POLITECNICO DI MILANO

Scuola di Ingegneria Industriale e dell'Informazione
Corso di Laurea Magistrale in Ingegneria Chimica
Dipartimento di Chimica, Materiali e Ingegneria Chimica "Giulio Natta"

HYDROXY FUNCTIONALIZED NANOSIZED GRAPHITE AS FILLER FOR NANOCOMPOSITES BASED ON NATURAL RUBBER AND POLYURETHANE

Relatore: Prof. Maurizio Stefano GALIMBERTI

Correlatore: Vincenzina BARBERA

Tesi di Laurea di:

Alessandro PORTA matr. 805037

Anno Accademico 2013 - 2014

Table of contents

List of Figure

Chapter I

Chapter II

Chapter III

Chapter IV

Chapter V

Chapter VI

Chapter VII

List of Tables

Chapter II

Chapter IV

Chapter V

Chapter VI

List of Schemes

Chapter III

Chapter IV

Chapter V

Chapter VI

List of abbreviation

6-PPD: (1,3-dimethylbutyl)-*N*'-phenyl-p-phenylenediamine

CB: Carbon Black

SWCNT: Single Walled Carbon Nanotubes

MWCNT: Multi Walled Carbon Nanotubes

DBP: Dibutyl phthalate

IR: Synthetic Rubber

NanoG: nano graphite

TBBS: *N*-tert-butyl-2-benzothiazyl sulfonamide

NR: Natural rubber

G-OH: Hydroxy functionalized nanographite

G-OH-M: Hydroxy functionalized nanographite via mechanical treatment

G-OH-T: Hydroxy functionalized nanographite via thermal treatment

G-OH-TM: Hydroxy functionalized nanographite via thermal and mechanical treatment

MDI: methylene diphenyl diisocyanate

G-A1: nanoG/maleic anhydride adduct obtained without hydrolysis

G-A2: nanoG/maleic anhydride adduct obtained with hydrolysis

G-S1: nanoG/ dodecanethiol adduct obtained without solvent

G-S2: nanoG/ dodecanethiol adduct obtained with solvent

DCT: dodecanethiol

MAH: maleic anhydride

PU: Polyurethane

Objectives and Introduction

Main objectives of the present thesis were:
(i) to modify nanosized graphite with high surface area (nanoG), introducing functional groups without substantially affecting the sp^2 hybridization of carbon atoms and promoting the delamination of graphite aggregates, moving in the direction of "few layers graphenes"
(ii) to obtain modified nanoG suitable for preparing nanocomposites with poly(1,4-*cis*-isoprene) from Hevea Brasiliensis (Natural Rubber, NR) or poly(urethane) (PU) as the polymer matrix
(iii) to prepare nanocomposites based on NR and PU, achieving even dispersion of the modified nanoG in the polymer matrices

Objectives for the modification reactions of nanoG were:
(i) to avoid dangerous reactions and harsh reaction conditions, toxic ingredients, complicated experimental procedures
(ii) to avoid further reaction steps on the modified nanoG, such as the reduction of graphite oxide. The objective is thus the possibility to use modified nanoG as obtained from the modification reaction.

NR was chosen as it is the most important rubber, it is a bio-based product and its production, with respect to a synthetic rubber, means a substantial reduction of energy consumption and environmental impact.
PU was chosen as it is the most versatile polymer and has a steady growing diffusion in the polymer market. Moreover, it can develop interesting synergy with functionalized nanoG: functional groups can take part in the formation of PU and graphite can contribute to solve the weak point of PU, that means the flame resistance.

Reaction was performed between nanoG and: (i) KOH, (ii) maleic anhydride (iii) 1-dodecanethiol. Reactions were performed in the absence of solvents, by using so called green method, such as ball milling, or by simply heating the reaction mixture. Products of the reactions were characterized by means of thermogravimetric analysis, infrared spectroscopy, X-Ray diffraction (XRD), transmission electron microscopy (TEM). The product of the reaction between nanoG and KOH, G-OH, bearing hydroxyl functional groups, was selected for the preparation of nanocomposites.

Stability of G-OH in water, in NR latex and in polyol mixture, also after centrifugation, was studied through UV spectroscopy. In particular, a concentration level typical of commercial products (4 mg/mL) was used.

In order to pursue ultimate dispersion of G-OH in the NR matrix, it was decided to prepare the nanocomposites by latex blending, that means by feeding G-OH in NR latex and precipitating the composite thanks to the addition of a mineral acid. Nanocomposites of G-OH in PU were prepared by dispersing G-OH in polyol mixture and by subsequently making the reaction with isocyanates.

NR based nanocomposites were then crosslinked by adding typical ingredients for a sulphur based vulcanization. Structure of the nanocomposites was studied by means of TEM and XRD. Dynamic-mechanical and tensile properties of the nanocomposites were investigated. Results were compared with those available in the literature for nanocomposites based on pristine nanoG.

Preliminary studies were performed on PU based nanocomposites, by means of nuclear magnetic resonance spectroscopy, XRD, TEM, TGA and differential scanning calorimetry.

SECTION I Background

Chapter I

1.1 Carbon

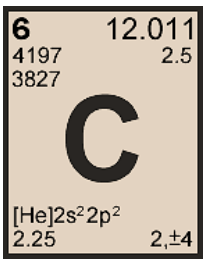

Figure 1.1 Carbon

Carbon is a chemical element with symbol C and atomic number 6, belonging to the group IVB of the periodic table (Fig. 1.1). It has an electronic configuration $1s^2 2s^2 2p^2$ and would seem therefore divalent. Is a fundamental element for life on earth, it can bind itself in long stable chains without a great expense of energy. [1]

It is the only atom present in all organic molecules, thanks to its ability to form multiple bonds and to give macromolecular structures.

So carbon can be tetravalent and all electrons of the external layer must be involved, assuming an electronic configuration like $1s^2\ 2s^1 2p^3$(Fig. 1.2).

Figure 1.2 Carbon electronic configuration in fundamental and excited state

The concepts of orbital hybridization and directed valence were developed by Linus Pauling after the description of hydrogen molecule with the valence bond theory. These concepts were applied to organic chemistry and in specific to the tetrahedral orientation of the bonds of

tetracoordinate carbon. Pauling thought that because covalent bond requires mutual overlap of orbitals, thus, stronger bonds would result from greater overlap. So orbitals that possess directional properties, like *p* orbitals, should be more effective than spherically symmetric *s* orbitals.

The electronic configuration of carbon atom in ground state is $1s^2 2s^2 2p^2$, and is not coherent with the tetrahedral bonding at carbon. Pauling proposed that four atomic orbitals ($2s$, $2p_x$, $2p_y$, $2p_z$) are replaces by four equivalent hybrid orbitals, named sp^3. The shape of these orbitals are shown in Figure 1.3 that show in particularly that the probability distribution in the sp^3 orbitals is highly directional, with a region of greatest probability concentrated to one side of the nucleus.

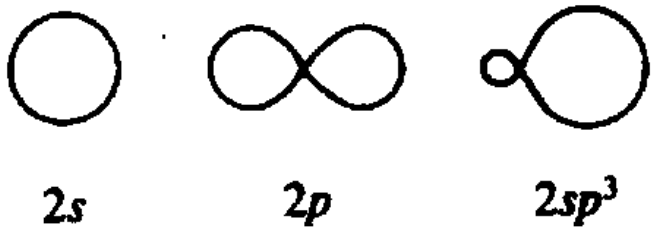

Figure 1.3 Cross section of angular dependence of orbitals

Orbital hybridization has two relevant consequences. First, carbon can form four bonds rather than two. Second, sp^3 orbitals are highly directional and provide for more effective overlap and stronger bonds. Thus, although isolated carbon atoms with one electron in each of four sp^3-hybridized orbitals would be at higher energy than the ground state, the energy required to promote two electrons from a $2s$ orbital to sp^3 is compensated by the creation of four bonds rather than two. Additionally, each bond is stronger thanks to the directional properties of hybrid orbitals. Tetrahedral geometry is predicted with mathematical description of hybridization. Experimentally, methane is found to be a perfect tetrahedron with H-C-H bond angle equal to 109.5°. The representation of valence bond in methane in Figure 1.4 shows the orbitals overlaps that give rise to four identical C-H bonds. These bonds are called σ bonds, in which the electron density have cylindrically symmetry about the internuclear axis.

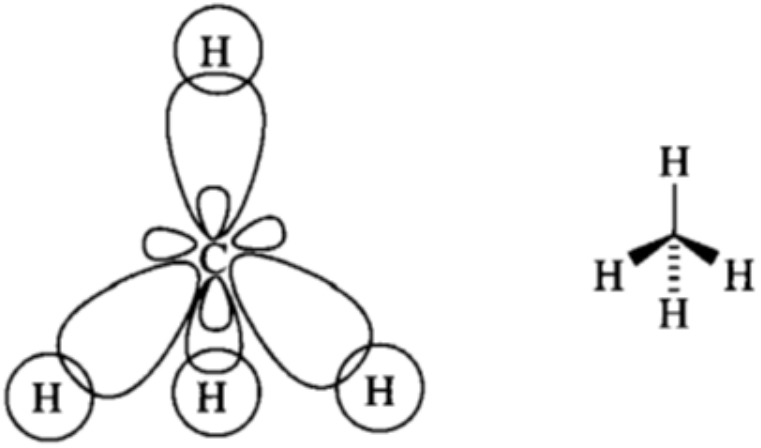

Figure 1.4 Valence bond structural representation of methane

The hybridization theory can be also applied to molecules with double or triple bonds. In ethylene (Fig. 1.5) each carbon is sp^2 hybridized and has three ligands. The 2*s* orbital and two of the 2*p* orbital generate three sp^2 orbitals that are orthogonal and coplanar to the remaining 2*p* orbital. The bond is formed between the two carbon atoms overlapping an sp^2 orbital of each. The four hydrogen are bonded with σ bonds involving the remaining two sp^2 hybrid orbitals and the hydrogen 1*s* orbital. This overlap is less effective than that of a σ bond and correspond to a π bond. The electron density in a π bond is concentrated below and above the plane of the σ bonds, thus the molecule is planar. In acetylene, the hybridization at each carbon atom is *sp*, and the carbon atoms are bonded by a σ bond and two π bonds, as shown in Figure 1.5. [2]

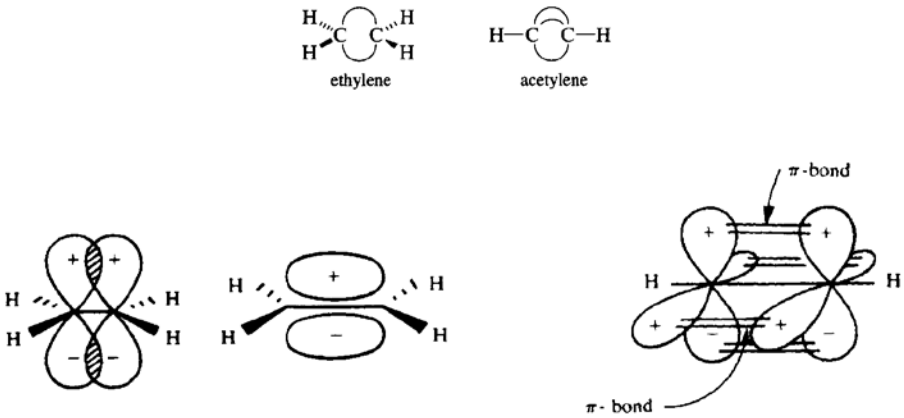

Figure 1.5 The π bond in ethylene and π bonds in acetylene

1.2 Carbon allotropes

"The term allotrope denotes forms of elements that differ in the way the atoms are bonded" P. Atkins, J.A. Beran, General Chemistry, 2nd Ed. Scientific American Books, 1990

Carbon–carbon bonds are stable and strong, they facilitate the formation of an enormous number of molecular forms. Carbon allotropes have different bonding arrangements and possess different physical and chemical properties.

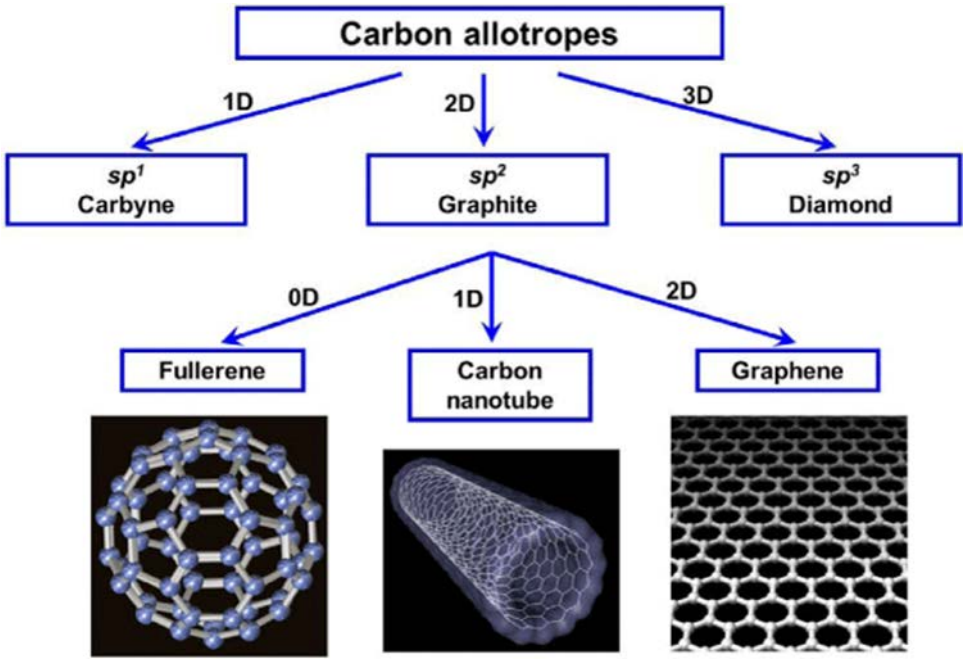

Figure 1.6 Carbon allotropes

For thousand years and until 25 years ago, amorphous carbon, graphite and diamond were considered the only three carbon allotropes.[3] In a *Nature Communication* of 1985 it was reported the discovering of another interesting allotrope of carbon, formed by 60 carbon atoms bounded themselves and having sp^2 ibridization. Due to this strange structure, Kroto named it *buckminsterfullerene* or fullerene. [4] Iijima and Donald Bethune found single walled nanotubes known as buckytubes six years later. [3] The first isolation of graphene, a two-Dimensional single atomic layer of graphite, was reported in 2004. [5] Fullerenes, graphene and CNTs have becomed important in modern science and technology because they provide exciting challenges and opportunities scientists thanks also to their unique properties.

1.2.1 Amorphous carbon

Before the advent of carbynes, nanotubes and fullerenes, amorphous carbons were considered the third allotropic form of carbon.[6] These materials have roughly planar layers of sp^2-hybridized carbon atoms but lack in long-range crystallinity, especially in the stacking direction. They contain an important fraction of sp^3 carbon atoms which crosslink neighboring layers forming a structure that comprises either amorphous and more graphitic regions. [7, 8] Amorphous carbons are usually prepared by pyrolysis of hydrocarbon precursors or organic polymer at temperatures below 1500 °C. The preparation history and the nature of the starting material strongly influence the structure and the final properties. [7] The so-called graphitizable carbons develop a graphitic structure by heating them to temperatures ranging from 1500 to 3000 °C.

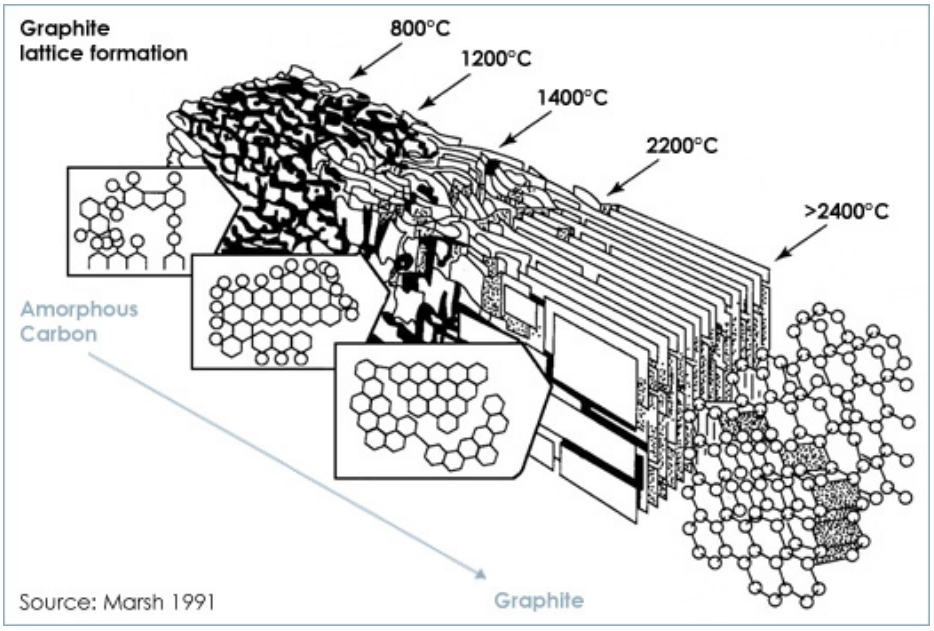

Figure 1.7 Graphitization

Carbons prepared from liquid precursors like petroleum pitch, show greater crystallinity or at least better graphitization. Graphitizable carbons are called ‘‘soft carbons’’. [8, 9] Materials prepared from the gas precursor can have a very high degree of three-dimensional order upon prolonged thermal treatment. [7] Carbon blacks, usually prepared from natural gas or acetylene, show a high degree of crystallinity with a small part of amorphous regions within the particles.[8]

Figure 1.8 Carbon black

Non-graphitizable carbons are called ‘‘hard carbons’’. They originate from solid precursors such as resins and polymers and have a highly disordered structure. [7 - 9] These carbons are isotropic in all properties, and do not develop significant graphitic structure even at high temperatures (2500–3000°C). Activated carbons are amorphous, usually hard, carbons that underwent physical or chemical activation.[7] The activation process results in a very high surface areas (~500–3000m^2 g^{-1}) and sometimes to a good microporosity. Chemical activation imply the addition of compounds such as H_2SO_4, H_3PO_4 and $ZnCl_2$ to the precursor feedstock previous carbonization. Physical activation refers to treatment of the carbon material with gases such as steam and carbon dioxide in the temperature range of 700–1100 °C. Activated carbons are industrially produced by the carbonization and physical activation of lignite, wood or coal for example. [7,11] Activated carbons have been used in gas separation, in water treatment, as catalysts and catalyst supports and also as filter materials or decolorizing agents.[7,11,12]

Carbon fibers are an important class of carbon materials closely related to multi-walled carbon nanotubes.[7] Their preparation is similar to that of amorphous carbon, often using pyrolysis of an organic precursor under specific conditions. The fibers can be amorphous or exhibit different degrees of crystallinity depending on the synthesis conditions, which will affect the ultimate properties and target applications.[8]

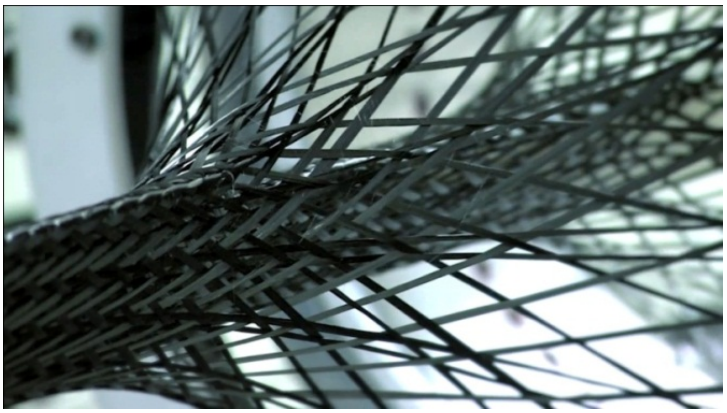

Figure 1.9 Carbon fibers

Also carbon aerogels can be formed from the pyrolysis of organic precursors. These materials usually show low density and very high specific surface areas. They can be produced in different forms, such as films, fine particles or monoliths. The final shape and properties depend strongly on the sample history.[13,14] Carbon aerogels are promising materials as adsorbents or catalysts.[13,14]

Figure 1.10 Carbon aerogel

1.2.2 Diamonds

Elemental carbon with sp^3 hybridization form a tetrahedral lattice that give rise to diamond in witch, each carbon atom covalently bonds to four others, forming three-dimensionally a series of tetrahedral in the three dimensions. Due to its structure diamond does not conduct electric current. It usually crystallizes with a cubic structure, and can be synthetized industrially. Thanks to their exceptional chemical and physical characteristics, diamonds have many applications. The

most important are the very high thermal conductivity and the low coefficient of thermal expansion, the extreme hardness, high resistance to chemicals and high index of optical dispersion. Diamonds are highly water repellent because water does not adhere to the surface, but form droplets that slip off very easily. A diamond put in water and then removed will be perfectly dry. The chemical resistance is very high in fact diamonds are resistant to most acids and bases, also in high concentrations. Diamond is the hardest natural mineral material known. It is the thermodynamically stable form of carbon above 60 kbar.[15] This extreme hardness is due to the presence of covalent bonds extended to the whole structure and in all directions.

Figure 1.11 Diamond

Above 1500°C diamond transforms into graphite, that is the thermodynamically stable allotrope at low pressure, under vacuum or inert atmosphere.[15] Under ambient conditions such transformation is negligibly slow.

1.2.3 Graphene

Graphene is defined by IUPAC as “A single carbon layer of the graphite structure, describing its nature by analogy to a polycyclic aromatic hydrocarbon of quasi infinite size”.

The discovery of graphene is simple like its structure. Even if graphene has been known since the early 1940s, the first isolation of the single graphene sheet has been reported only in 2004 [5]. Novoselov and Geim won the Nobel Prize for physics in 2010 for the isolation of one of this atom-thick form of carbon allotrope through an experiment simple but functional. They used the tape to peel off a layer of graphite from its block.

It is possible to consider CNTs, fullerenes, and graphite as different structures formed from the honeycomb lattice called ‘graphene’ (Fig. 1.11). Every carbon atom in graphene is covalently

bonded to three other carbon atoms with sp^2 hybridization forming a two-dimensional (2D) honeycomb lattice structure. The C–C bond length is 1.42 Å.

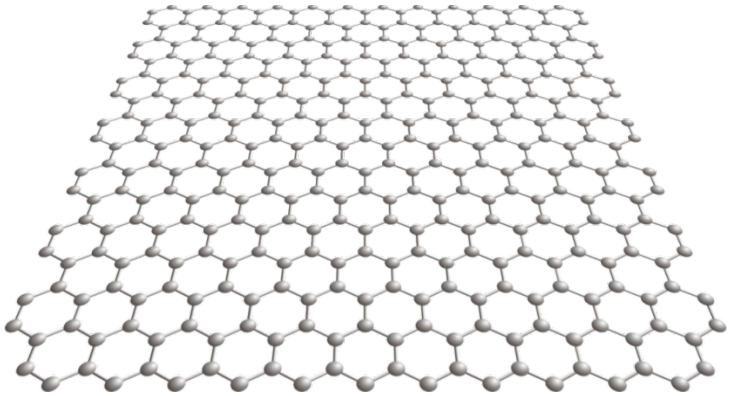

Figure 1.12 Structure of graphene

Graphene is the thinnest and the strongest material known. The experimental investigation shows that monolayer graphene has a breaking strength of *40 N/m and a Young's modulus of *1.0 TPa.[14] Graphene can sustain current densities of six orders of magnitude higher than copper. It has a thermal conductivity of *5000 Wm^{-1} K^{-1} at room temperature [16] and it is impermeable to gases [17]. Significant progress has been recently made to fabricate graphene devices, for example transistors [18,19] and also studies about the chemistry of graphene sheets have been reported.[20, 21] Graphene is a very important area of research in this decade because of its potential applications in nanotechnology. Various defects such as vacancies [22], Stone–Wales (SW),[23] substitution atoms [24, 26] and poredefects [26] can occur in graphene sheet. Different kinds of defects have been observed experimentally [17] using HRTEM and atomic force microscopy. The characteristics and concentrations of typical defects in graphene sheets are unclear, in fact, the chemistry of graphene has remained largely unexplored.[17] Graphene can be involved in chemical reactions like any other molecule; its chemistry is expected to play important role in the production of materials based on graphene. Chemical transformation, that can probably be induced even locally, is considered one of the best method to detect imperfections in the graphene sheet.[27] The functionalized graphene can be useful for specific applications. Studies have shown that the edges of graphene have significant influence on their chemical reactivity and properties.[28, 29] It has been recently reported that single graphene

sheet is about 10 times more reactive than bi- or multi-layers of graphene and that reactivity of edges is at least two times higher than the reactivity of the bulk single graphene sheet [28, 29].

1.2.4 Graphite

Figure 1.13 Example of use of graphite

Graphite is a crystalline and polymorphic form of elementary carbon. The graphite structure consists in six-membered rings in which every carbon atom is bonded with three near neighbours forming an equilateral triangle. The layers in graphite are kept together by van der Waals forces with an energy of 0.2 eV/atom. Weak bonding perpendicular to the layers results in easily parallel sliding of the sheets.

Two types of spatial arrangement of carbon layers are possible: the sequence ABABAB. . . is characteristic of the hexagonal structure of graphite (Fig. 1.12a) while the sequence ABCABC... occurs in the rhombohedral modification (Fig. 1.12b). The hexagonal one is the thermodynamically stable form of graphite in a wide range of pressures and temperatures ($T < 2000$ °C, $P < 1.31010$ Pa [130 kbar]). The rhombohedral one is a metastable phase, disappearing at elevated temperatures ($T > 2000$ °C). The described structure of graphite refers to its ideal crystalline forms.

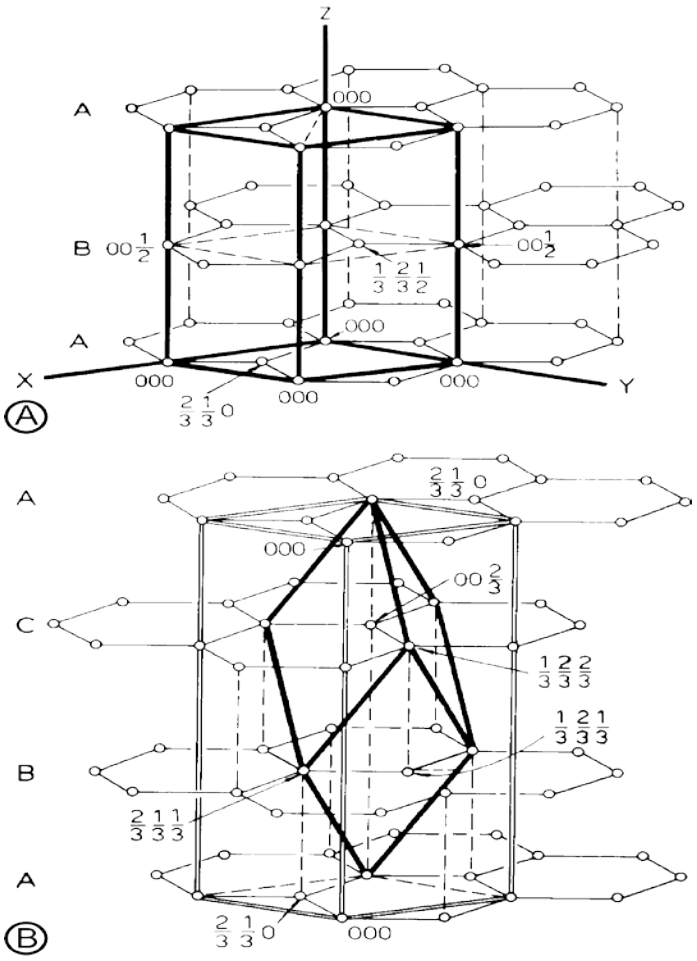

Figure 1.14 Structure of graphite

In nature graphite appears in less perfect forms and in a variety of disordered types. These forms show many degrees of graphitization of carbon contained in the organic matter or carbonaceous substance dispersed in metamorphic or sedimentary rocks. They are named anthracite, meta-anthracite and semigraphite according to the content of H and C and the degree of order in the structure. Graphite is anisotropic, being a good thermal and electrical conductor within the layers but a poor electrical and thermal conductor perpendicular to the layers.

Due to the anisotropy, the carbon layers can slide one respect to each another quite easily making graphite a good pencil material and lubricant. Graphite is also able to undergo chemical reactions by allowing the reactant, or intercalate, to insert between the graphene layers. These reactions are known as intercalation reaction. Compression of exfoliated graphite flakes without a binder form a flexible and resilient sheet known as flexible graphite used as gasket material. [18]

1.2.5 Carbon Nanotubes

Structural model of Carbon Nanotubes (CNTs) has the resemblance of a ‘‘Russian doll’’ because is based on concentric cylinders capped at ends. The existence of CNTs was reported for the first time in 1952 but this report did not reach the scientific community. Iijima detected CNTs in 1991 and his work is considered as the pioneering one for the nanotechnology revolution of the modern era.[27] According to Iijima,[54] the detection of CNTs was unexpected but not entirely accidental. Iijima had motivation in finding out new carbon allotropes due to the discovery of Buckminsterfullerene by Kroto et al.[4] Single-walled CNTs (SWCNTs) and Multi-walled CNTs (MWCNTs) are the two structural forms of CNTs.

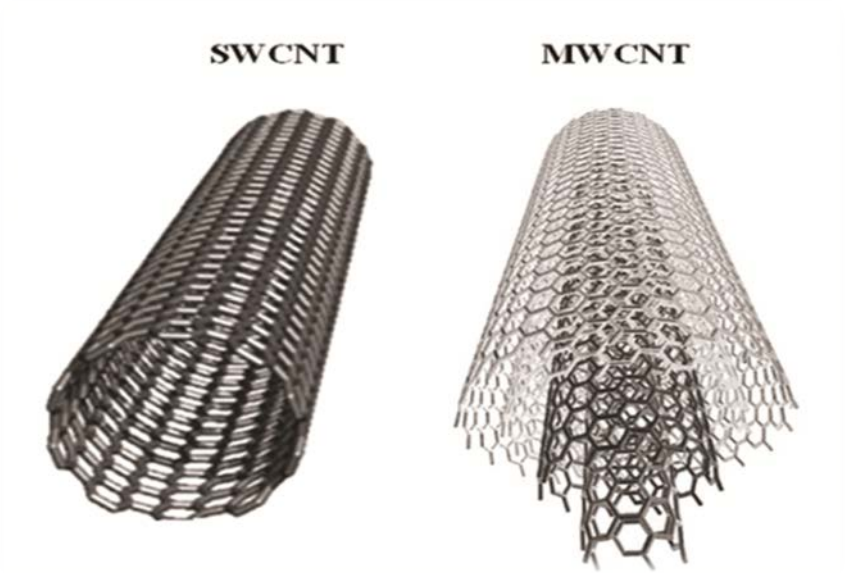

Figure 1.15 Single-walled nanotubes (SWCNT) and multi-walled nanotubes (MWCNT)

Wide range of methods such as laser ablation, arc-evaporation of graphite, vapor phase decomposition, and chemical vapor deposition (CVD) are available for the syntheses of SWCNTs and MWCNTs.[31, 32] The mechanism of formation of SWCNTs and MWCNTs remains unclear.[20] An ideal MWCNT consists in cylindrical tubes weakly bonded through van der Waals forces. CNTs have diameters ranging from one nanometer to tens and lengths up to centimeters. They can be closed by a hemispherical fullerene-type cap or open-ended, depending on the synthesis method.[33] SWCNTs can be viewed as the wrapping of a graphene sheet into an infinite cylinder (Fig. 1.16).

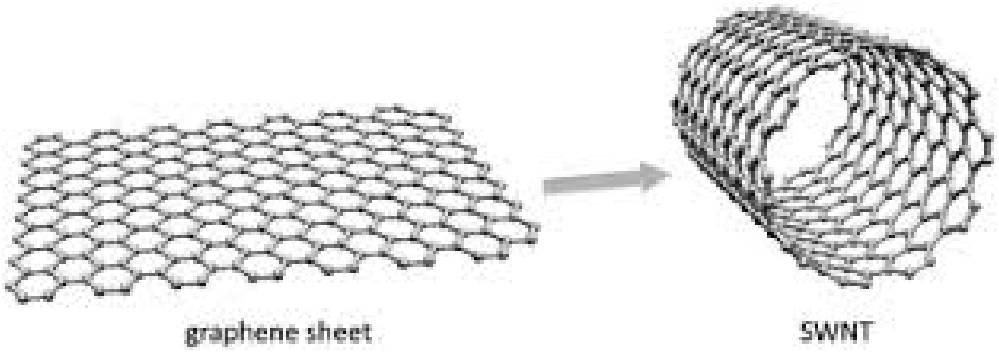

Figure 1.16 Schematic of the roll-up of a graphene sheet to form a SWCNT structure

CNTs is a large family with a wide variety of properties and sizes that are determined by their composition and structure, including defects, number and ordering of the walls, surface functionalization and other features. It is now possible to identify, disperse, isolate and sort various types of CNTs.[34–37] Specific methods have been found to grow long SWCNTs and to control the nanotube diameters.[38, 39] High resolution transmission electron microscopy (HRTEM) is useful in determining the diameter distribution of SWCNTs [40] SWCNTs in particular have stimulated intense experimental and theoretical studies due to their unique mechanical, structural, thermal, electronic, and chemical properties and also for their potential applications in diversified areas.[41–45]

1.2.6 Fullerenes

Fullerenes have one of the most important places in modern material. Fullerene C60 is the most abundant and representative of the fullerene family. It was produced for the first time on industrial scale in 1990.[19] Production of important quantity of C60 allowed scientists to study and understand its properties and chemistry. C60 has 20 hexagon rings placed at the centers of icosahedral faces and 12 pentagons located around the vertices. The C60 molecule was named as ‘‘Buckminsterfullerene’’ in honor of the renowned architect Buckminster Fuller, who designed geodesic domes.

Figure 1.17 Buckminsterfullerene

Fullerenes are represented by the formula Cn. They have 3n/2 edges, 12 pentagonal faces and (n - 20)/2 hexagonal faces.[21] The second most abundant fullerene is C70 and was characterized using mass spectroscopy by Kroto et al. [4] and Kra¨tschmer et al. [19] independently. C60 has a spherical shape similar to the common soccer ball while C70 belongs to a class of non-spherical fullerenes and it looks like rugby ball. The self-assembly process giving rise to the ‘‘soccer-ball’ structure from hot carbon vapor is not fully understood; different mechanisms have been proposed for the formation of fullerenes. Fullerenes are classified into two types: classical and non-classical fullerenes. Classical fullerenes are closed carbon cages containing 12 pentagons and different number of hexagons. Non-classical fullerenes can have heptagons, octagons, and an additional number of pentagons or squares. At ambient pressure and temperature, C60 crystals show face centered cubic (fcc) structure, while the C70 crystals adopt to a hexagonal close packed (hcp) structure. The average diameter of C60 and C70 fullerenes is about 7 and 9 Å respectively. Among 1812 possible isomers of structure with 60 carbon atoms, the Buckminsterfullerene C60 is the most stable because none of the pentagons are in contact with each other. The IPR is a very essential and important rule in governing the geometry of fullerenes. The rule asserts that the most stable fullerenes are those in which all pentagons are surrounded by five hexagons. The smallest fullerene that obeys the IPR is C60 and the C70 is the second. There is only one isomer for C60,that satisfies the IPR instead there are 8149 possible isomers of structure for C70. However, only one of them obeys IPR.[46, 47] There are no IPR fullerenes between C60 and C70. The number of possible isomers that obey to IPR rule increases

rapidly with increase in the size of the fullerenes. Fullerenes that violate IPR rule were reported to be thermodynamically less stable and aromatic than the IPR-obeying isomers.[48 - 51]

The isolation and characterization of large fullerenes are really difficult by the presence of many different isomers. Understand the energetic and electronic properties and structure of the family of fullerenes is important because these systems can be used in nanotechnology applications. In fast if hexagons are added or removed, the fullerene structure begins to loose its roundness. Kroto's group developed the experimental method for the formation of quasi-icosahedral shaped carbonaceous particles called giant fullerenes.[52, 53]

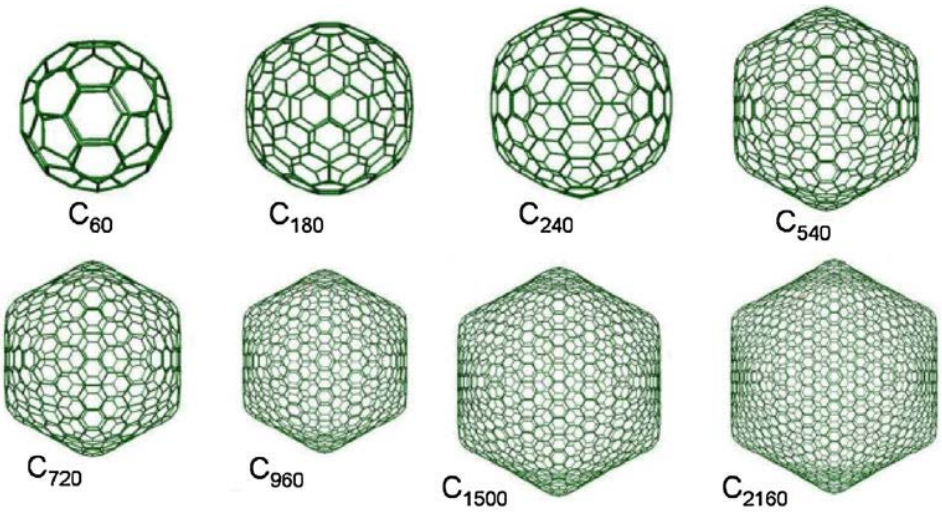

Figure 1.18 Giant Fullerenes

Majority of the giant fullerenes are of two kinds, one being Cn = 60k2 and the other Cn = 20k2; where n is the number of carbon atoms and k is any positive integer.[54] Few structures belong to the 180k2 family. Figure 1.18 shows some of the giant fullerene structures. C180 and C720 belong to the 180k2 family whereas all other structures belong to the 60k2 family of icosahedra fullerenes.

1.2.7 Other nanostructures

During the investigation of sp^2-hybridized carbon allotropes, attention has been also paid towards the development of more synthetic carbon allotropes.[55] The construction principle of incorporating both sp^3- and *sp*-hybridized atoms into carbon lattice offers limitless structural

possibilities: the simplest example is one-dimensional carbyne formed by infinite chains of *sp*-hybridized carbon atoms (Fig. 1.19).

Figure 1.19 One-dimensional *sp*-carbyne

Considering that this allotrope itself is still elusive, many model compounds called end-capped polyynes have been synthesized and characterized. The combination of sp^3-, sp^2- and *sp*-hybridized carbon atoms allows many possible two- and three-dimensional carbon allotropes like graphyne (Fig. 1.20).[36]

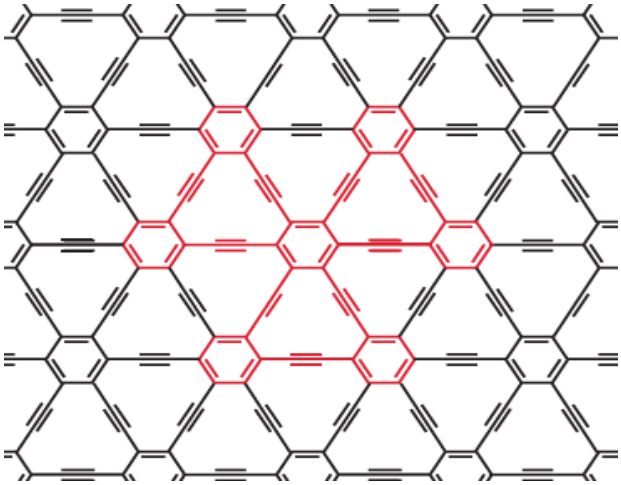

Figure 1.20 Two-dimensional *sp*-sp^2-graphyne

Significantly large molecular fragment of graphyne have been synthesized. Studies suggests that the material has attractive self-assembly and optoelectronic properties. Allotropes with a skeleton of sp^3- and *sp*-hybridized carbon are the class least-studied of hybrid allotropes. The prediction of impressive mechanical properties motivates the study of these materials, for example hardness for allotropes like yne-diamond (Fig. 1.21).

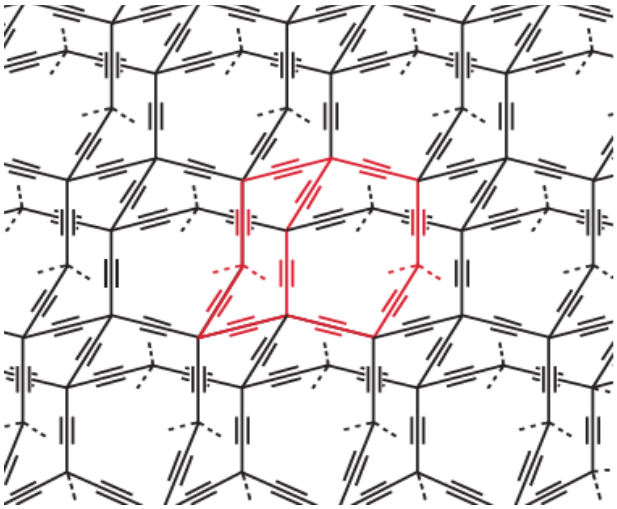

Figure 1.21 Three-dimensional *sp*-*sp*^{3}-yne-diamond

A variety of low-molecular structures of these networks have been synthesized however the synthesis of this carbon allotropes is still very difficult.

1.3 Chemical modifications on *sp*^{2} Carbon allotropes

The chemical modification of carbon allotropes is important to improve the solubility in water or in organic solvent. In recent years, several approaches to obtain the functionalization of carbon allotropes were improved. The main approaches for the functionalization of carbon allotropes can be grouped into two main categories: (a) the covalent attachment of chemical groups, through reactions on the conjugated skeleton, and (b) the noncovalent supramolecular adsorption or wrapping of various functional molecules. In this thesis we dealt mainly with graphite then will be reported more examples of this specific allotrope

1.3.1 Non covalent modification

Weak and reversible noncovalent interactions, such as hydrogen bond (HB) and aromatic π–π interactions, metal coordination, hydrophobic and van der Waals forces, and/or electrostatic effects are key features in supramolecular chemistry. Although much less strong than hydrogen bonding, aromatic π–π interactions and ring-current effects associated with the presence of aromatic moieties represent another important type of weak interaction.

In this frame, the surface of carbon allotropes can be modified via van der Waals forces and π-π interactions, by adsorption or wrapping of polynuclear aromatic compounds, surfactants, polymers, or biomolecules. The main advantage of the non covalent functionalization, as compared to the covalent one, is that with the former, chemical functionalities can be introduced without affecting the structure and electronic network of the tubes. For example, in literature, is reported that the transport properties and electrochemical performance of polyelectrolyte membranes were improved through the dispersion of chitosan-wrapped carbon nanotubes, for direct methanol fuel cell applications.[56] Nakashima and co-workers have reported evidence for the interaction of the nanotube sidewall and the pyrene moiety in the aqueous dispersion/solution finding that sonication of solid single-walled carbon nanotubes (p-SWNT) in an aqueous solution of a pyrene-carrying ammonium ion gave a transparent dispersion/solution.[24]

1.3.2 Covalent modification

The presence of defects on carbon allotropes results in a locally enhanced chemical reactivity of the graphitic nanostructures. In general, carbon allotropes show mainly three types of defects:

- Unsaturated bonds: due to lack of binding of C atoms with the surrounding atoms and involve the presence of vacations, replacement, dislocations and atoms in interstitial position;
- Topological defects: mainly consist of pentagons and hexagons present in the hexagonal cells structure, and can lead to deformations and variations of the chirality. In this category are also the so-called defects of Stone-Wales, consisting in the presence of two pairs of pentagons and heptagons generated by a 90° rotation of one of the bonds in the hexagonal lattice;
- Defects of re-hybridization: come from the presence of a line of elements sp^3 hybridized, within a lattice with sp^2 hybridization.

To obtain covalent functionalization of carbon sp^2 allotropes there are mainly two types of approaches, in particular: defect-group and covalent sidewall functionalization. For example, it is possible mill pristine graphite, in the presence of dry ice, to achieve high yield of edge-selectively carboxylate graphite.[25] It is also possible to perform more aggressive reaction on

graphite: the oxidation of graphite to graphitic oxide can be accomplished by treating graphite with a mixture of concentrated sulfuric acid, sodium nitrate and potassium permanganate.[57]

1.3.3 Carbocatalysis

In literature, there are many example of reactions performed using carbon allotropes as support [58]. It is know that supported catalysts are of special interest in organic synthesis, because they allow the dispersion and stabilization of small metallic particles. The most important carbon support material is *activated carbon*, followed by carbon black and graphite or graphitised materials.[59] They can be also efficient catalysts and not only a catalyst support,[60] infact "carbocatalysis" is a new field used in chemical reactions.[61]

1.4 References

[1] Primo Levi, The periodic table

[2] Carey, Sundberg – Advanced Organic Chemistry part A: Structure and mechanisms

[3] Pierson HO (1993) Handbook of carbon, graphite, diamonds andfullerenes: processing, properties and applications. Noyes Publications,New Jersey, USA

[4]. Kroto HW, Heath JR, O'Brien SC, Curl RF, Smalley RE (1985)Nature 318:162

[5]. Novoselov KS, Geim AK, Morozov SV, Jiang D, Zhang Y,Dubonos SV, Grigorieva IV, Firsov AA (2004) Science 306:666

[6] Mantell CL, Carbon and Graphite Handbook, Interscience Publishers, New York, Ch. 2 (1968).

[7] Winter M and Besenhard JO, in Lithium Ion Batteries –Fundamentals and Performance, ed. by Wakihara M andYamamoto O, Wiley–VCH, Weinheim, Germany, Ch.6 (1998).

[8] Mantell CL, Carbon and Graphite Handbook, InterscicencePublishers, New York, Ch. 6 (1968).86 Pierre AC and Pajonk GM, Chemistry of aerogels and theirapplications. Chem Rev 102:4243–4265 (2002).

[9] Dresselhaus MS and Endo M, Relation of carbon nanotubes to other carbon materials. Topic Appl Phys 80:11–28 (2001).

[10] Byrne JF and Marsh H, in Porosity in Carbons, edbyPatrick JW Halsted Press, New York, Ch. 1 (1995).

[11] Chung DDL, Graphite. J Mater Sci 37:1475–1489 (2002).

[12] Al–Muhtaseb SA and Ritter JA, Preparation and propertiesof resorcinol–formaldehyde organic and carbon gels. AdvMater 15:101–114 (2003).

[13] Moreno–Castilla C and Maldonado–Hodar FJ, Carbon aerogelsfor catalysis applications: An overview. Carbon43:455–465 (2005).

[14] Lee C, Wei X, Kysar JW, Hone J (2008) Science 321:385

[15] Rode AV, Gamaly EG, Christy AG, Fitz Gerald JG, HydeST, Elliman RG, et al, Unconventional magnetism inall–carbon nanofoam. Phys Rev B 70:054407-1–054407-9(2004).

[16] Balandin AA, Ghosh S, Bao W, Calizo I, Teweldebrhan D, MiaoF, Lau CN (2008) Nano Lett 8:902

[17] Meyer JC, Kisielowski C, Erni R, Rossell MD, Crommine MF, Zettl A (2008) Nano Lett 8:3582

[18] *Idem., J. Mater. Eng. Perf.* **9**(2) (2000).

[19] Kra¨tschmer W, Lamb LD, Fostiropoulos K, Huffman DR (1990) Nature 347:354

[20] Dresselhaus MS, Dresselhaus G, Ph Avouris (eds) (2001) Carbon nanotubes: synthesis, structure, properties, and applications.Springer-Verlag, Berlin

[21] Fowler PW, Manolopoulos DE (1995) An atlas of fullerenes. Oxford University Press, New York

[22] Jiang D, Cooper VR, Dai S (2009) Nano Lett 9:4019 154. Zhu ZH, Hatori H, Wang SB, Lu GQ (2005) J Phys Chem B 109:16744

[23] Stone AJ, Wales DJ (1986) Chem Phys Lett 128:501 152. Carlson JM, Scheffler M (2006) Phys Rev Lett 96:046806

[24] Nakashima, N., Tomonari, Y., & Murakami, H. (2002). Water-Soluble Single-Walled Carbon Nanotubes via Noncovalent Sidewall-Functionalization with a Pyrene-Carrying Ammonium Ion. Chemistry Letters, (6), 638-639.

[25] Jeon, I. Y., Shin, Y. R., Sohn, G. J., Choi, H. J., Bae, S. Y., Mahmood, J., ... & Baek, J. B. (2012). Edge-carboxylated graphene nanosheets via ball milling.Proceedings of the National Academy of Sciences, 109(15), 5588-5593.

[26] Miwa RH, Martins TB, Fazzio A (2008) Nanotechnology 19: 155708

[27] Iijima S (1991) Nature 354:56

[28] Peralta-Inga Z, Murray JS, Grice ME, Boyd S, O'Connor CJ, Politzer P (2001) J Mol Struct (Theochem) 549:147

[29] Sharma R, Nair N, Strano MS (2009) J Phys Chem C 113:14771

[30] Iijima S (2007) Nat Nanotechnol 2:590

[31] Dresselhaus MS, Dresselhaus G, Ph Avouris (eds) (2001) Carbon nanotubes: synthesis, structure, properties, and applications.Springer-Verlag, Berlin

[32] Ajayan PM (1999) Chem Rev 99:1787

[33] Lu J, Yuan D, Liu J, Leng W, Kopley TE (2008) Nano Lett8:3325

[34] Harris PJF (2003) Carbon nanotubes and related structures.Cambridge University Press, Cambridge, UK

[35] Strano MS (2003) J Am Chem Soc 125:16148

[36] Arnold MS, Green AA, Hulvat JF, Stupp SI, Hersam MC (2006)Nat Nanotechnol 1:60
[37] Strano MS (2007) Nat Nanotechnol 2:340
[38] Ouyang M, Huang J, Lieber CM (2002) Acc Chem Res 35:1018
[39] Zhang H, Cao G, Wang Z, Yang Y, Shi Z, Gu Z (2008) J Phys Chem C 112:12706
[40] Pesce PBC, Araujo PT, Nikolaev P, Doorn SK, Hata K, Saito R,Dresselhaus MS, Jorio A (2010) Appl Phys Lett 96:051910
[41] Matsuo Y, Tahara K, Nakamura E (2003) Org Lett 5:3181
[42] Cioslowski J, Rao N, Moncrieff D (2002) J Am Chem Soc124:8485
[43] Bahr JL, Tour JM (2002) J Mater Chem 12:1952
[44] Hirsch A (2002) Angew Chem Int Ed 41:1853
[45] Vostrowsky O, Hirsch A (2004) Angew Chem Int Ed 43:2326
[46] Manolopoulos DE, Fowler PW (1992) J Chem Phys 96:7603
[47] Brinkmann G, Dress AWM (1998) Adv Appl Math 21:473
[48] Schmalz TG, Seitz WA, Klein DJ, Hite GE (1988) J Am Chem Soc 110:1113
[49] Liu X, Klein DJ, Seitz WA, Schmalz TG (1991) J Comput Chem 12:1265
[50] Aihara J (1995) J Am Chem Soc 117:4130
[51] Diederich, F. & Kivala, M. Adv. Mat. 22, 803‑812 (2010).
[52] Kroto HW, McKay KG (1988) Nature 331:328
[53] Kroto HW (1990) Chem Br 26:40
[54] Tang AC, Huang FQ (1995) Phys Rev B 51:13830
[55] Diederich, F. & Kivala, M. Adv. Mat. 22, 803‑812 (2010).
[56] Hasani-Sadrabadi, M. M., Dashtimoghadam, E., Majedi, F. S., Wu, S., Bertsch, A., Moaddel, H., & Renaud, P. (2013). Nafion/chitosan-wrapped CNT nanocomposite membrane for high-performance direct methanol fuel cells. RSC Advances, 3(20), 7337-7346.
[57] Hummers Jr, W. S., & Offeman, R. E. (1958). Preparation of graphitic oxide.Journal of the American Chemical Society, 80(6), 1339-1339.
[58] Serp, P., & Figueiredo, J. L. (Eds.). (2009). Carbon materials for catalysis. John Wiley & Sons.
[59] A.J. Bird, in: A.B. Stiles (Ed.), Catalyst Supports and Supported Catalysts, Butterworths, Boston, 1987, p. 107.

[60] Dreyer, D. R., & Bielawski, C. W. (2011). Carbocatalysis: Heterogeneous carbons finding utility in synthetic chemistry. Chemical Science, 2(7), 1233-1240.
[61] Navalon, S., Dhakshinamoorthy, A., Alvaro, M., & Garcia, H. (2014). Carbocatalysis by graphene-based materials. Chemical reviews, 114(12), 6179-6212.

Chapter II

2.1 Natural Rubber

Natural rubber is a biopolymer consisting of isoprene units (C5H8)n linked together in a *cis*- 1,4-configuration (Fig. 2.1). Its unique properties are due to its intrinsic structure, its high molecular weight.

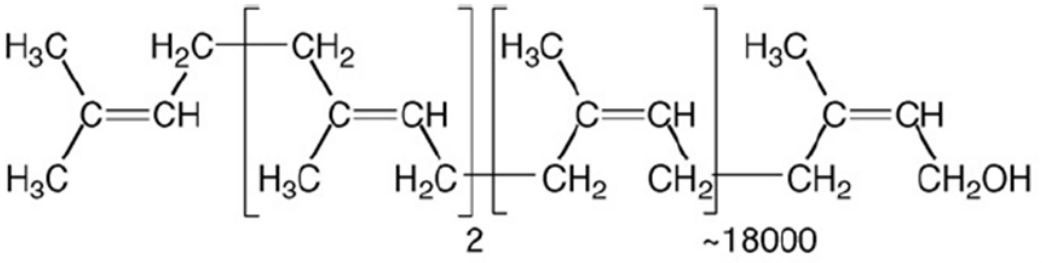

Figure 2.1 Structure of natural rubber

NR outstanding properties: great strength [1,2] and tack [3,4] in the uncrosslinked state and, in the crosslinked state, very high tensile strength [5,6] and crack growth resistance, both in static [7-11] and in fatigue [12-19] loading conditions. In particular, the crack growth resistance makes NR the ideal rubber for highly demanding applications such as the ones for heavy truck and airplane tyres and for base isolators to restrict transmission of seismic vibrations. Beneficial for the mentioned NR properties is the strain induced crystallization (SIC), that is the rapid development of crystallization under straining.

NR has unique properties [20] and can not be replaced in large scale applications of rubber, such as the one in tyre. In fact 75% of NR is use in tyre compounds and the remaining 25% for latex products and various industrial uses.

Moreover, with respect to a synthetic rubber, NR requires much lower energy for its production and has much lower impact on the environment.[21] Data are summarized in Table 2.1

Table 2.1 Energy consumption for rubber production and carbon footprint

	Energy Consumption (MJ/kg)	**Carbon Footprint (kg CO_2 / kg)**
Natural Rubber	8	0.4
Synthetic Rubber	110	5.0

2.2 Elasticity and Vulcanization

2.2.1 Enthalpic and entropic elasticity

The most important property of elastomers is their ability to undergo large reversible elastic deformations, with practically no residual deformations or changes in shape. This behavior is achieved when flexible polymer chains are cross-linked to a three-dimensional network and the system is in the rubbery state (T > Tg). The material concept which allow such an unique behavior is the entropy-elasticity.

The basic differences in the behavior of elastomers and ideal elastic solids are governed by specific mechanisms of energy storage during deformation.

The capability to store energy changes with temperature. In particular, glass transition temperature (Tg) is the temperature which marks the transition, for an elastomer, from enthalpic elasticity to entropic elasticity.

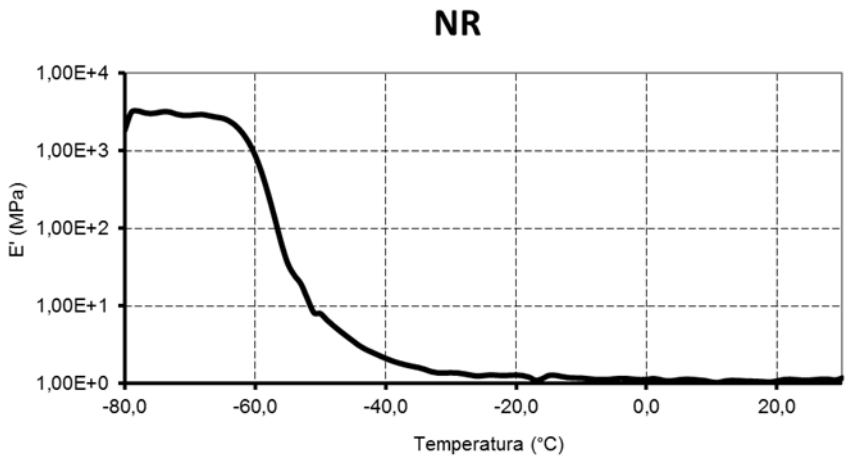

Figure 2.2 Transition from entahalpic and entropic elasticity

Below Tg, an elastomers is endowed with enthalpic elasticity. *Enthalpic elasticity* In ideal elastic solid the atoms or molecule groups are located in well ordered spatial lattices. By applying deformation forces, the interatomic or intermolecular distances are increased over their equilibrium values. The internal energy of the deformed system is increased also. Consequently, when a stress σ is applied the body deforms to a strain ε. The mechanical energy necessary to deform the body is stored by the change of internal energy. The sample recovers its original dimensions completely and instantaneously when the stress is removed. For an ideal system a complete deformation cycle occurs without energy losses. The strain is always proportional to the stress and is independent of the rate at which the body is deformed. The equation that steers the enthalpic elasticity is known as the Hooke law

$$\sigma = Y \varepsilon$$

Above Tg, polymer chains can undergo large deformations. In accordance with the first principle of thermodynamics, the heat absorbed by the system is related to the variation of the internal energy and to the work spent to deform the specimen. Since heat is given off during elongation, according to the second principle of thermodynamics, it follows that a part of the elastic response is associated with an entropy reduction. For an ideal elastomers, the variation of enthalpy can be disregarded. The following equation can be written for the entropic elasticity.

$$f = \left(\frac{\partial G}{\partial L}\right)_{P,T} \cong -T\left(\frac{\partial S}{\partial L}\right)_{P,T}$$

The retractive force is related to the variation of entropy with the elongation. As the entropy decreases with the elongation, it appears from the equation that the retractive force increases with the temperature.

In Figure 2.3 below, it is reported the initial elastic modulus measured by applying sinusoidal shear stress to neat IR crosslinked with a sulphur based system. It is evident that the initial modulus increases with the temperature.

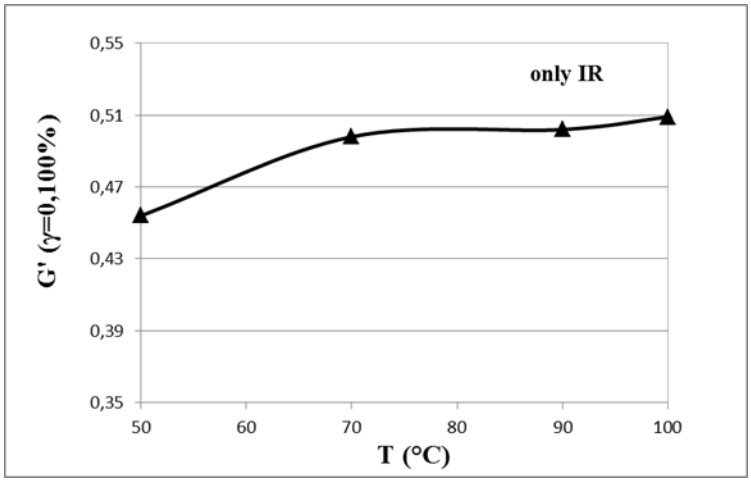

Figure 2.3 Dependence of modulus from Temperature. Taken from lesson of M. Galimberti, Chemistry for elastomers and composite materials technologies, Politecnico di Milano

2.2.2 Vulcanization

Vulcanization is a process applied to transform a polymer, with suitable molecular characteristics, into a rubbery material.

According to ISO definition 1382 (1982) of Rubber – Vocabulary a rubber is defined “a family of polymeric materials that are flexible and elastic. A rubber can be substantially deformed under stress, but immediately and forcibly return to approximately its original length after removal of tensile load.” The Glossary of terms relating to Rubber and Rubber-Like materials reports the ASTM definition n°- 184, 1956 of elasticity “the property of matter to recover its initial shape

and dimension after removal of the stress, traction, compression and torsion, that cause the deformation." Therefore, an elastic rubber must have the property of springback.

Rubbery materials forcibly retract to their approximately original shape after a rather large mechanically imposed deformation. The term "forcibly" makes reference to the retractive force, that has been described above.

Vulcanization can be defined as a process which increases the retractile force and reduces the amount of permanent deformation remaining after removal of the deforming force. Thus vulcanization increases elasticity while it decreases plasticity. It is generally accomplished by the formation of a crosslinked molecular network.

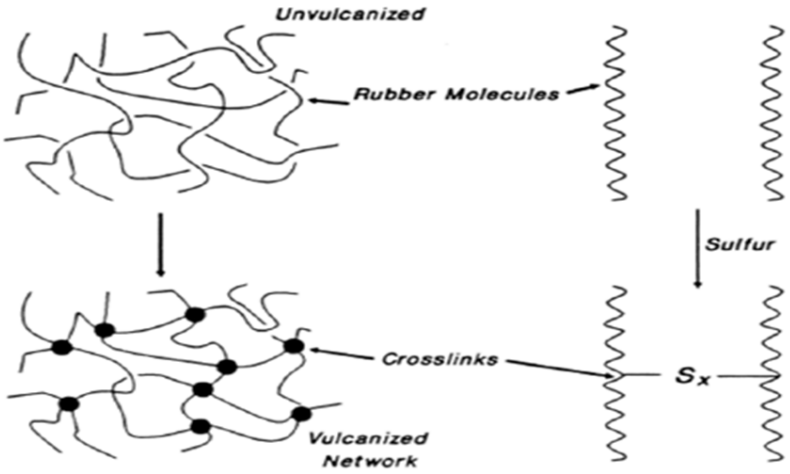

Figure 2.4 Schematically represented of network formation

According to the theory of rubber elasticity,[22] the retractile force to resist a deformation is proportional to the number of network supporting polymer chains per unit volume of elastomer. A supporting polymer chain is a linear polymer molecular segment between network junctures. In an unvulcanized linear high polymer (above its melting point), only molecular chain entanglements constitute junctures. Vulcanization, thus, is a process of chemically producing network junctures by the insertion of crosslinks between polymer chains. A crosslink may be a group of sulfur atoms in a short chain, a single sulfur atom, a carbon to carbon bond, a polyvalent organic radical, an ionic cluster, or a polyvalent metal ion. The process is usually carried out by heating the rubber and mixed with vulcanizing agents in a mold under pressure. Vulcanization causes profound changes at the molecular level. It should be noted that static

modulus increases with vulcanization to a greater extent than does the dynamic modulus. The dynamic modulus is a composite of viscous and elastic behavior, whereas static modulus is largely a measure of only the elastic component of rheological behavior. Hysteresis is reduced with increasing crosslink formation. Hysteresis is the ratio of the rate-dependent or viscous component to the elastic component of deformation resistance. It is also a measure of deformation energy that is not stored (or borne by the elastic network) but that is converted to heat. Vulcanization then causes a trade-off of elasticity for viscous or plastic behavior. The vulcanization reaction is an irreversible process that gives rise to the formation of a three-dimensional network structure of polymer chains chemically bonded to one another, converting a plastic material into an elastic one. The physical properties of a rubber material are largely depending on the state of cure of the final compound. The cure process consists essentially in the heat transfer by conducting through the rubber mass and the cure reaction which starts around 120–170°C depending on the nature of the elastomer. If the temperature is too low, the reaction is not properly achieved, and the final material exhibits little interest for industrial application. On the other hand, if the temperature is too high, the final material is burnt, loosing the quality of the elasticity. The vulcanization curves of a rubber compound are currently obtained by monitoring the increase of the torque required to maintain a given amplitude of oscillation at a given temperature in an oscillating disc rheometer (MDR). It has been assumed that the increase in torque during vulcanization is proportional to the number of cross-links formed per unit of volume of rubber. The torque is automatically plotted versus time to give a so-called cure curve or rheograph. A typical curing curve of a rubber is shown in Figure 2.5

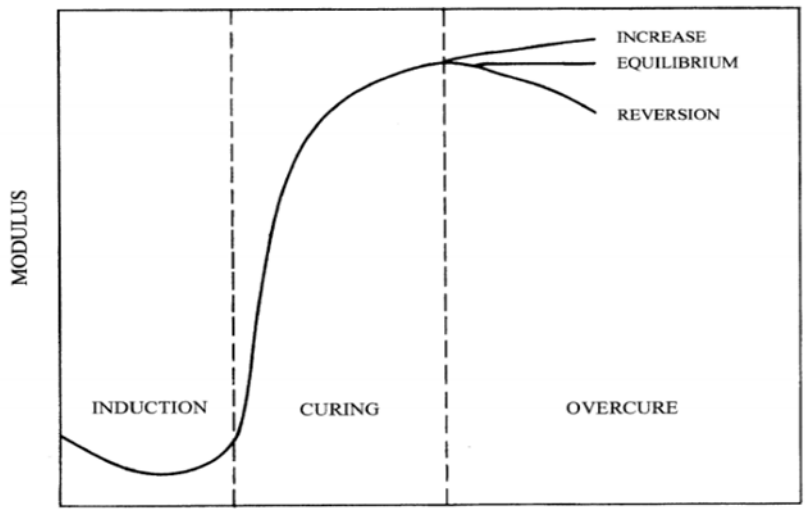

Figure 2.5 Typical curing curve of a rubber

The curve gives a rather complete picture of the overall kinetics of crosslink formation and it is therefore extensively used to control the quality and uniformity of rubber stocks. Three regions are clearly observed: the first region is the scorch delay or induction period, during which most of the accelerator reactions occur. The second period is due to the curing reaction, during which the network structure is formed. It defines the curing speed, that is, the greater or lesser degree of activation of the reaction between the rubber and the cross-linking system. In the last period, once the optimum vulcanization is achieved, a plateau is observed. The network matures by overcuring reversion, equilibrium, or additional but slower cross-linking, depending on the nature of the compound. The overcuring reversion corresponds to a loss of the mechanical behavior of the material due to the breakdown of bonds, in particular, polysulfide bonds. The main parameters obtained from the MDR curve provide information about the reaction kinetics and the cross-link density and are detailed below:

- Scorch Time (t_{s1}). It is the time required for the torque value to increase by 1 in. pounds over the minimum. It indicates the time available before onset of vulcanization and, it provides a good assessment of the scorch safety of a rubber compound. Lower scorch time values correlate with an increased likelihood of premature cross-linking (precocity).

- Optimum Cure Time (t_{90}). It is the time in which 90% of the delta torque is reached. This is a useful estimate of the overall cure rate at a given temperature. As overheating the material could lead to reversion processes.

- The Minimum Torque Value (M_L). It represents an index of material viscosity and can be related to the dispersion of the filler and the filler–polymer interaction. In general, it indicates the extent of the mastication.

- The Maximum Torque (M_H). It represents the highest level of cross-linking possible at a given vulcanization temperature.

- The Delta Torque ($\Delta S' = M_H - M_L$). It is the difference between the maximum and the minimum torque, and it is a quantitative assessment of the crosslinking density of a vulcanizate. So, it is an efficient means of measuring the effects of additives on the cure efficiency.

2.3 Reinforcement

Elasticity is a fascinating property. However, it is not enough to allow the large scale application of rubbery materials. To achieve such application, rubbery materials have to be reinforced. Typically, reinforcement of a rubbery materials is carried out by using particulate fillers, such as carbon black and silica. Such reinforcing fillers are called nano-structured.

2.3.1 Nanostructured fillers

In Figure 2.6 is shown the TEM micrograph of carbon black N326.

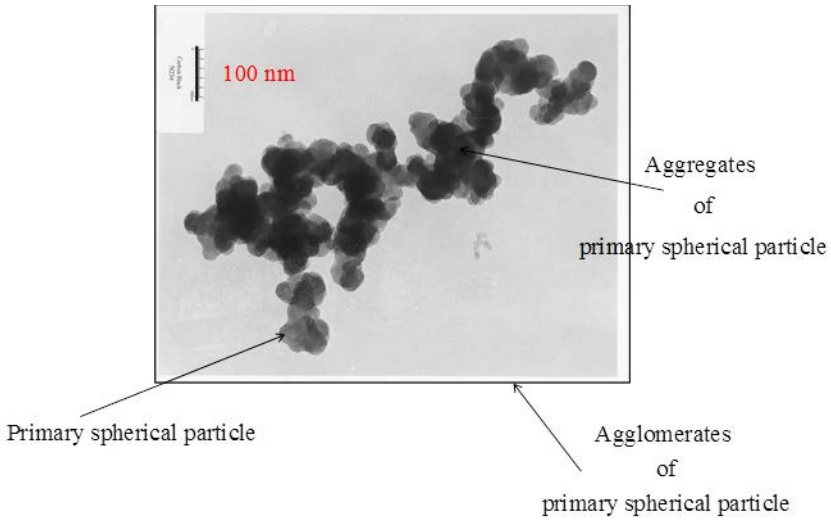

Figure 2.6 TEM micrograph of carbon black N326. Taken from lesson of M. Galimberti, Chemistry for elastomers and composite materials technologies, Politecnico di Milano

Nanostructured fillers are formed by primary spherical particles, that are fused together to form aggregates.[23] Aggregates cannot be separated into primary particles by thermomechanical mixing. They are packed together leaving different amount of voids in between the primary particles. These voids represent the so called structure: the higher is the amount of voids, the higher is the structure. Such voids are able to occlude the polymer chains, transforming them into a rigid phase, such as a filler. Structure is a key feature of nanostructured fillers, as it allows to develop reinforcement at large strain. Aggregates are joined together, through Van der Waals interactions, to form agglomerates, that can be broken by applying energy, by means of thermo-mechanical mixing but also under the normal operating conditions of rubber goods, such as, for example, a tyre. Large amount of nanostructured fillers, at least about 50 parts per hundred rubber (phr), is required to have appreciable reinforcement.

2.3.2 Contributions to the modulus

Reinforcing fillers have strong impact on static and dynamic behavior of polymer melts and elastomers. Figure 2.7 shows the complex modulus of an elastomeric material as the sum of different contributions . Three of them are independent of the strain amplitude.

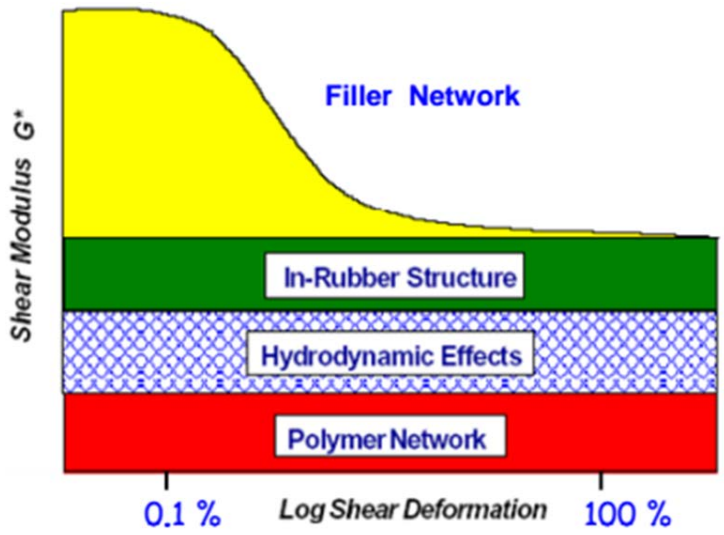

Figure 2.7 Typical behavior of the complex shear modulus versus dynamic shear deformation

They are due to: polymer network, hydrodynamic effect and the so called in-rubber structure. The contribution to the modulus that arises from the so called “in rubber structure” is exactly due to the structure of the reinforcing filler, that means to the ability of the nanostructured filler to occlude the polymer chains in the voids between the primary particles. In the presence of modulus of filled polymer melts and elastomers that does not depend on the strain amplitude, the modulus enhancement as a consequence of the presence of a spherical filler is given by the Guth-Gold-Smallwood equation (Guth and Gold, 1944; Guth, 1945; Smallwood, 1944):

$$E/E_0 = 1 + 0.67f\Phi + 1.62\, f^2\, \Phi^2$$

where E and E_0 are the initial modulus of filled and unfilled material, respectively, Φ is the filler volume fraction, the quadratic term accounts for the mutual disturbance caused by the spherical particles and f is a shape factor that allows to apply the equation to non-spherical fillers. The shape factor f is the ratio between the largest and the smallest dimension. The contribution that depends on the strain amplitude is due to the filler network, that is formed for Φ values above a critical threshold, that is the filler volume fraction at which filler percolation occurs. However, reinforcing fillers have a high surface area and a high structure so they easily interact with each other, forming aggregates, and with the elastomer. The polymer chains that remains adsorbed on

the filler structure or occluded in the filler voids, form the so called occluded rubber, that is not anymore free to move but it behaves very similar to the reinforcing filler. Therefore the volume fraction of filler that appears in the equation above has to be corrected to take into account the occluded rubber. The corrected volume fraction is through the following equation that makes reference to the volume of the adsorbed DBP

$$\phi_c = \frac{\phi}{2} \cdot \left[1 + \frac{1 + 0.02139 \cdot \mathrm{DBP}}{1.46}\right]$$

The φ_c values derives from the filler volume φ and from the amount of polymer chains that cannot be deformed The last contribution to the modulus instead depends on the strain amplitude, thus is not linear. This phenomenon is called Payne effect In the presence of a filler network, filler aggregates are joined together either by direct contact or via layer of polymer shell around them. Different theories explain the reduction of modulus with the strain amplitude. The traditional theory of Payne refers to the thixotropy of the composite materials. The Payne effect is a particular feature of the stress-strain behaviour of rubber, especially rubber compounds containing fillers. It is named after the British rubber scientist A. R. Payne, who made extensive studies of the effect (e.g. Payne 1962). The effect is observed under cyclic loading conditions with small strain amplitudes, and is manifest as a dependence of the viscoelastic storage modulus on the amplitude of the applied strain. Above approximately 0.1% strain amplitude, the storage modulus decreases rapidly with increasing amplitude. At sufficiently large strain amplitudes (roughly 20%), the storage modulus approaches a lower bound. In that region where the storage modulus decreases the loss modulus shows a maximum. The Payne effect depends on the filler content of the material and vanishes for unfilled elastomers. Physically, the Payne effect can be attributed to deformation-induced changes in the material's microstructure, i.e. to breakage and recovery of weak physical bonds linking adjacent filler clusters. More recent theories invoque either the presence of a glassy shell of polymer surrounding the filler particle, that is removed when the strain occurs, or the reduction of the network density, due to the desorption of polymer chains upon stretching. The modulus at minimum deformation depends on the filler network. Filler is the main character. Modulus is due to interactions between filler particles and between filler and polymer. The filler most important feature to determine the modulus at low strain is the

filler surface area. The filler volume takes into account the occluded rubber. This means that the modulus at moderate deformations is a function of the filler structure. The surface area determines the modulus at first plateau. The structure determines it at the second plateau.

2.3.3 The role of the shape factor f

It is worth dwelling upon the role of the shape factor *f* on the mechanical reinforcement. In Figure 2.8, is reported the modulus enhancement as a function of filler volume fraction, for different shape factor *f*.

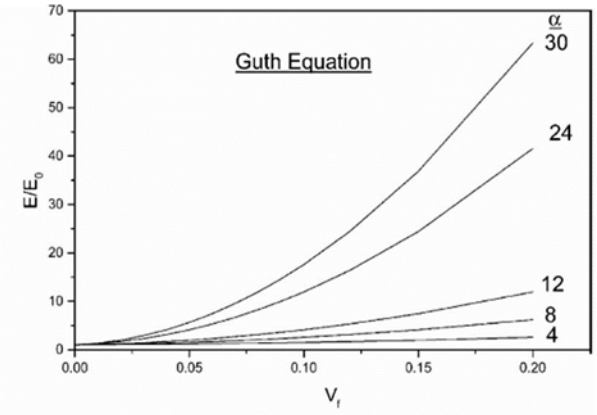

Figure 2.8 Modulus enhancement as a function of filler volume fraction, for different shape factor *f*

It is evident that the modulus enhancement is much larger as the shape factor increases.

In the case of traditional nanostructured fillers, such as carbon black and silica, it has been already reported that the primary particles are fused together to form aggregates (see Figure 2.6 for carbon black). The shape factor *f* is given by the ratio of the largest to the lowest dimension of the aggregates.

2.4 Nanofillers

2.4.1 Geometry of nanofillers and surface area

Over the last years, the so called nano-fillers [24, 25] appeared in the rubber world. They are characterized by primary particles with at least one dimension below 100 nanometers,[26] that

can be individually dispersed in the rubber matrix. Low dimension means high surface area. In Table 2.2 below, correlation between dimension of primary particles and surface area is shown for various carbon black grades.[27]

Table 2.2 Correlation between dimension of primary particles and surface area for various carbon black grades

Designation	d,[a] nm	S_{BET},[b] m^2/g
N-110	17–25	130–145
N-220	19–28	100–120
N-330	24–32	75–85
N-550	36–50	46–48

[a] Electron micrographs.
[b] BET nitrogen adsorption.

Moreover, fillers with high shape factor can be endowed with high surface area.
In the graph below in Figure 2.9, taken from ref. [28] it is reported the dependence of surface area to volume ratio on the aspect ratio.

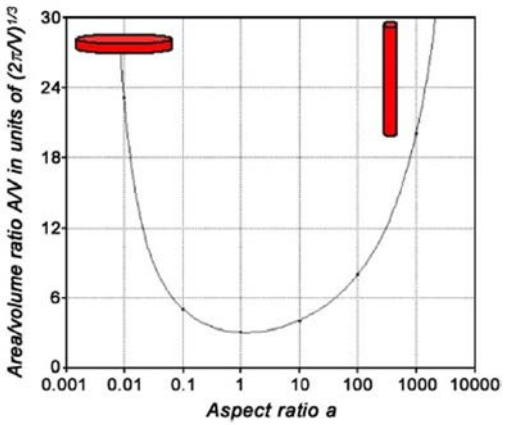

Figure 2.9 Dependence of surface area to volume ratio on the aspect ratio (shape factor *f*)

It is evident that the ratio increases in the presence of sheets and rods. More in detail, the ratio increases more for sheets than for rods. Graphene is a sheet and carbon nanotube is a rod. This justifies the large interest for graphene as filler for polymer nanocomposites.

2.4.2 The shape factor f of nanofillers

It is thus worth examining how to estimate the shape factor *f* of nanofillers. In the case of a nanofiller made by sheets stacked to make the so called tactoid, the shape factor *f* is given by the ratio of the largest side of the sheet to the thickness of the tactoid. In Figure 2.10, is reported a nanocomposite made by a montmorillonite in natural rubber.[29] Tactoids are indicated.

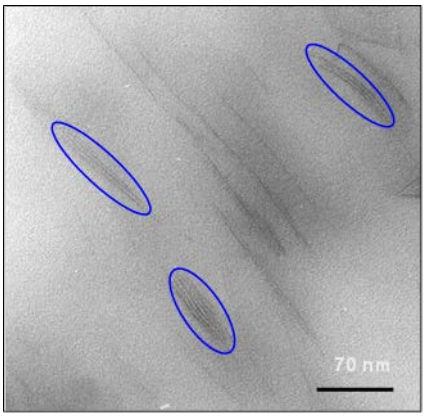

Figure 2.10 Nanocomposite made by a montmorillonite in natural rubber [29]

In the case of CNT, the shape factor *f* is given by the ratio of the length to the diameter of the tube In Figure 2.11, is reported a nanocomposite made by a multiwalled CNT in natural rubber.[29]

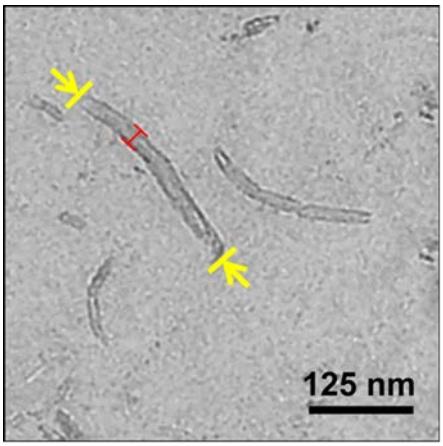

Figure 2.11 Nanocomposite made by a MWCNT in natural rubber [29]

Determination of the shape factor *f* can be complex indeed.

Many TEM micrographs are needed to estimate the dimensions of sheets aggregates and tubes. In the literature, the *f* factor is calculated from the Guth equation: E/E_0 values are plotted as a function of the filler volume fraction and the f factor is obtained from the best fitting of experimental data.

In the case of stacks of sheets, an alternative way could be based on the determination of the length of crystalline domains in the direction parallel and orthogonal to structural layers. Such determination can be done from X-Ray analysis. The application of the Scherrer equation (see Experimental Section) to the diagnostic reflections allows to estimate the thickness of crystallites. However, such determination gives only the length of crystallites. Stacks of sheets are visualized in Figure 2.12. X-Ray determination gives the thickness of ordered stacked layers, shown in Figure 2.12 a, but not the thickness of layers that include disordered stacked layers, as in Figure 2.12b.

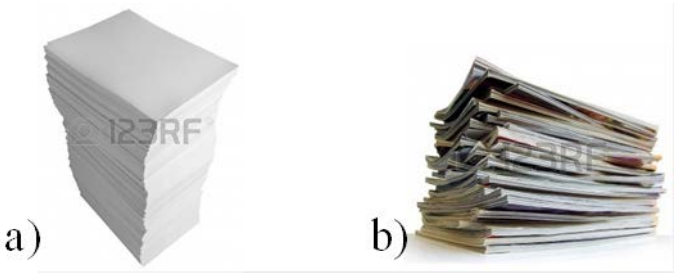

Figure 2.12 Sheets stacked in ordered (a) and disordered (b) way

2.4.3 "Structure" of nanofillers

If every single particle of a nanofiller is dispersed in the matrix, one can not talk anymore about structure. In fact, it was reported above that the stricture is given by the voids left among the primary particles of a nanostructured fillers, fuse together.

This has large impact on the mechanical reinforcement. In fact, nano-fillers could give high initial modulus, that depends on surface area, and low modulus at high deformation, that depends on structure. Therefore nano-fillers could promote strong non-linearity of modulus and so high Payne effect.

2.5 NR based nanocomposites

As mentioned in “Introduction and Objectives”, objectives of the present thesis were: (i) to prepare modified nanosized graphite, (ii) to obtain even dispersion of such modified graphites in NR and PU as the polymer matrices (iii) to study the effect of such graphites on the polymers, at lest preliminarly. Hence, it was not the objective of the present thesis to study the properties of polymer nanocomposites based on nanosized graphite, correlating the nanocomposite properties with the nanofiller characteristics.

As a consequence, in the introduction to the present thesis, chapter are not dedicated to the exame of polymer nanocomposites based on carbon allotropes. However, it is worth reporting few comments, indicating literature on the subject.

There are some papers in the literature dedicated to nanocomposites based on rubbers and nanosized graphite: Rubber are: natural rubber,[30] poly(styrene-co-butadiene) [31] poly(butadiene-co-acrylonitrile) [32] fluoroelastomers,[33] synthetic poly(1,4-*cis*-isoprene).[34] A review appeared in a series of book dedicated to nanocomposites based on Natural Rubber,[35] reporting an overall exam of nanofillers in NR matrix.

In the present thesis, preliminary investigation on the effect of nanosized graphite on mechanical reinforcement is performed. It is thus worth reporting what is available in the literature on this aspect.

In Ref. [34], tensile measurements were reported on nanocomposites based on IR and containing an increasing amount of nanoG, the same nanoG used in the present thesis, from 1 to 60 phr. The percolation threshold of nano-G was calculated by applying the Huber-Vilgis model.[35]Double logarithmic plot was prepared with the excess of initial modulus $(E - E_0)/E_0$ vs the nano-G content. Two straight lines were identified, with slope 0.9 and 3.5, below and above the percolation threshold, found to be at 21.2 phr. The slope values were not far from the ones calculated for CB (1 and 4) and the network formation occurred at a level not much lower than the one typical of CB (about 30 phr).

Hybrid nano-G/CB filler systems were prepared in IR as the matrix. In samples containing 60 phr of CB, a discontinuity was observed for the dependence of the excess of modulus on nano-G content, at about 6 phr as nano-G content, as if nano-G was able to establish a continuous network in the polymer matrix.

2.6 References

[1] Kawahara S., Isono Y., Sakdapipanich J. T., Tanaka Y., Aik-Hwee E., Rubber Chem.Technol., 2002, 75, 739-746.

[2] Hamed G. R., Rubber Chem. Technol., 1981, 54, 403-414.

[3] Hamed G. R., Rubber Chem. Technol., 1981, 54, 576-595.

[4] Wool R. P., Rubber Chem. Technol., 1984, 57, 307-319.

[5] Thomas A. G., Whittle J. M., Rubber Chem. Technol., 1970, 43, 222.

[6] Gent A. N., Zhang L. Q., Rubber Chem. Technol., 2002, 75, 923-934.

[7] Lake G. J., Rubber Chem. Technol., 1972, 45, 309-328.

[8] Hamed G. R., Rubber Chem. Technol., 1994, 67, 529-536.

[9] Hamed G. R., Kim H. J., Gent A. N., Rubber Chem. Technol. 1996, 69, 807.

[10] Lake G. J., Rubber Chem. Technol., 1995, 68, 435-460.

[11] Hamed G. R., Rattanasom N., Rubber Chem. Technol., 2002, 75, 935-942.

[12] Busse W. F., Industrial & Engineering Chemistry, 1934, 26, 1194-1199.

[13] Cadwell S. M., Merrill R. A., Sloman C. M., Yost F. L., Industrial & Engineering Chemistry Analytical Edition, 1940, 12, 19-23.

[15] Mars W. V., Fatemi A., International Journal of Fatigue, 2002, 24, 949-961.

[16] Mars W. V., Fatemi A., Rubber Chem. Technol., 2004, 77, 391-412.

[17] Papadopoulos I. C., Thomas A. G., Busfield J. J. C., Journal of applied polymer science, 2008, 109, 1900-1910.

[18] Mars W. V., Rubber Chem. Technol., 2009, 82, 51-61.

[19] Saintier N., Cailletaud G., Piques R., Materials Science and Engineering: A, 2011, 528, 1078-1086.

[20] Eng, A.H., Ong, E. L. in: Hevea Natural Rubber Handbook of elastomers *Eds.*, *CRC Press*, **2000**, 29-6

[21] Source: International Rubber Conference, September 2014, Beijing [22] Flory. P. J., “Principles of Polymer Chemistry,” Cornell Univ. Press, Ithaca, NY, 1953, Chap. 11.

[23] Kakub T., Matsuura A., Kawahara S., Tanaka Y., Rubber chemistry and technology, 1998,71, 70

[24] Maiti M., Bhattacharya M. and Bhowmick A. K., Rubber Chem. Technol., 2008, 81, 384
[25] M. Galimberti, V. Cipolletti, V. Kumar, Natural Rubber Based Composites and Nanocomposites S. Thomas, C. H. Chan, L. A. Pothan, Ramanan, J. Maria Eds., Royal Society of Chemistry, 2014, Chapter 2, Print ISBN: 978-1-84973-631-2. PDF eISBN: 978-1-84973-765-4, DOI:10.1039/9781849737654-00034
[26] Vocabulary – Nanoparticles, PAS 71, 2005 BSI.
[27] Hamed, Rubber Chemistry and Technology, 2000
[28] Advanced in Polyolefin nanocomposites, Edited by Vikas Mittal, CRC Press, 2011, 12, 330-332
[29] TEM micrograph taken form the lessons of the Course "Chemistry for elastomers and Composite Materials", Prof. M. Galimberti, Politecnico di Milano
[30] A. K. Bhowmick, M. Bhattacharya, S. Mitra, J. Elastom. Plast. 42, 517 (2010).
[31] M. Bhattacharya, M. Maiti, A. K. Bhowmick, Polym. Eng. Sci., 49, 81 (2009).
[32] F. R. Al-Solamya, A. A. Al-Ghamdib, W. E. Mahmoud, Polym. Adv. Technol. 23, 478, (2012).
[33] V. Sridhar, D. Xu, T. T. Pham, S. P. Mahapatra, J. K. Kim, Polym. Comp. 334 (2009).
[34] M. Galimberti, V. Kumar, M. Coombs, V. Cipolletti, S. Agnelli, S. Pandini, L. Conzatti, *Rubber Chemistry and Technology*, June 2014, Vol. 87, No. 2, pp. 197-218
[35] G. Huber, T. A. Vilgis, Kaut. Gummi Kunstst. 52, 102 (1999).

Chapter III

3.1 History of polyurethane

The discovery of polyurethane [PU] is dated 1937 by Otto Bayer and his coworkers at the laboratories of I.G. Farben. The interest was first focused on PU obtained by aliphatic diisocyanate and diamine, with the formation of polyurea, until interesting properties of PU obtained from an aliphatic diisocyanate and glycol were discovered.

Polyisocyanates became commercially available in 1952, when the industrial scale production of PU was supported by toluene diisocyanate (TDI) and polyester polyols. In the following years (1952-1954), various polyester-polyisocyanate systems were studied by Bayer.

Polyester polyols were replaced by polyether polyols due to their several benefits such as low cost, ease of manipulation, and improved hydrolytic stability. DuPont introduced Poly(tetramethylene ether) glycol (PTMG) as the first commercially available polyether polyol in 1956.

In the years that follows, PU evolved from flexible to rigid foams (1967) as various polyether polyols, and polymeric isocyanate became available. These rigid PU foams showed good thermal and flame resistance.

PU Reaction Injection Moulding [PU RIM] technology was introduced in 1969 producing high performance PU material and in 1983 was produced the first plastic-body automobile in the USA.

In 1990s, because of the growing awareness of the dangers of using chloro alkanes as blowing agents, several other blowing agents appeared in the market (e.g., carbon dioxide, 1,1,1,3,3-pentafluoropropane).

In the meantime, two-pack PU, PU-polyurea spray coating technology became available, that brought considerable advantages to be insensitive to humidity with fast reactivity.

Then bloomed the strategy of the use of vegetable oil based polyols for the production of PU. Interest in the PU was born due to the simplicity of synthesis and application protocol, few basic reactants and excellent properties of the final product.

3.2 Raw materials

PU are produced by chemical reaction between a di/poly isocyanate and a diol or polyol, making repeating urethane groups, usually, in presence of a chain extender, catalyst, and/or other additives.

3.2.1 Polyols

Polyols are substances bearing plurality of hydroxyl groups. They can also contain ester, ether, acrylic, metal and other functionalities, besides hydroxyl groups.

Polyester polyols (PEP) hold ester and hydroxylic groups along the backbone. They are usually prepared by a condensation reaction between glycols and a aliphatic or aromatic dicarboxylic acid/anhydride. The properties of PU also depend on the degree of cross-linking and on molecular weight of the starting PEP. Highly branched PEP imply rigid PU with good heat and chemical resistance, PU produced with less branched PEP provide good flexibility (at low temperature) but low chemical resistance. Similarly, low molecular weight polyols provide rigid PU and high molecular weight polyols yield flexible PU.

Polyether polyols (PETP) are cheaper than PEP. They are made by addition reaction of ethylene or propylene oxide and alcohol in presence of acid or base catalyst. PU produced from PETP show high water permeability and low Tg, that limits their use in coatings and paints. ACP is an acrylated polyol made by free radical polymerization of hydroxyl ethyl acrylate or methacrylate with other acrylics. ACP produce PU with better thermal stability. These PU find applications as coating materials.

Polyols can further be modified with metal salts forming hybrid polyols (MHP). PU obtained with MHP show good thermal stability and anti-microbial behavior.

3.2.2 Isocyanates

Isocyanates are essential starting materials required for PU production containing two or more -NCO groups per molecule. They can be aromatic or aliphatic, like TDI, xylene diisocyanate (XDI), methylenediphenyl diisocyanate (MDI), 4,4’-dicyclohexylmethane diisocyanate (H12MDI), isophorone diisocyanate (IPDI), meta-tetramethylxylylene diisocyanate (TMXDI), hydrogenated xylene diisocyanate (HXDI), 2,2,4-trimethylhexamethylene diisocyanate (TMDI),

1,6 hexamethylene diisocyanate (HDI), phenylene diisocyanate (PPDI), norbornane diisocyanate (NDI), naphthalene 1,5-diisocyanate (NDI). Figure 3.1 shows examples of some common isocyanates.

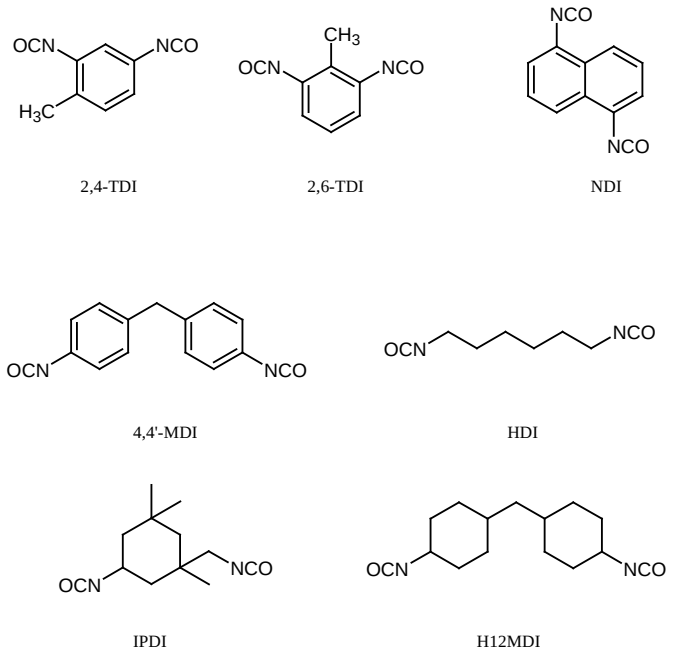

Figure 3.1 Common isocyanates

The isocyanate group is R-N=C=O, where the reactivity of isocyanate is given by the positively charged carbon atom, that is available for the attack of nucleophiles. Scheme 3.1 shows resonances structures that justify the presence of partial positive charge on the carbon atom. Oxygen and nitrogen atoms are then available for attack by electrophiles.

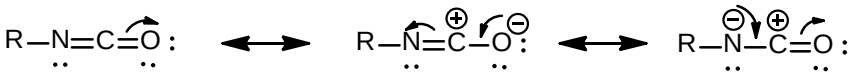

Scheme 3.1 Resonance in isocyanate

When R is an aromatic group, the negative charge is delocalized on R (Scheme 2), so, the aromatic isocyanates are more reactive than aliphatic ones.

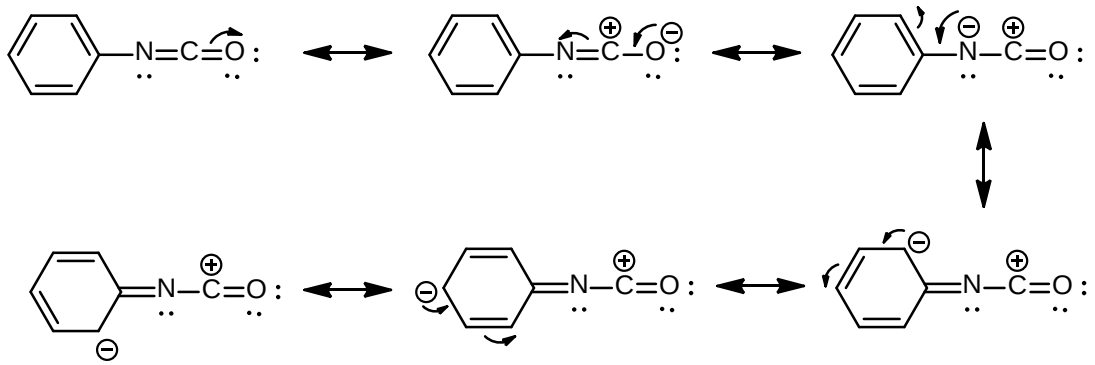

Scheme 3.2 Resonance in aromatic isocyanate

Nature of the substituent also determines the reactivity. In diisocyanates, the presence of the electron attracting second isocyanate increases the reactivity of the first isocyanate. The reactivity of the two-NCO groups depends on the position of –NCO groups. The two-NCO groups in isophorone diisocyanate differ in their reactivity, as a consequence of their different location. Para substituted aromatic diisocyanates are more reactive that their ortho analogues, essentially as a consequence of the steric hindrance conferred by the second –NCO functionality. Meta-tetramethylxylylene diisocyanate serves as an aliphatic isocyanate since the two isocyanate groups are not in conjugation with the aromatic ring.

Another isocyanate of increasing interests is vinyl terminated isocyanate since along with the –NCO group, the extra vinyl group provides sites for crosslinking. The choice of the isocyanate depends on the desired properties of the final product. To prepare rigid PU, aromatic isocyanates are chosen, however, PU produced with these isocyanates has lower oxidative and ultraviolet stabilities.

3.2.3 Additives

Besides a polyol and an isocyanate, additives are required during PU production, to control and modify the reaction, and also to modify or finish the final product. Such additives are catalysts, chain extenders, colorants, fillers and others.

Catalysts are added to improve reaction rates or for deblocking the blocked isocyanates. Many aromatic and aliphatic amines (e.g. DABCO) or organometallic compounds (e.g., dibutyltin diacetate, dibutyltin dilaurate) are used as catalysts. The catalytic activity of tertiary amines is determined by their structure and by their basicity. The catalytic activity passes through the

formation of a complex between amine and isocyanate: the electrons on nitrogen atom of tertiary amine are donated to the positively charged carbon atom of the isocyanate. Catalytic activity decreases with the steric hindrance on the nitrogen atom and increases with basicity. Metal catalysts are better than tertiary amines because they are comparatively less volatile and less toxic.

Important effect on PU molecular structure have the chain extenders. Low molecular weight diols (ethylene glycol, 1,4-butanediol, 1,6-hexanediol), hydroxyl-amines (diethanolamine and triethanolamine), cyclohexane dimethanol, are used as chain extenders in PU production.

Because isocyanates are too sensitive to water even in traces, moisture scavengers, such as zeolite, are incorporated to eliminate water during PU synthesis.

Blowing agents like CO_2 or hydrazin are used to produce PU foams.

3.3 Chemistry of PU

3.3.1 Building blocks for the preparation of PU

PU are produced by (i) condensation polymerization reaction of diamine with bischloroformates (Scheme 3.3) and (ii) addition polymerization reaction of diisocyanates with polyol, or other compounds having a multiplicity of active hydrogen atom (Scheme 3.4).

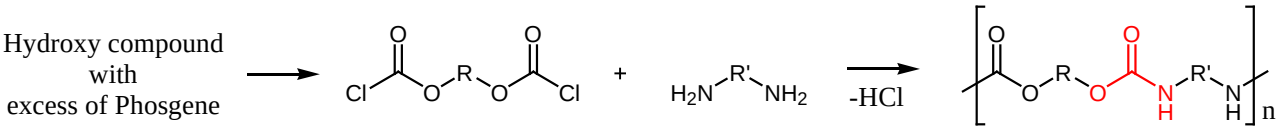

Scheme 3.3 Reaction of bischloroformate with diamine

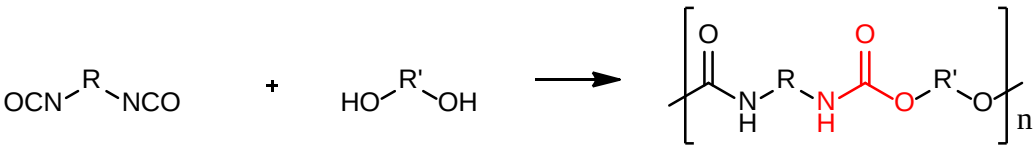

Scheme 3.4 Reaction of diisocyanate with di or poly hydroxy compound

The second method is more interesting from the industrial point of view because in this method no by-product is formed. The isocyanate reactions are divided into two classes, (a) addition (primary and secondary) reaction with materials containing active hydrogen (Schemes 3.5 and 3.6), (b) self-addition reaction (Scheme 3.7).

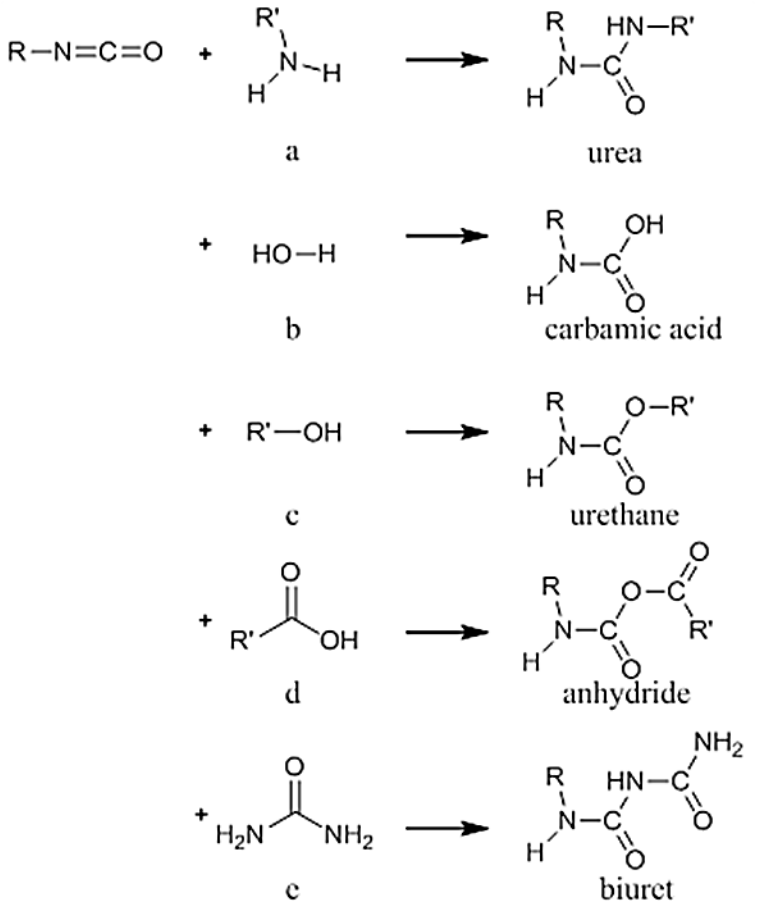

Scheme 3.5 Primary addition reactions of isocyanate with (a) amine, (b) water, (c) alcohol, (d) carboxylic acid, (e) urea

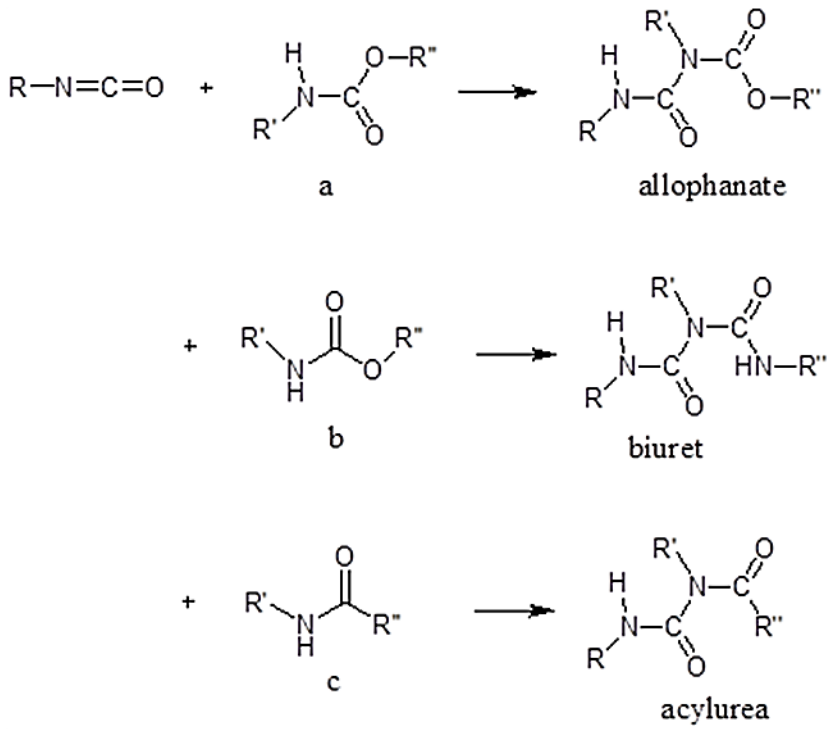

Scheme 3.6 Secondary addition reactions of isocyanate with (a) polyurethane, (b) polyurea and (c) polyamide

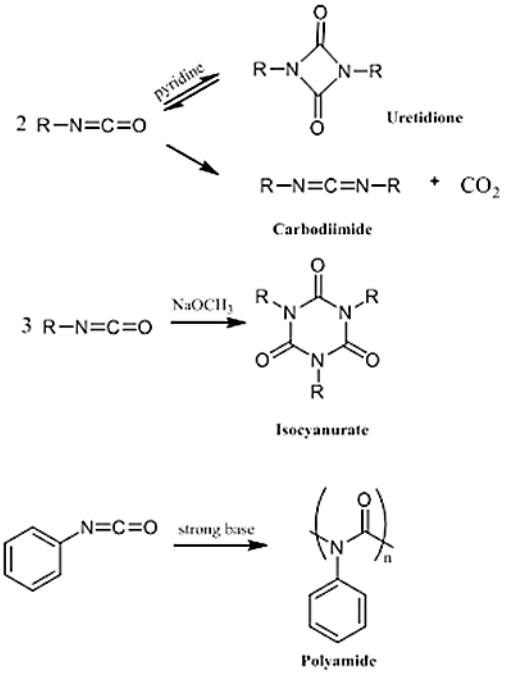

Scheme 3.7 Self -addition reactions of isocyanate

CO_2 is released in some of the reactions: this helps in the formation of PU foams.

It is well-known that when a diol reacts with diisocyanate, a linear PU is formed while branched or cross-linked PU results with the reaction of polyol. Branched or cross-linked PU are also formed when a material containing three or more isocyanate groups reacts with a diol.

3.3.2 Mechanism

The reaction of an isocyanate with compounds with active hydrogens takes place with or without a catalyst. The reactions of self-addition of isocyanates usually do not proceed as fast as the reactions with compounds with active hydrogens.

3.3.2.1 Reaction in the absence of a catalyst

The active compound itself behaves as a catalyst in the reaction as shown in Scheme 3.8.

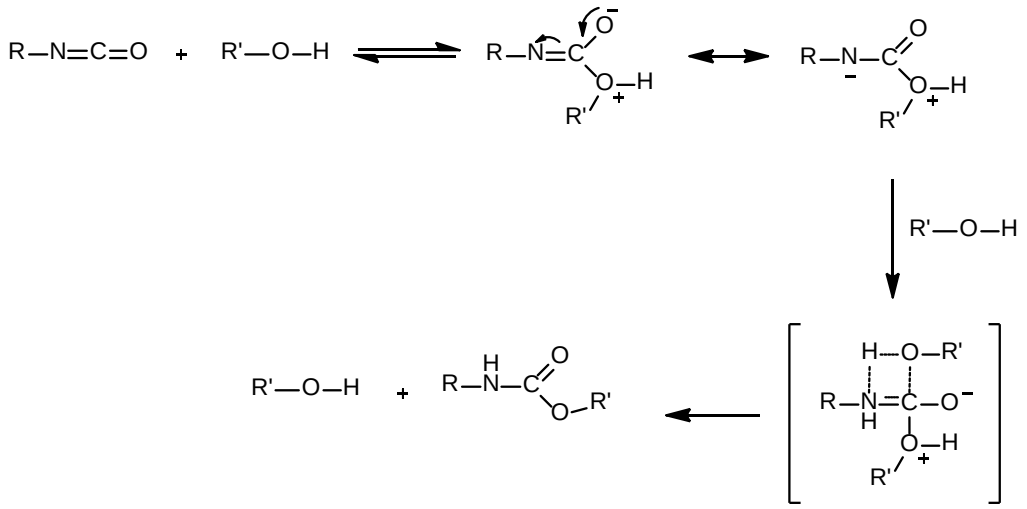

Scheme 3.8 Isocyanate reaction in the absence of a catalyst

In the reactions proceeding without a catalyst, the electrophilic carbon of the isocyanate is attacked by the nucleophilic centre of the active hydrogen compound; hydrogen is added to –NCO group. The aromatic isocyanates are more reactive than the aliphatic isocyanates and steric hindrance at –NCO or HXR' groups reduce the reactivity.

3.3.2.2 Reaction in the presence of a catalyst

The reactions of class (a) are extremely sensitive to catalysis. The various isocyanate reactions are influenced by different catalysts to different extents. Many commercial applications of isocyanates use catalysed reactions. Metal compounds and tertiary amines are most widely used catalysts for the reaction (Schemes 3.9 and 3.10). The mechanism is similar to that of the uncatalyzed reaction (Scheme 3.8). The metal salts and tertiary amines catalyze the reaction as reported in the Schemes. The base strength of the amines is closely parallels to the catalytic activity except when steric hindrance becomes pronounced. Catalysts made of amines are also effective for self-addition reactions while metal salt are less active in this sense.

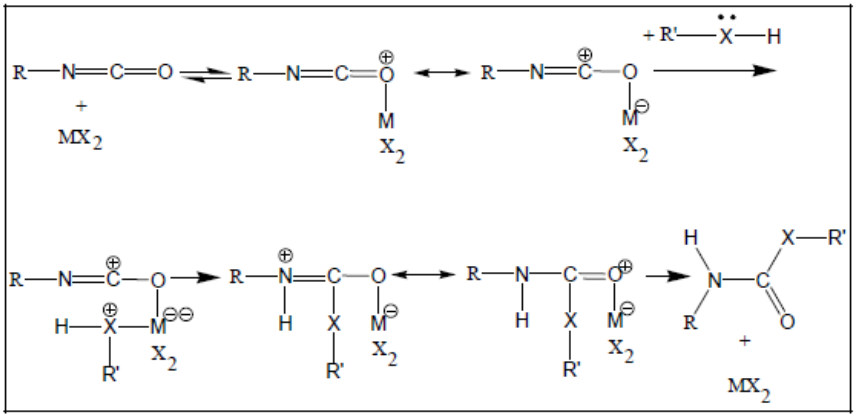

Scheme 3.9 Metal salts catalyzed reaction

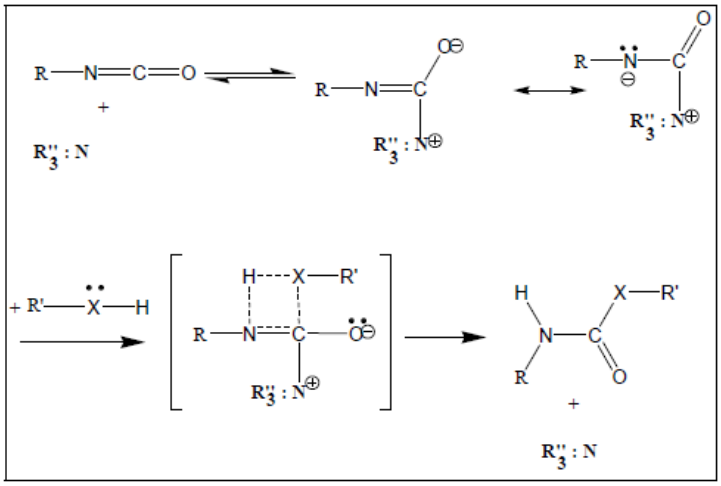

Scheme 3.10 Tertiary amine catalyzed reaction

3.4 Nanocomposites based on TPU

The objectives of the present thesis are written in “Introduction and Objectives” and summarized in Chapter 2. Hence it was not the objective of the present thesis to study the properties of polymer nanocomposites based on PU, correlating the nanocomposite properties with the nanofiller characteristics. As a consequence, in the introduction to the present thesis, there is not a summary dedicated to the exam of PU nanocomposites based on carbon allotropes. However, it is worth reporting few comments, indicating literature on the subject.

The interest on PU is essentially due to two main reasons: (i) polyurethanes are the most versatile polymers, ranging from elastomers to thermoplastics, to thermoset to foams, (ii) the presence of PU in the market is steadily increasing. They are very interesting materials.

In particular, looking at the literature, attention was focused on thermoplastic polyurethanes (TPU), that belong to the larger family of thermoplastic elastomers (TPE). TPE is a family of rubber-like materials that can be processed and recycled like thermoplastic materials. TPU displays properties of both elastomers and thermoplastics and find many applications such as coatings, adhesives, foams, rubbers, and thermoplastic elastomers.[7] Interest of this thesis was mainly in the direction of elastomeric materials. This is why the recipe adopted for the preparation of polyurethanes (see Chapter 6) was suitable for having elastomeric products.

However, it is known that TPU exhibit poor resistance to heat and this limits its applications.[8] Objective of the work begun with this thesis is the improvement of thermal resistance of TPU thanks to nanosized graphite. It will be explained in Chapter 6 that the low amount on nanographite used was in line with the amount of carbon allotropes used for improving the flame resistance of polymer matrices.

To improve the heat resistance, inorganic nanomaterials have been introduced, as additives into polymer systems has resulted in polymer nanostructured materials exhibiting a multiplicity of high performance characteristics beyond what traditional polymer composites possess.[9] These improved properties include higher thermal and flame resistance, moisture and chemical resistance, decreased permeability, charge dissipation, and thermal/electrical conductivity.

Looking at the literature on nanocomposites based on TPU and graphite, it is clear that the objective was to obtain even dispersion of graphite in the PU matrix, to achieve the strongest impact by the nanofiller. In particular, in ref. [10], a method was reported based on a solvent, one

single solvent, to prepare graphite nanoplatelet (GNP) filled thermoplastic polyurethane (TPU) nanocomposites. Uniform dispersion of GNPs was demonstrated in the TPU matrix. Storage modulus of the nanocomposites was increased with increasing GNP content. Large deformation at break was maintained. Moreover, TGA analysis showed that the incorporation of GNPs could improve the thermal stability of the nanocomposites and cone calorimetry results showed that the GNPs could act as intumescent flame retardant and significantly reduced the heat release rate (HRR), thus improving the flame retardancy of the TPU matrix.

3.5 References

[1] Lligadas G., Ronda J.C., Galia`M., Cadiz V. Plant Oils as Platform Chemicals for Polyurethane Synthesis:Current State–of–the–Art. Biomacromolecules 2010; 11: 2825– 2835.

[2] Petrović Z. S. Polyurethanes from Vegetable Oils. Polymer Reviews 2008; 48:109– 155.

[3] Chattopadhyay D.K., Raju K.V.S.N. Structural Engineering of Polyurethane Coatings for High Performance Applications. Progress in Polymer Science 2007; 32: 352– 418.

[4] Paul, S. Surface Coating–Science and Technology. New York: John Wiley & Sons; 1985.

[5] Nylen P., Sunderland E. Modern Surface Coatings. London: John Wiley & Sons; 1965.

[6] Malcolm P S. Polymer Chemistry An Introduction. 3rd Edn. New York: Oxford University Press, Oxford; 1999.

[7] Woods, G., *The ICI Polyurethanes Book*, Wiley, New York, 1990.

[8] Fabris, H. J., *Advances in Urethane Science and Technology*, Technomic, New York, 1976.

[9] J. H. Koo, O. A. Ezekoye , J. C. Lee , W. K. Ho, M. C. Bruns, Chapter 16 in "Rubber Clay Nanocomposites – Science, Technology, Applications" M. Galimberti Editor, Wiley and Sons, First Edition: October 2011

[10] H. Quan, B.-Q. Zhang, Q. Zhao, R. K. K. Yuen, R. K. Y. Li, Composites: Part A **40**, 1506 (2009).

SECTION II Results and Discussions

Chapter IV

4.1 Introduction

Today, a fascinating challenge in the field of nanocomposite materials is to find new methods, simple and industrially replicable, to obtain graphene or few layers graphene.

Single or few layers of graphene are obtained through micromechanical cleavage,[1] epitaxial growth of graphene films [2] or oxidation of graphitic nanofiller to graphite oxide (GO) followed by thermal or chemical reduction.

The latter method is considered as the best practice but is however characterized by several drawbacks. The oxidation requires strong acids and oxidation agents and harsh reaction conditions, thermal reduction occurs at high temperature and under controlled conditions, efficient chemical reducing agents can be toxic, hazardous and expensive, such as, for instance, those based on hydrazine. Moreover, it is very hard to completely restore the sp^2 hybridization of the carbon atoms.

4.2 Alternative methodologies for the preparation of graphene derivatives

Clearly, a process that gets both of the following features, single sheet and sp^2 hybridization of carbon atoms, in a controlled manner would help to overcome on of the major major problems today associated with the use of graphene and few layer graphene.

Moreover, the nanosized graphite (graphene or few layer graphene) should, ideally, contain functional groups suitable to promote its dispersion in media such as the polymer matrices.

This chapter describes the methodologies selected in the present thesis, aimed at obtaining few layer graphene and graphene, with functional groups suitable for promoting even dispersion in polar media:

- without using strong acids and oxidizing agents

- without using harsh reaction conditions
- without using toxic reagents
- preserving as much as possible the sp^2 hybridizations of the carbon atoms.

Methodologies for the preparation of graphene derivatives, alternative with respect to those considered as the best practice in the field, were studied.

4.3 Chemical modification of nanosized graphite: alternative methods

4.3.1 Alternative methods used in this thesis

Chemical modifications were performed on nanosized graphite. They are summarized in Table 4.1.

Table 4.1. Chemical modifications performed on nanosized graphite

Reagent	Main experimental conditions	Expected functional groups
nanoG; KOH; water	(i) ball milling at 300 rpm for 10h (ii) heated flask 70°C for 4h	-OH
nanoG; maleic anhydride	Heated flask 110°C for 3h	-COOH
nanoG; dodecanethiol	Heated flask 70°C for 3h	$-S-(CH)_{11}CH_3$

These methods are profoundly different from a chemical point of view. The red line of this methods is the aim of disturbing, as little as possible, the conjugated nature of the allotrope.

The first method is the treatment of graphite with KOH through two different approaches: (i) mechanochemical, (ii) thermal. The objective is the introduction of hydroxyl functional groups on the edges of graphene layers. The functionalized graphite can be called edge hydroxy-graphite, indicated in the text below as G-OH. Such reaction was reported in a paper in the scientific literature.[3] In the present thesis, starting from this report, different experimental conditions were explored.

The second method has also the objective of introducing polar groups. It is based on the Diels-Alder reaction of the aromatic rings of graphite with maleic anhydride. Indications on this reaction are reported in the scientific literature.[4]

The third method appears different. First of all, the objective of this modification is the introduction of apolar substituents. Moreover, the type of the reaction is different: 1-dodecanethiol is reacted with nanoG with the help of radicalic initiator [5].

4.3.2 Methods adopted in the literature

The best practice for the preparation of graphite with oxygenated functional groups is considered the oxidation with strong oxidizing agents, in the presence of mineral acids. The Brodie's [6] or Staudenmaier's [7] methods use potassium chlorate with a mixture of sulfuric and nitric acid. The Hummers' [8] method uses potassium permanganate with a mixture of sodium nitrate and concentrated sulfuric acid.

These methods use harsh reaction conditions, are to some extent dangerous, as they put together reducing and oxidizing agents, require complex procedures to wash the oxidized graphite.

Staudenmaier and Hummers methods are summarized in Scheme 4.1 and Scheme 4.2 respectively.

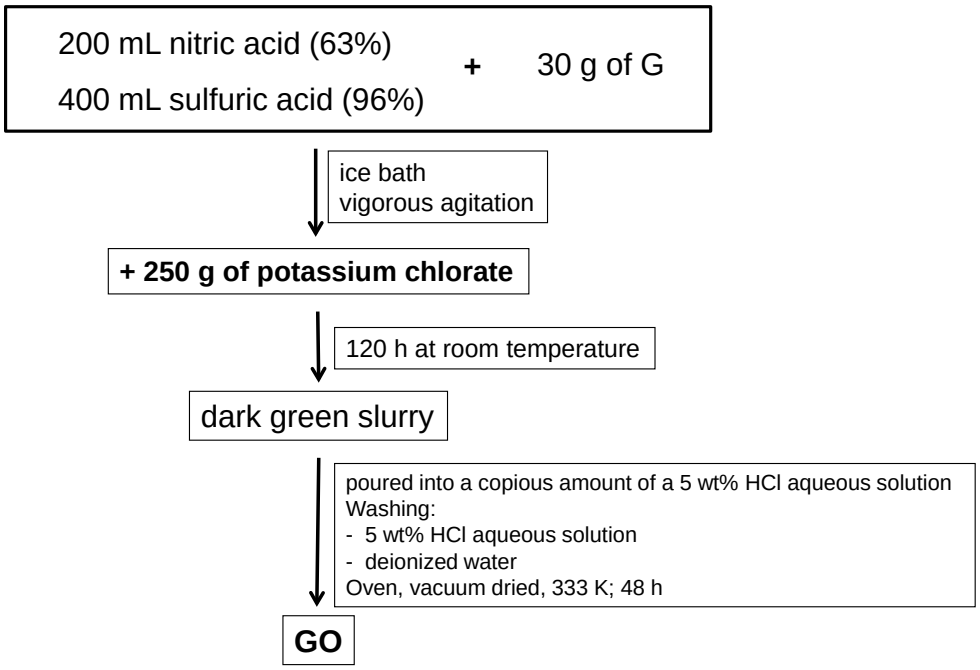

Scheme 4.1 Staudenmaier's method

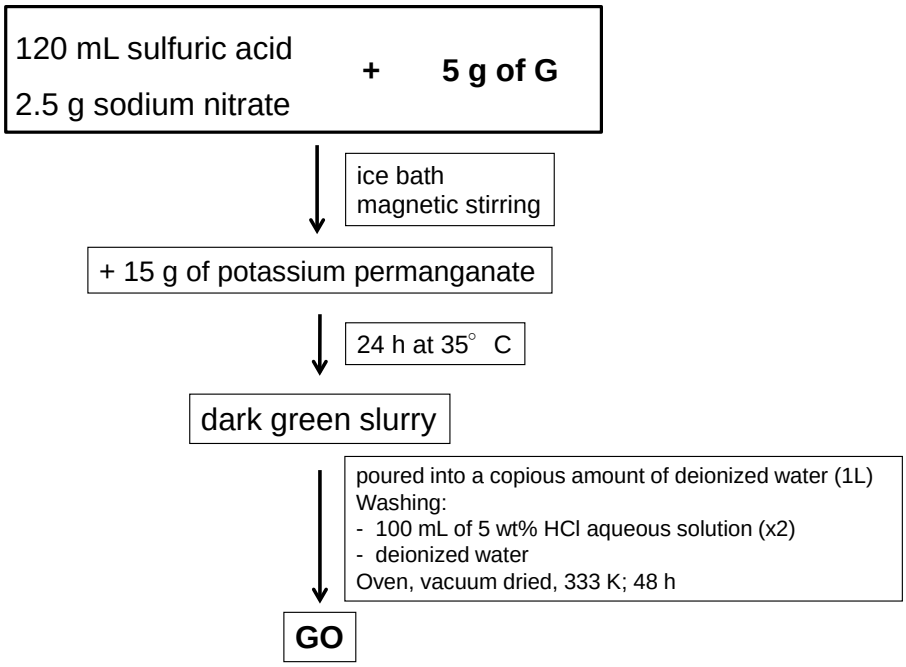

Scheme 4.2 Hummers' method

It is worth noting that such methods leads to largely oxidized graphite, GO. To have the desired properties of graphite, GO has to be reduced. This means a further reaction, that is successful to different extent. It is acknowledged in the field that sp^2 hybridization of carbon atoms is not completely restored.

4.4 Characterization of pristine nanosized graphite

The following nanosized graphite was used: Synthetic Graphite 8427® from Asbury Graphite Mills Inc., with 99,5% as carbon content. In the text below, such nano-graphite is indicated as nanoG. Data already available [9] on surface area and DBP absorption number are reported in Table 4.2. Data on CB N110 and CNT are also shown for comparison.

Table 4.2 BET surface area and DBP absorption number

Carbon filler	**BET surface area (m^2/g)**	**DBP absorption number (mL/100g)[a]**
CB N110	137	113
CNT	200	316
nanoG	330	162

[a] mL of absorbed di-isobutyl-phtalate / 100 grams of CB

CB N110 is one of the reinforcing carbon black with the highest surface area. CNT are well known, thanks to their shape, for having high surface area. From the data in Table 4.2 it is thus clear that the nanoG adopted in this thesis has very high surface area. This was chosen for favouring the modification reaction. Moreover, the very high surface area should favour the interaction of nanoG with the polymer matrix.

To verify the actual accessibility of nanoG to the polymer chains, it is useful to examine the values of absorbed di-iso-butyl phthalate reported in Table 4.2. Oil absorption is a typical test performed on reinforcing fillers, to investigate their ability to interact with the polymer matrix. It appears that there is not the same correlation for the three carbon allotropes between surface area and oil absorption numbers. In particular, nanoG shows low value of oil absosrption. In literature,[9] this was explained with the presence of stacked layers in nanoG aggregates: graphene layers are more accessible to small nitrogen molecules rather than to the polymer chains.

4.5 The reactivity of graphitic substrates

As already reported in Chapter 1, graphite is structurally formed by carbon atoms arranged in hexagonal fused rings. Each layer is held to the others by Van der Waals forces. This macromolecular system can be assimilated to polycyclic aromatic hydrocarbons (PAH), such as perylene or coronene, represented in Figure 4.1, Figure 4.1a and Figure 4.1b, respectively.

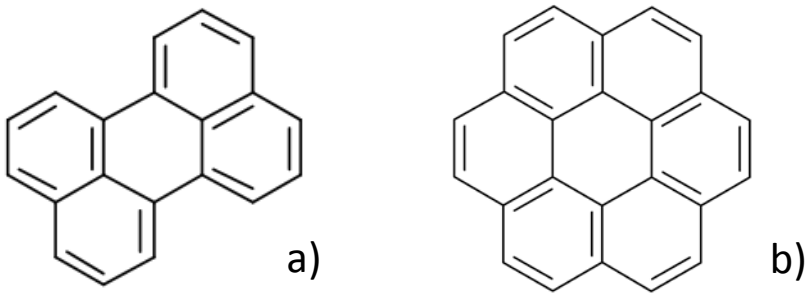

Figure 4.1 Perylene (a), coronene (b)

It is known that the ratio of hydrogen to carbon decreases, as these extended aromatic compounds become larger. For example, the symmetrical hexacyclic compound coronene has a H/C ratio =1/2, compared with 1 for benzene. In fused ring systems further extended in space, the H/C ratio would approach zero, and the resulting compound would be a pure form of carbon (i.e. graphite).

As in PAH, also in graphite the base structural unit is benzene, and, within structural defects, each carbon atom has sp^2 hybridization.

On the basis of these considerations, it is clear that, modifications on graphite or its derivatives, should have, as reference, the benzene reactivity.

In organic chemistry it is known that the functionalization of aromatic systems is very difficult because of the stability due to aromaticity. The electrons in the π system of benzene ring are responsible for the reactivity. While aromatic compounds are best represented by a continuous electron density evenly distributed around the aromatic core, the alternating single and double bonds, that are commonly drawn, are very useful models when predicting the reactivity of aromatic compounds. Many reactions common to alkenes (characterized by carbon-carbon double bonds) also work in a similar fashion with the "double bonds" in aromatic compounds, though generally the activation barrier is higher for the aromatic compounds, as a consequence of the stabilizing force of aromaticity (ca. 36 kcal/mol). However, aromatic compounds can participate in a variety of chemical reactions such as nucleophilic aromatic substitution.

4.6 Synthesis of graphite derivatives: reaction with KOH

4.6.1. Considerations on the reaction with KOH

Usually, to perform a nucleophilic aromatic substitution on benzene ring, is required the presence of a good leaving group: the nucleophile binds the ring taking the place of the leaving group.

In the case of graphite, the terminal rings are formed by carbon bound to hydrogen atoms, therefore, in theory, the nucleophilic substitution reactions are unlikely. The introduction of hydroxy functions on the ring is possible through long step reactions (ie. Diazonium salts). [10]

In this work, the insertion of the OH on the edges of graphite has been obtained by a treatment in excess of KOH.[11] In scheme 4.3, it is shown the proposed mechanistic pathway for this reaction.

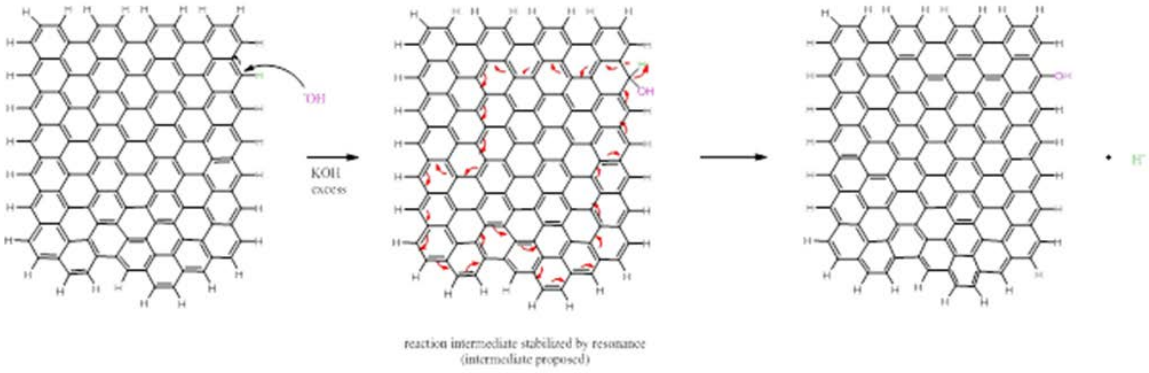

Scheme 4.3 Proposed mechanistic pathway

It was hypothesized that the insertion of hydroxyl anion occurs on peripheral carbon, through a two-step mechanism: (i) nucleophilic initial addition (in this case hydroxide ion) to the aromatic ring, followed by (ii) loss of a hydride from the negatively charged intermediate. This is possible because the intermediate reaction stabilizes the anion on the entire conjugated system and facilitates the expulsion of the hydride during the aromatization. Such hypothesized mechanism, that can be seen responsible for the functionalization of graphite, implies thus a reaction intermediate that exist in a considerable number of resonance hybrids. This large stabilization could be named as "wave effect".

4.6.2. Experimental conditions

The hydroxy-graphite derivatives [3] were prepared by mixing potassium hydroxyde and pristine graphite and providing mechanical energy, thermal energy or both together, as explained in detail in the experimental part.

To allow an easier reading of the results reported below, Table 4.3 summarizes types of nanosized graphite, conditions for their modifications and labels adopted to indicate them.

Table 4.3. Nanosized graphites: conditions for the modifications and labels

Type of treatment	**Conditions**	**Label**
None	=	NanoG
Thermal	KOH; water. heated flask 70°C for 4h	G-OH-T
Mechanical	KOH; ball milling at 300 rpm for 10h	G-OH-M
1. Thermal 2. Mechanical	1. KOH; water. heated flask 70°C for 4h 2. ball milling at 300 rpm for 10h	G-OH-TM

Procedure adopted for the treatments of nanoG are summarized in Scheme 4.4.

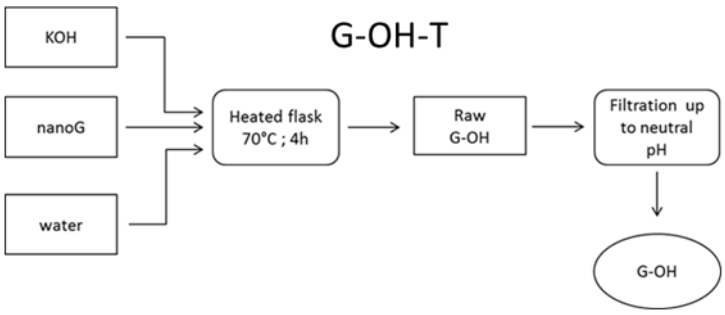

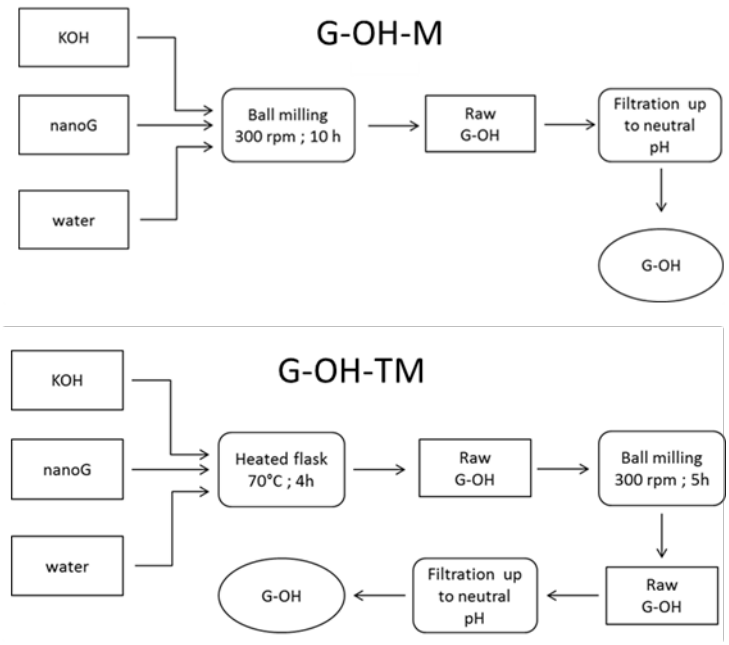

Scheme 4.4 Procedure for preparing the hydroxy-graphite derivatives by thermal treatment (G-OH-T), mechanical treatment (G-OH-M), thermal and mechanical treatment (G-OH-TM)

In Table 4.4, quantities of reagents are indicated.

Table 4.4. Synthesis of G-OH: amount of reagents

G-OH	**Graphite (mmol)**	**KOH (mmol)**	**H_2O (mL)**
G-OH-T	39	39	22
G-OH-M	14	356	6.5
G-OH-TM	208	208	117

4.7 Characterization of hydroxy-graphite (G-OH)

4.7.1 Degree of functionalization of G-OH

Thermogravimetric analysis (TGA) was used to quantitatively estimate the degree of functionalization. TGA curves of graphite and G-OH-M are shown in Figure 4.2.

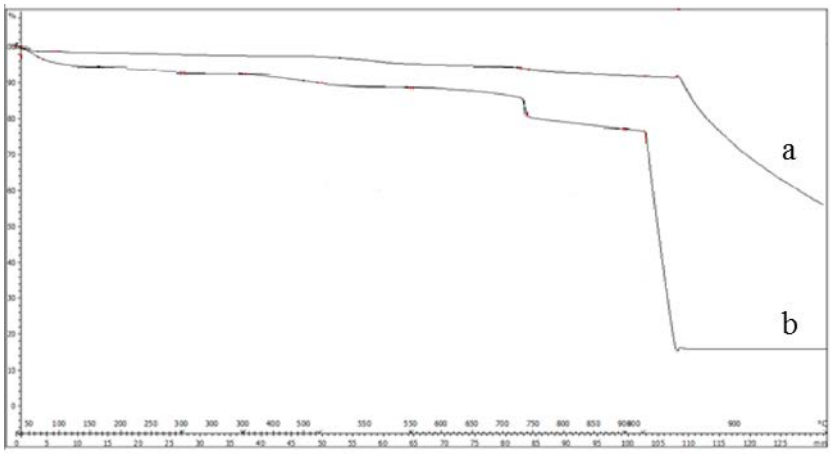

Figure 4.2 TGA thermograms under N_2 of graphite (a) and G-OH-M (b)

TGA trace of nanoG shows lower weight loss below 700°C. Compared with nanoG, G-OH-M shows lower thermal stability.

TGA trace, of G-OH-M, reveals a four-step decomposition profile, corresponding to:

(i) the removal of water (first step), T < 150°C

(ii) decomposition of oxygen-containing groups (second step)

(iii) removal of alkenilic groups (third step)

(iv) thermal degradation of graphite (fourth step), T > 700°C.

In Table 4.5, weight losses at the different steps are reported.

Table 4.5. Weight losses of nanoG and G-OH samples, from TGA analysis

Sample	**Weight loss [%]**		
	T < 150°C	**150°C < T < 700°C**	**T > 700°C**
nanoG	n.d.	5.2	92.3
G-OH-T	3.1	9.8	84.1
G-OH-M	5.9	17.2	74.7
G-OH-TM	5.8	17.3	73.9

The weight loss of nanoG seems to indicate that pristine nanoG contains minor amounts of functional groups that can undergo degradation below the typical temperature for the degradation of graphite. Investigation through IR spectroscopy (reported below in paragraph 4.7.2) is helpful in assessing the nature of these functional groups. Adsorbed water was not detected.

Much larger weight loss in the temperature range from 150 to 700°C was detected for G-OH-T, G-OH-M and G-OH-TM. In particular, the largest amount was in G-OH-M samples. In both these samples, weight loss was found at temperatures below 150°C. This weight loss could be attributed, as mentioned above, to water loss. Interestingly, the larger amount of weight loss at T > 150°C goes along with larger weight loss at T < 150°C. It could be hypothesized that G-OH containing larger amount of oxygenated functional groups holds larger amount of water.

It is finally worth observing that the onset temperature of the last step degradation becomes appreciably lower in G-OH samples, with respect to nanoG, presumably due to the combustion of the edge carbons coming from the degradation of oxygen-containing functional groups. Electric

4.7.2 Functional Groups in nanoG and G-OH samples

Functional groups present in nanoG and hydroxy graphite were investigated through IR spectroscopy in KBr pellet. Figure 4.3 shows the FTIR spectra of pristine nanoG, G-OH-T, G-OH-M, G-OH-TM.

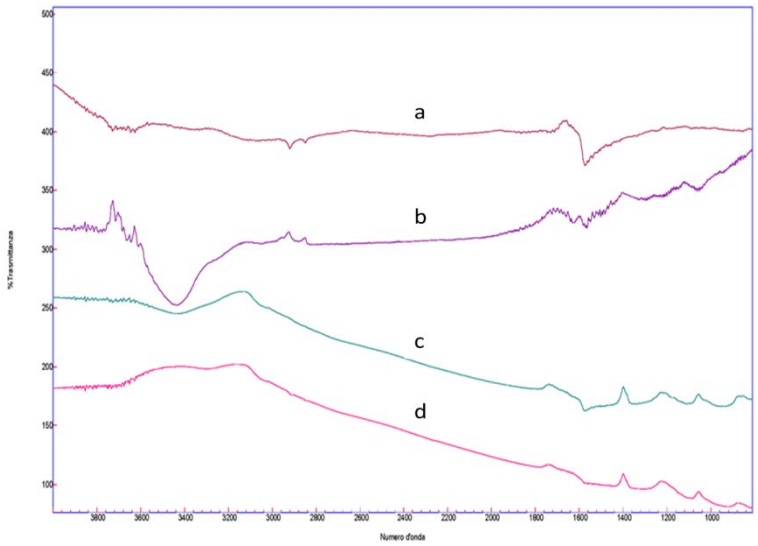

Figure 4.3 FTIR spectra (KBr pellets) of nanoG(a), G-OH-TM(b), G-OH-M(c) and G-OH-T(d)

The FTIR spectrum of the pristine nanoG (Fig. 4.3a) shows a weak band at 1632 cm^{-1} and a strong peak at 3400 cm^{-1} that are characteristic of the vibration mode of adsorbed water molecules and of bound moisture in KBr (Fig. 4.3a), which was used for the preparation of the IR specimen.

Due to the functionalization at the edges, G-OH-T, G-OH-M and G-OH-TM display their characteristic peaks for hydroxyl group at around 3282 (O-H stretching), 1353 (in plane O-H bend) and 1108 (C-O stretch) cm^{-1}. Moreover, they show prominent peaks at 2917 cm^{-1} (methylene C-H stretch, ν_{as}) and 2848 cm^{-1} (methylene C-H stretch, ν_s), that are attributable to sp^3 C−H and sp^2 C−H, respectively. It is also visible: the =C-H stretching at 3000 cm^{-1}, 1786 – 1669 (combination bands), 1560 – 1448 (C-C aromatic ring stretch), 967 (out of plane , =C-H bend) cm^{-1}

Hence, the FTIR spectra confirmed that nanoG underwent changes in all the reactions.

By taking into consideration results from TGA and IR analysis, it can be commented that the mechanochemical reaction, driven by ball milling, permits the insertion of hydroxyl groups at edges of graphite thanks to the reaction with KOH.

4.7.3 Structure of nanoG and G-OH

Structure of nanoG and G-OH was studied by means of TEM and X-Ray diffraction analyses.

4.7.3.1 TEM analysis

Samples for TEM analysis were prepared by pipetting a few millilitres (5 drops) of dispersion onto holey carbon mesh grids. Figure 4.4 shows micrographs of nanoG (Fig. 4.5a) and and G-OH-M (Fig. 4.4b). Pristine nanoG material is visible as a group / bundles of unordered carbon layers with reduced lateral size. Figure 4.4b shows agglomerates of point particles covered and sometimes connected by layers characterized by very thin and very small dimensions.

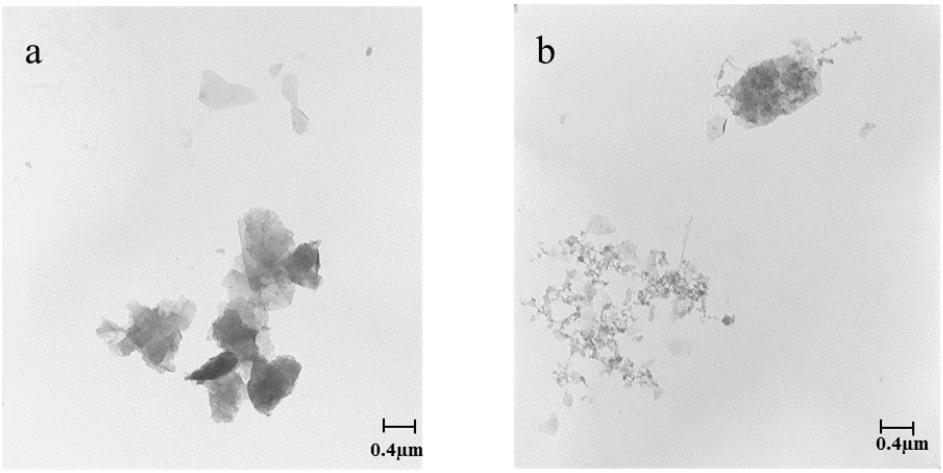

Figure 4.4 TEM micrograph of graphite (a) and G-OH-M (b)

4.7.3.2 X-Ray diffraction

Figure. 4.5 shows wide angle X-Ray diffraction patterns taken on powders of nanoG (Fig. 4.5a), G-OH-T (Fig. 4.5b)**,** G-OH-M (Fig. 4.5c), G-OH-TM (Fig. 4.5d) and GO hummers (Fig. 4.5e). (002) reflection is clearly visible in the pattern of pristine nanoG and remains at the same 2θ value in the pattern of all of the G-OH samples, indicating that the oxidation reaction did not promote expansion of the interlayer distance. It is also worth commenting that such interlayer distance, that can be calculated by applying the Scherrer equation to the 2θ value, is slightly larger than the one of ordered graphite samples (d002 = 0.335 nm).[12] There is, instead, a large change in the position of (00ℓ) reflections in the pattern of GO obtained by oxidizing nanoG with the Hummers method.[8] (001) reflection is at 2θ = 10.45 and corresponds to an average interlayer spacing of 0.9 nm. These differences are justified by the presence of oxygen-containing functional groups attached on both sides of the graphene sheet and the atomic scale roughness arising from structural defects.

The number of stacked layers was calculated by applying the Scherrer equation (Equation 1):

$D_{hk\ell} = K\,\lambda / (\beta_{hk\ell} \cos\theta_{hk\ell})$ (1)

where: K is the Scherrer constant, λ is the wavelength of the irradiating beam (1.5419 Å, CuKα), $\beta_{hk\ell}$ is the width at half height, and $\theta_{hk\ell}$ is the diffraction angle. The introduction of a correction factor has to be used in case $\beta_{hk\ell}$ is lower than 1°.

The number of stacked layers was found in a range, whose extremes were 35 for nanoG and 23 for G-OH-M**.**

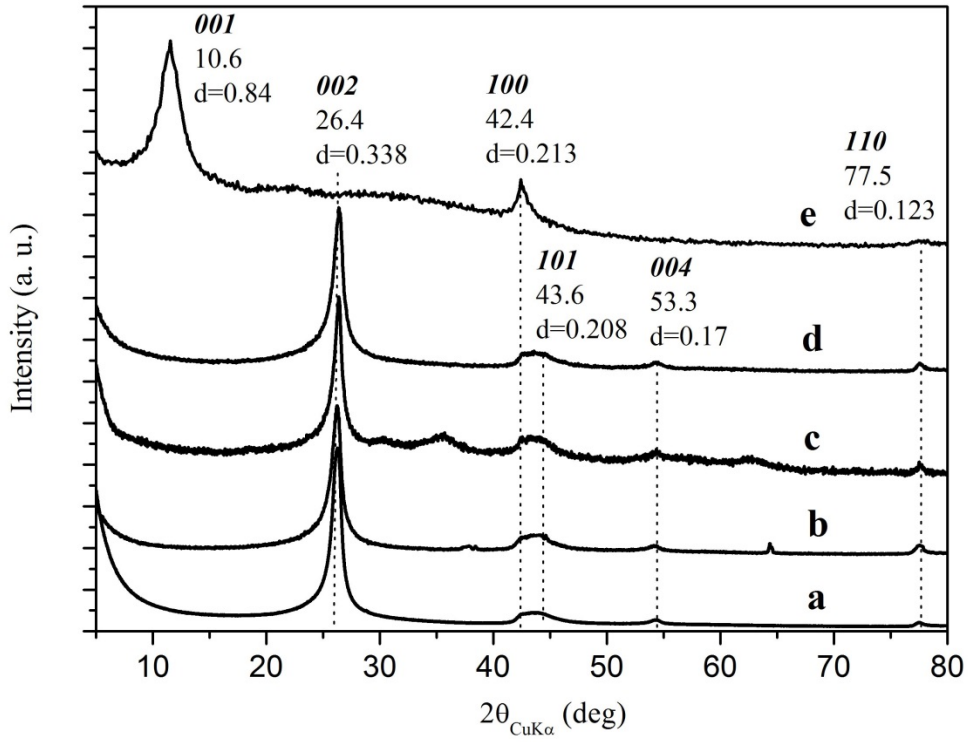

Figure 4.5 XRD patterns of graphite (a), G-OH-T (b), G-OH-M (c)**,** G-OH-TM (d) and GO hummers (e)

4.7.4 Overall comment on characterization results

Characterization results shown in the previous paragraphs demonstrate that the reaction of nanoG with KOH led to nanosized graphite containing hydroxyl functional groups. The amount of

functional groups could be estimated sufficient to allow the dispersion of G-OH in polar media, such as water and polyols.

4.8 Dispersions of G-OH in H_2O and in polyol mixture

4.8.1 Dispersion in water

Dispersion of G-OH in water was studied, taking G-OH-TM as the sample. As reported in the experimental part, aqueous solutions of G-OH at different concentrations (0.01, 0.02, 0.05, 0.1, 0,2 0,3 0.5 mg/mL) were prepared through a mild sonication and analyzed by UV-Vis absorption analysis. UV absorbance as a function of the wavelength is shown in Figure 4.6.

In Figure 4.6a it is shown that the absorbance monotonously increases with G-OH-TM concentration.

The stability of the solution with 1 mg/mL concentration was investigated also by taking UV-Vis spectra after 1 week. In Figure 4.6b, it is evident that the absorbance detected for the solution (1 mg/mL) freshly prepared and after 1 week did not change. The centrifugation at 2000 rpm for 10 minutes led to a slight decrease of absorbance.

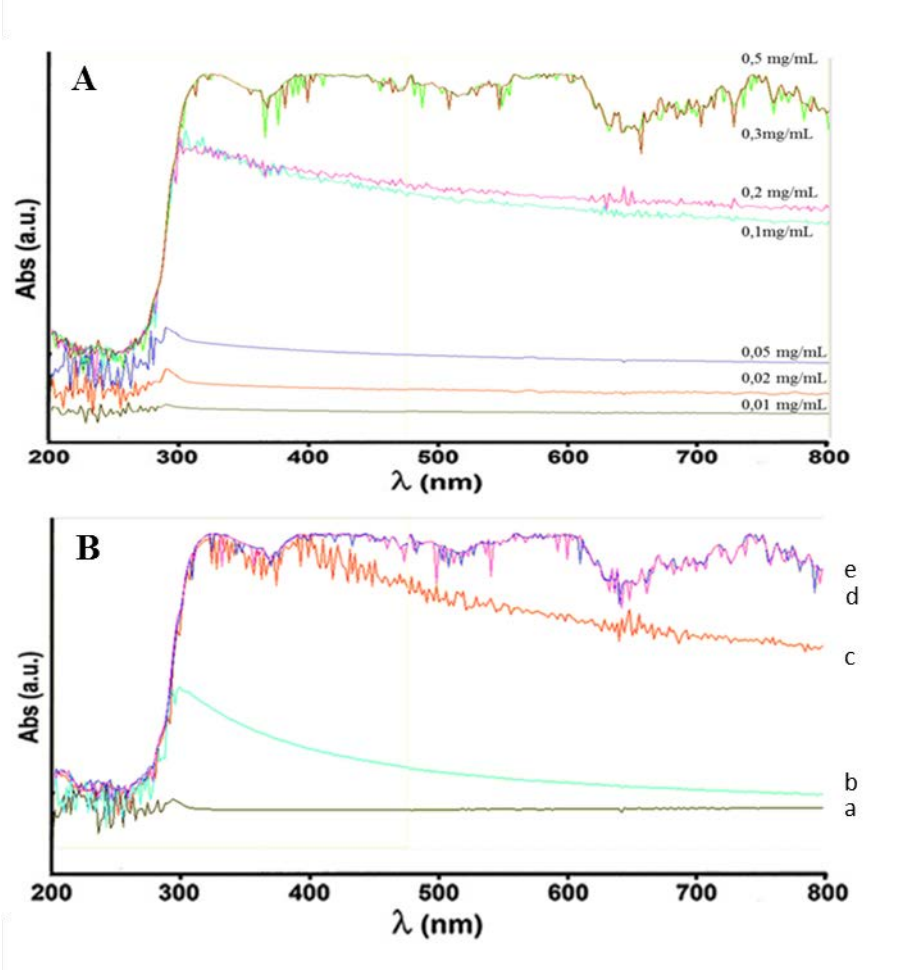

Figure 4.6 Dependence of UV-Vis absorbance on concentration of G-OH water solutions (A) and UV-Vis spectra of graphite in water (a), UV-Vis spectra of G-OH-TM after centrifugation at 4000 rpm for 1 hour (b), after centrifugation at 2000 rpm for 10 min (c), after sonication (d) and after 1 week (e) (B)

Graph in Figure 4.7 shows how experimental data of absorbance as a function of concentration are well interpolated by a straight line. Lambert-Beer law is then respected so it can be assumed that G-OH-TM form easily a solution with water thanks to –OH functional groups.

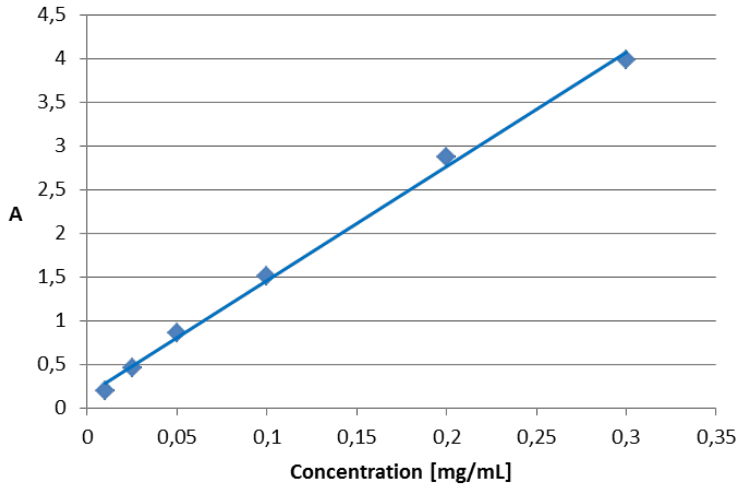

Figure 4.7 Linear relationship between the absorbance at 260 nm and the concentration of water solution of G-OH-TM

Stability of G-OH solution was also checked for a sample with 4 mg/mL concentration, typical level of commercial products of G-OH from oxidation according to the Hummers method.[8]

4.8.2 Dispersion in polyol mixture

In Figure 4.8, is shown the UV-Vis absorbance for polyol solution of G-OH-TM (1 mg/mL) in polyol mixtures, treated under different conditions: after sonication, after 1 week without centrifugation, after centrifugation at 2000 rpm for 10 min, after centrifugation at 4000 rpm for 1 hour. Only the centrifugation at 4000 rpm leads to appreciable reduction of absorbance.

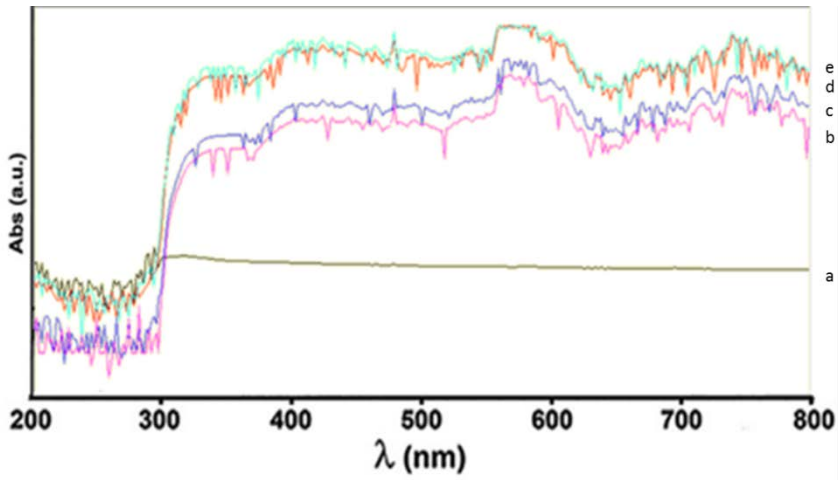

Figure 4.8 Dependence of UV-Vis absorbance on concentration of G-OH-TM polyol solutions and UV-Vis spectra of graphite in polyol (a), UV-Vis spectra of G-OH-TM in polyol after centrifugation at 4000 rpm for 1 hour (b), after centrifugation at 2000 rpm for 10 min (c), after sonication (d) and after 1 week (e)

4.8.3 Visual inspection of G-OH solutions

Figure 4.9 shows aqueous suspension (1 mg/mL) of nanoG (Fig. 4.9c), and solution (1mg/mL) of G-OH-TM in water (Fig. 4.9b) and polyol (Fig. 4.9a).

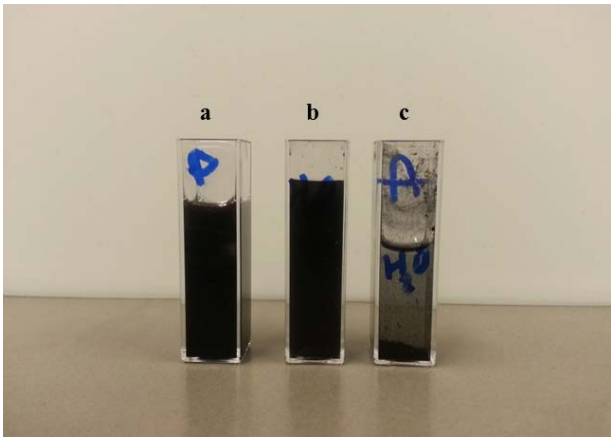

Figure 4.9 G-OH-TM solutions in polyol (a) and water (b). Water suspension of graphite (c)

4.9 Synthesis of graphite derivatives: reaction with maleic anhydride

4.9.1. Considerations on the reaction of graphite with maleic anhydride

Polycyclic aromatic hydrocarbons, such as anthracene, are able to react with dienophile such as maleic anhydride, giving a reaction known as Diels Alder.[13] Diels Alder is a pericyclic reaction leading to the formation of cycles through the reaction between a conjugated electron-rich diene and an electron-poor alkene (dienophile). [14 - 15] When polycyclic aromatic hydrocarbons react with maleic anhydride, they behave as dienes.

In literature there are many studies about Diels Alder on graphite and derivatives, that behave either as diene or dienophile.[16]

Aim of this part of the work was to prepare cycloadducts from the reaction of graphite and maleic anhydride.

4.9.2. Experimental conditions

The reaction between graphite and maleic anhydride was performed at 110° C for 3 hours, in the absence of additional solvents or reagents.

The reaction conditions were optimized through the reaction of maleic anhydride with a model substrate, anthracene, reported in Scheme 4.5.

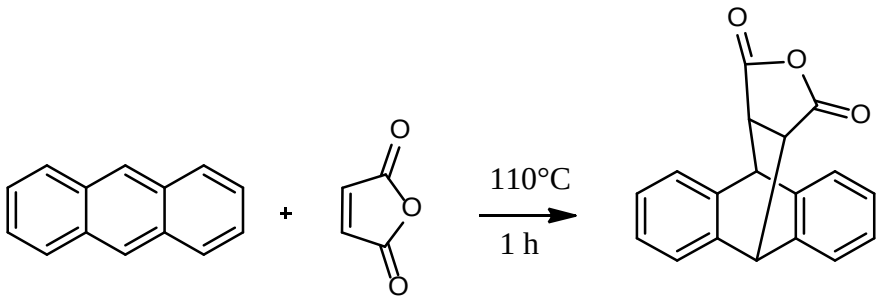

Scheme 4.5 Diels Alder adduct from reaction between anthracene and maleic anhydride (9,10,11,15-tetrahydro-9,10-[3,4]furanoanthracene-12,14-dione)

The obtained compound was: 9,10,11,15-tetrahydro-9,10[13,16]furanoanthracene-12,14-dione. Anthracene and maleic anhydride were mixed at 110°C for 1 hour and the cycloadduct obtained was characterized by NMR spectroscopy.

The presence in the spectrum of the characteristic peaks at 4.82 and 3.51 ppm (Fig. 4.10) unambiguously reveals that the synthesized compound was the expected adduct.

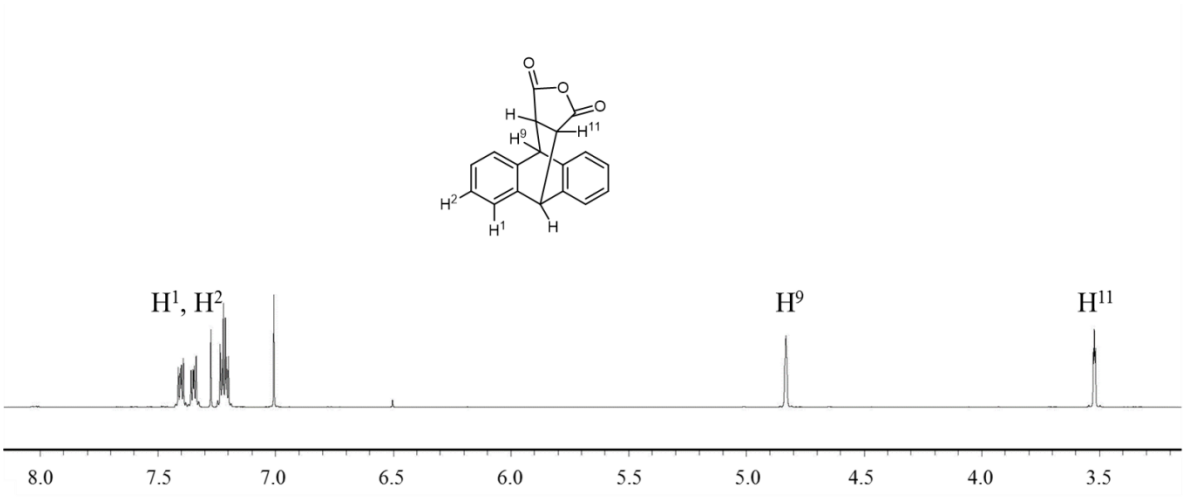

Figure 4.10 400 MHz ^{1}H NMR spectra in $CDCl_3$ of 9,10,11,15-tetrahydro-9,10-[3,4]furanoanthracene-12,14-dione

Reaction between graphite and maleic anhydride, as described in the experimental part, was performed at the same temperature. Procedures adopted are shown in Scheme 4.6. The first procedure leads to the preparation of the nanoG/maleic anhydride adduct. The second procedure has, as the last, step, the hydrolysis of anhydride group.

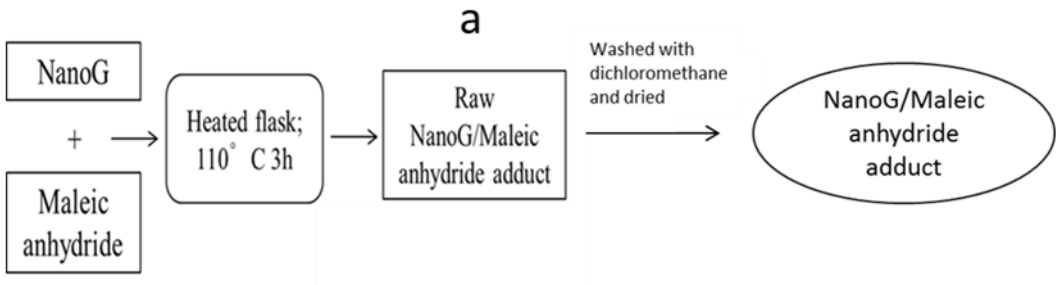

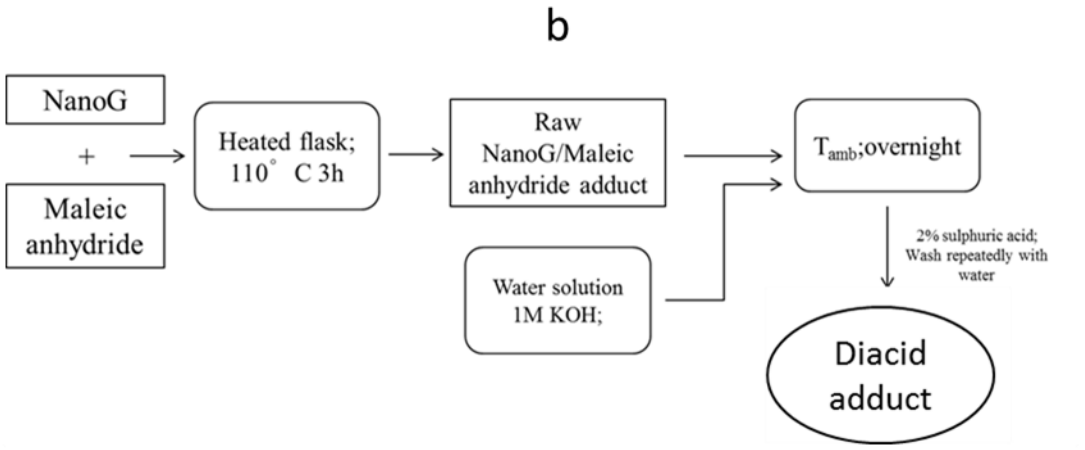

Scheme 4.6 Procedure followed for the reaction between nanoG and maleic anhydride: method followed for sample G-A1 (a) and G-A2 (b)

In Table 4.6, are indicated main experimental conditions, in particular the molar ratio of reagents, calculated taking into consideration the molar amount of benzene rings in nanoG. Maleic anhydride was used in excess, larger in the first run.

Table 4.6 Reaction of nanoG with maleic anhydride: molar ratio of reagents and hydrolysis

Sample	**Molar ratio benzene ring / MA**	**Hydrolysis**
G-A1	1 : 2.9	-
G-A2	1:2	Basic hydrolisis

4.10 Characterization of adduct of graphite with maleic anhydride

4.10.1 Thermogravimetric analysis

As reported above thermogravimetric analysis (TGA) was used to estimate the degree of functionalization. TGA curves of graphite adducts are shown in Figure. 4.11.

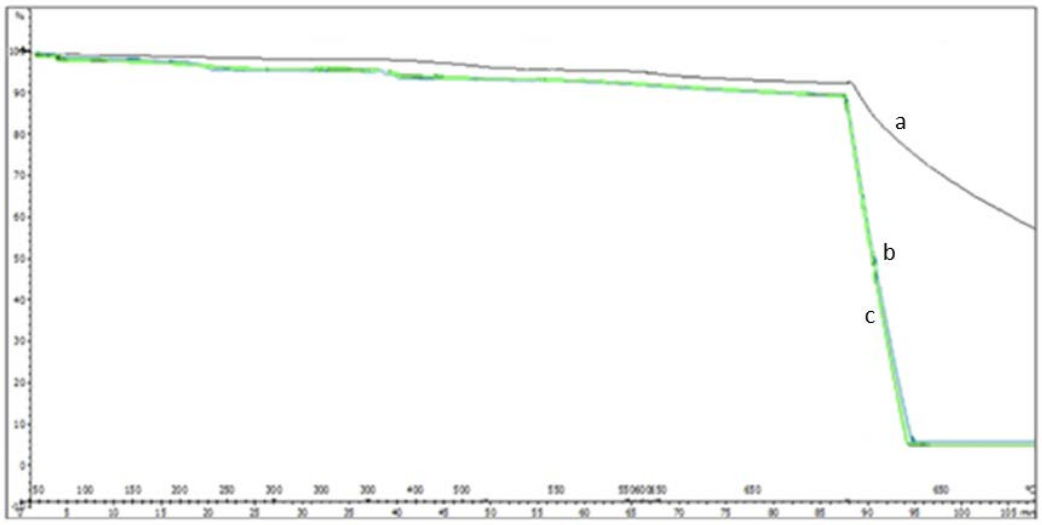

Figure 4.11 TGA thermograms under N_2 of nanoG (a) and nanoG/MAH adducts: G-A1 (b), G-A2 (c)

Figure 4.11 shows the thermogravimetric analysis of nanoG (a) and nanoG/MAH adducts: G-A1 (b), G-A2 (c).

Weight losses in the three thermographs are indicated in Table 4.7

Table 4.7 Weight losses of nanoG and nanoG/MAH adducts, from TGA analysis

Sample	**Weight loss [%]**		
	T < 150°C	**150°C < T < 700°C**	**T > 700°C**
nanoG	n.d.	5.2	92.3
G-A1	1.17	1.97	95.4
G-A2	1.22	2 + 2.26	90.6

Thermal plot of both adduct samples show the first weight loss at about 72°C (1.20% w), that is probably due to the unreacted maleic anhydride, that remained adsorbed on graphite.

In the first sample (G-A1) there are only three weight losses: the first at about 70°C, unreacted anhydride (1.17%); the second at 467°C (1.97%) relative to the adduct and the last from 600°C is the combustion of graphite.

The TGA of the second sample of graphite (G-A2), obtained by conducting the reaction in the molar ratio of 1 to 2 (benzene rings / anhydride), shows 4 weight losses: the first at about 70°C relative to unreacted anhydride (1.22%); the second at 256°C (2%) and the third at 488°C (2.26%) relative to the carboxylic groups and linked anhydride respectively; the last from 600°C is combustion of graphite .

In the second sample there is 4 weight losses because in the second reaction was also carried out the basic hydrolysis of the linked anhydride.

4.10.2 Infrared spectroscopy

Structure of G-A2 was investigated through FTIR spectroscopy in KBr pellet. Figure 4.12 shows the FTIR spectra of G-A2 and pristine graphite powders. The FTIR spectrum of the pristine graphite (Fig. 4.12a) shows only a weak band at 1632 cm^{-1}, which is characteristic of the vibration mode of adsorbed water molecules. The strong peak at 3400 cm^{-1} is attributable to the bound moisture in KBr (Fig. 4.12), which was used for the preparation of the IR specimen.

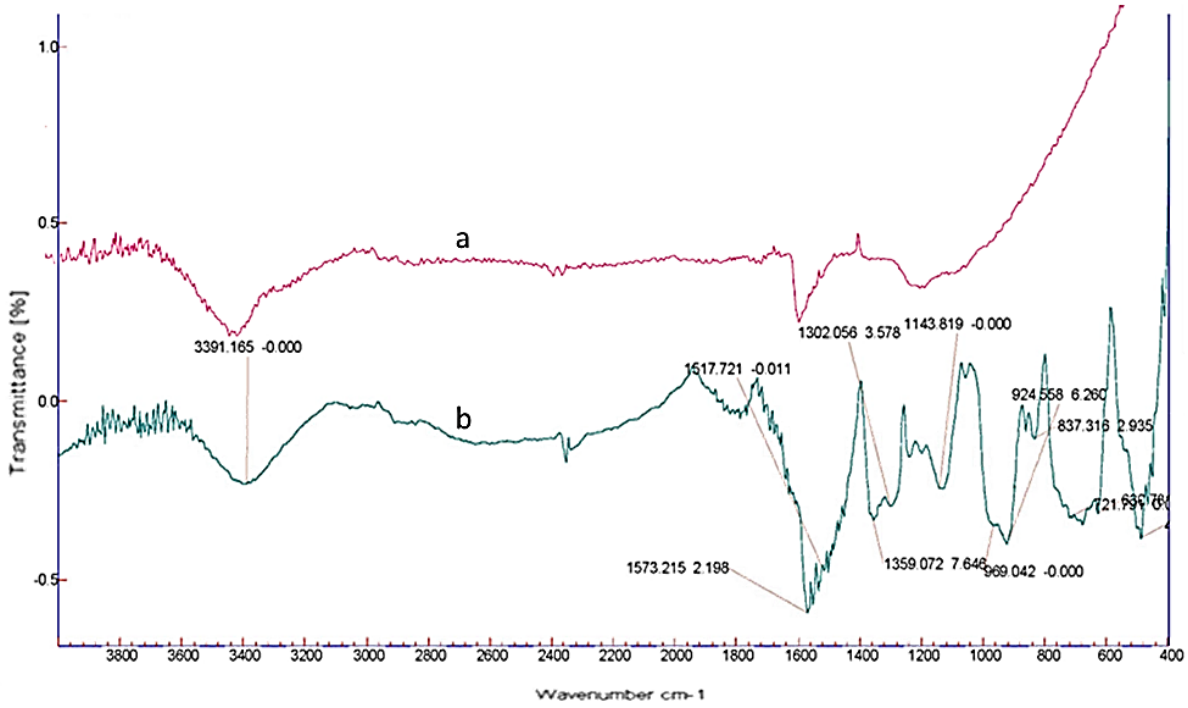

Figure 4.12 FTIR of graphite (a) and G-A2 (b)

Figure 4.12b shows the spectrum of the adduct hydrolyzed: prominent peak at 3391 is related to OH stretching from water of KBr pellet. Under this peak could be the OH stretching of carboxylic acid, because at 1302 cm^{-1} is possible to see the CO stretch of acid group. 1820-1780 C=O stretch anhydride; 1573 - 1517 (C-C aromatic ring stretch); 1359 (OH bending); 969 (out of plane, =C-H bend) cm^{-1}.

4.10.3 Comments on characterization results

Modification of nanoG with maleic anhydride was successful. However, after hydrolysis, unreacted anhydride, linked anhydride and carboxylic groups are present. The reaction should be better optimized in order to improve the efficiency for the introduction of carboxylic groups.

4.11 Synthesis of graphite derivatives: reaction with 1-dodecanethiol

4.11.1 Considerations on the reaction of graphite with 1-dodecanethiol

Reaction between graphite and 1-dodecanethiol was performed in the presence of a radicalic initiator, azobisisobutyronitrile (AIBN). Hypothesized mechanism for the reaction is represented in Scheme 4.7: addition occurs on double bonds of defective rings.

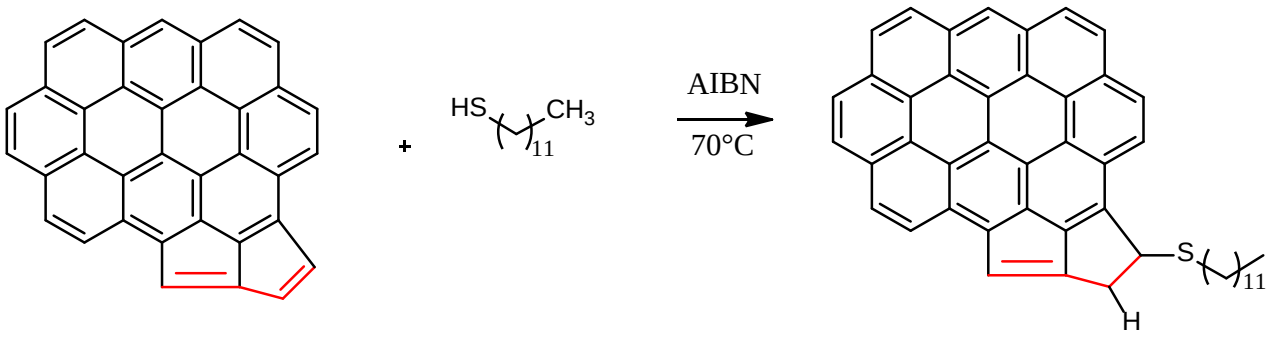

Scheme 4.7 Radicalical addition on the defects of graphite

4.11.2. Experimental conditions

The reaction between nanoG and 1-dodecanethiol was carried out at 70°C, either in the absence or in the presence of solvent. The procedure followed is briefly reported in Scheme 4.8 and more in detail in the experimental part.

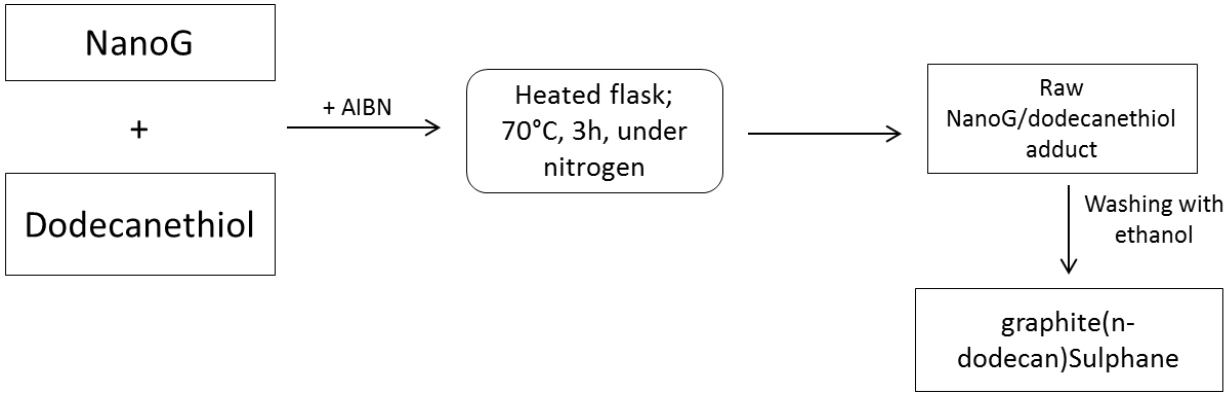

Scheme 4.8 Procedure followed for the reactions of graphite with dodecanethiol

Product from the reaction in the absence of solvent is labeled G-S1.

Product from the reaction in the presence of solvent is labeled G-S2.

Main experimental conditions are in Table 4.8

Table 4.8 Reaction of nanoG with maleic anhydride: molar ratio of reagents and hydrolysis

Sample	**Molar ratio 1-dodecanethiol/ benzene ring in graphite**	**Solvent**
G-S1	1.4 : 1	-
G-S2	1: 2.8	Ethanol

GS-1 was synthesis was performed using a large excess of dodecanethiol (1:1.4 moles of benzene ring and dodecanethiol respectively), while for GS-2 dodecanethiol was used in defect (2.8: 1 moles of benzene ring and dodecanethiol respectively) and ethanol was added as solvent.

4.12 Characterization of adduct of graphite with 1-dodecanethiol: graphite(n-dodecan)Sulphane

4.12.1 Thermogravimetric analysis

Thermogravimetric analysis was used to estimate the degree of functionalization. TGA curves of nanoG (a), nanoG(n-dodecan)Sulphane products G-S2 (b) and G-S1(c) are shown in Figure 4.13.

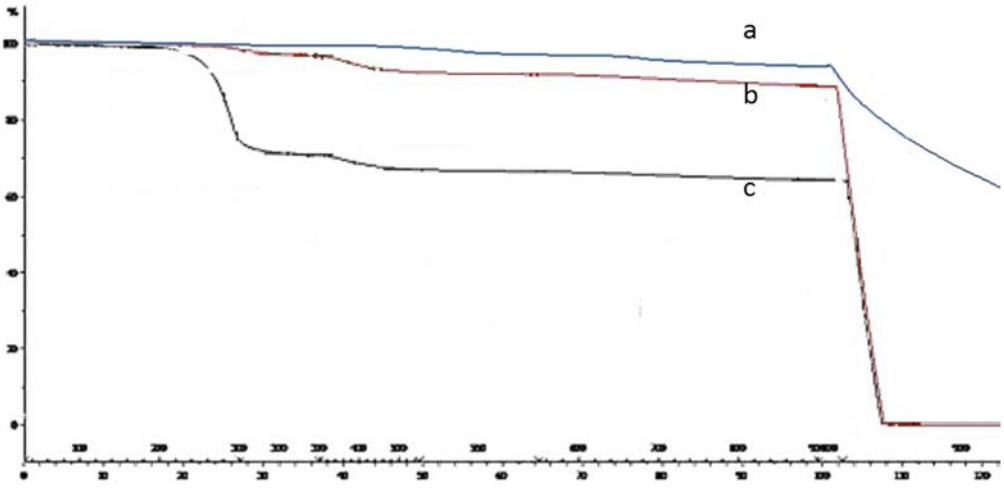

Figure 4.13 TGA thermograms under N_2 of graphite (a), G-S2 (b) and G-S1 (c)

Weight losses in the three thermographs are indicated in Table 4.9

Table 4.9. Weight losses of nanoG and nanoG/DCT adducts, from TGA analysis

Sample	**Temperature**		
	150°C < T < 300°C	**300 < T < 700°C**	**T > 700°C**
nanoG	5.2		92.3
G-S1	28	3.85	66.2
G-S2	2.7	3.27	91.8

Figure 4.16 shows thermogravimetric traces of G-S1 and G-S2.

G-S1 (3 weight losses): the first is supposed to be the excess of dodecanethiol (292°C, 28% w). If one considers that the dodecanethiol boils at this temperature, this hypothesis seems plausible. The second loss at 378°C (3.85% w) is the alkilthio moiety; the last is graphite.

G-S2 (3 losses in weight): the first is supposed to be the excess of dodecanethiol (292°C, 2.7% w). The second loss at 378°C (3.27 w%) is the alkilthio moiety; the last is graphite.

The degree of functionalization obtained in both reactions was calculated considering the second and third weight losses in the thermogravimetric trace.

Calculated values are as follows:

G-S1: 5.68%,

G-S2: 3.48%.

4.11.3 Infrared spectroscopy

Figure 4.14 shows G-S1 and G-S2 FTIR spectra:

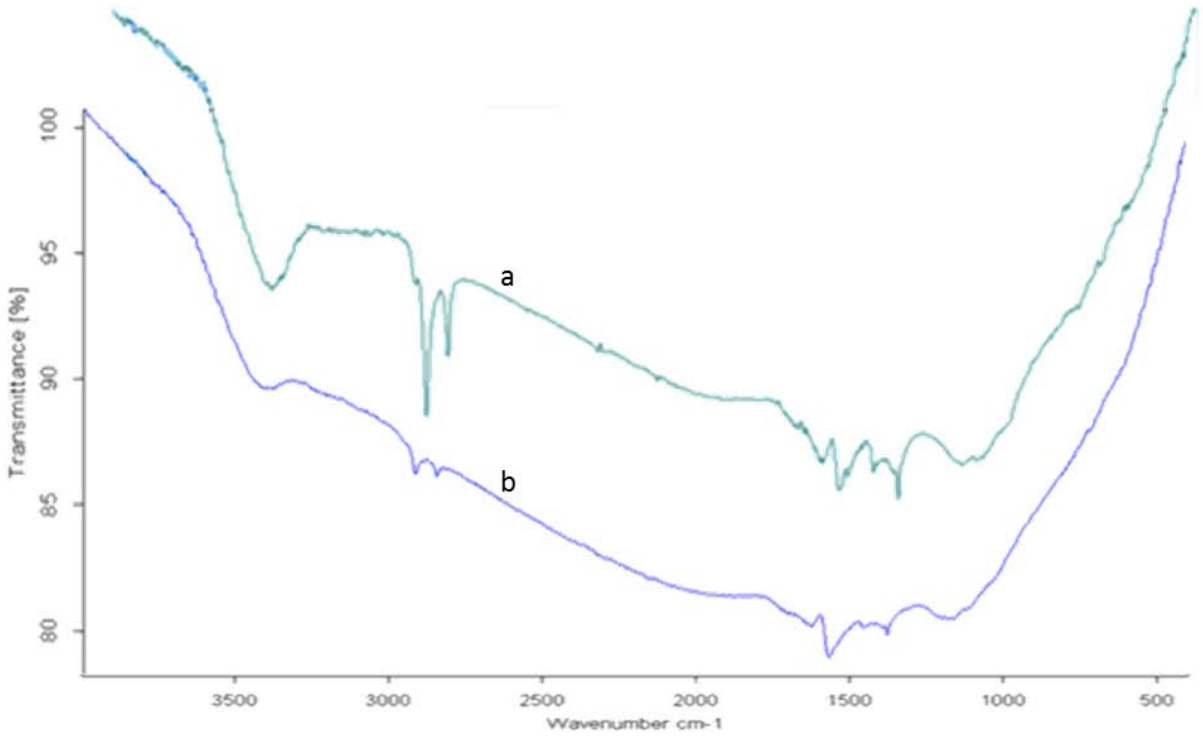

Figure 4.14 FTIR spectra of G-S1 (a) and G-S2 (b)

Prominent peak at 3410 OH stretching and weak band at 1632 cm^{-1} are characteristic of the vibration mode of adsorbed water molecules from water of KBr pellet.

Peaks at 2918 cm^{-1} (methylene C-H, asymmetrical stretching), 2849 cm^{-1} (methylene C-H, symmetrical stretching), can be attributed to sp^3 C−H and sp^2 C−H, respectively. Stretching due to aromatic rings are at: 3000 cm^{-1} for =C-H and at 1573 cm^{-1} for C-C.

The presence of intense absorptions at 2918 and 2849 cm^{-1} is due to the presence of long alkyl chains.

4.12.3 Comments on characterization results

Modification of nanoG with 1-dodecanethiol was successful. It seems that the procedure in the presence of solvents could be better for preparing an adduct with very little amount of unreacted thiol.

4.13 Conclusions

The modification of nanosized graphite with very high surface area, nanoG, was performed successfully with the following reagents:

(i) KOH

(ii) maleic anhydride

(iii) 1-dodecanethiol

The reaction with KOH led to appreciable amount of modification, with the introduction of hydroxyl groups essentially in peripheral positions. Reaction was carried out in the absence of solvents or catalysts, via ball milling or simply by heating the reaction flask, thus through methods that are considered as green methods. Ball milling brought to reduction of crystalline order in the direction orthogonal to structural layers. This combination of reaction and experimental procedure led to the formation of few layers graphene, as confirmed by transmission electron microscopy. It is worth noting that few layers graphene were prepared without harsh and dangerous oxidation reactions (such as those performed according to Staudenmeier and Hummers methods) and by using water as the only solvent.

G-OH (treated first by heating and then via ball milling) was suspended in water and gave rise to stable solutions, up to 4 mg/mL, typical level of commercial products of G-OH from oxidation according to the Hummers method.

The reaction with maleic anhydride led to the introduction of clearly detectable anhydride groups and, after hydrolysis, of carboxylic groups. Reaction procedure should be improved, to avoid the presence of unreacted anhydride and to improve the efficiency for the introduction of carboxylic groups.

The reaction with 1-dodecanethiol led to the introduction in nano-G of hydrocarbon chains. This demonstrates that carbon allotropes are able to react with sulphur, at least through radicalic addition.

Aim of this thesis was to perform modification of nanosized graphite in order to promote its compatibility with matrices such as natural rubber and poly(urethanes). Literature on nanocomposites demonstrate that best dispersion of nanosized fillers is obtained via latex blending. Dispersions in natural rubber could be thus prepared by blending modified nanoG with NR latex.

In the light of these considerations, modification of nanoG with polar groups should be preferred. Between the two modifications with polar groups, the one with KOH appears to be more promising, mainly because of the possibility of removing KOH up to neutral pH of the carbon allotrope and of selectively introducing OH groups, that appear suitable for dispersion in water and for the affinity with polyols and for the reactivity with isocyanates. The stability of G-OH from KOH solutions in water and polyols is a clear indication in this direction.

4.14 References

[1] Terrones, M., Botello-Méndez, A. R., Campos-Delgado, J., López-Urías, F., Vega-Cantú, Y. I., Rodríguez-Macías, F. J., ... & Terrones, H. (2010). Graphene and graphite nanoribbons: Morphology, properties, synthesis, defects and applications. Nano Today, 5(4), 351-372.

[2] Keun Soo Kim1,3,4, Yue Zhao7 , Houk Jang2 , Sang Yoon Lee5 , Jong Min Kim5 , Kwang S. Kim6 , Jong-Hyun Ahn2,3, Philip Kim3,7, Jae-Young Choi5 & Byung Hee Hong1,3,4 Nature Vol 457| 5 February 2009

[3] Lu Yan,a Mimi Lin,a Chao Zeng,a Zhi Chen,a Shu Zhang,a Xinmei Zhao,b Aiguo Wu,b Yaping Wang,a Liming Dai,*ac Jia Qu,*a Mingming Guod and Yong Liu; J. Mater. Chem., 2012, 22, 8367

[4] Sarkar, S., Bekyarova, E., & Haddon, R. C. (2012). Chemistry at the Dirac point: Diels–Alder reactivity of graphene. Accounts of chemical research, 45(4), 673-682.

[5] Yang, X. H., Guo, J. W., Yang, S., Hou, Y., Zhang, B., & Yang, H. G. (2014). A free radical assisted strategy for preparing ultra-small Pt decorated CNTs as a highly efficient counter electrode for dye-sensitized solar cells. Journal of Materials Chemistry A, 2(3), 614-619.

[6] Brodie, B. C. Phil. Trans. R. Soc. London 1859, 149, 249−259.

[7] Staudenmaier, L. Ber. Dtsch. Chem. Ges. 1898, 31, 1481−1487.

[8] Hummers, W. S.; Offeman, R. E. J. Am. Chem. Soc. 1958, 80, 1339.

[9] Agnelli, S., Cipolletti, V., Musto, S., Coombs, M., Conzatti, L., Pandini, S., ... & Galimberti, M. (2014). Interactive effects between carbon allotrope fillers on the mechanical reinforcement of polyisoprene based nanocomposites. Express Polymer Letters, 8(6).

[10] Jay R. Lomeda , Condell D. Doyle , Dmitry V. Kosynkin , Wen-Fang Hwang and James M. Tour. Am. Chem. Soc., 2008, 130 (48), pp 16201–16206

[11] Yan, L., Lin, M., Zeng, C., Chen, Z., Zhang, S., Zhao, X., ... & Liu, Y. (2012). Electroactive and biocompatible hydroxyl-functionalized graphene by ball milling. Journal of Materials Chemistry, 22(17), 8367-8371.

[12] Mauro, M., Maggio, M., Cipolletti, V., Galimberti, M., Longo, P., & Guerra, G. (2013). Graphite oxide intercalation compounds with rotator hexagonal order in the intercalated layers. Carbon, 61, 395-403.

[13]. Sauer, J., & Sustmann, R. (1980). Mechanistic Aspects of Diels-Alder Reactions: A Critical Survey. Angewandte Chemie International Edition in English, 19(10), 779-807.

[14] Rideout, D. C., & Breslow, R. (1980). Hydrophobic acceleration of Diels-Alder reactions. Journal of the American Chemical Society, 102(26), 7816-7817

[15] Evans, D. A., & Johnson, J. S. (1999). Diels-Alder Reactions. Comprehensive asymmetric catalysis, 3, 1177.

[16] Sarkar, S., Bekyarova, E., Niyogi, S., & Haddon, R. C. (2011). Diels− Alder Chemistry of Graphite and Graphene: Graphene as Diene and Dienophile.Journal of the American Chemical Society, 133(10), 3324-3327.

Chapter V

5.1 Introduction

In this Chapter, are discussed nanocomposites based on NR and G-OH: preparation, structure, sulphur based crosslinking, dynamic-mechanical and tensile properties. Results are briefly commented in the light of the existing scientific literature.

5.2 Preparation of nanocomposites

Elastomeric nanocomposites were prepared with poly(1,4-*cis*-isoprene) from Hevea Brasiliensis (Natural rubber, NR) and different amounts of G-OH. Typical formulation was adopted, with ingredients for sulphur based crosslinking. Only the amount of G-OH was changed in the different nanocomposites. Formulations are shown in Table 5.1. The amount of G-OH in the nanocomposites was checked by means of thermogravimetric analysis, performed on the crosslinked composites, presented below in Paragraph 5.3. Nanocomposites were labelled indicating the actual content of G-OH.

Table 5.1 Formulations of NR-based nanocomposites with G-OH as the filler[1,2]

Ingredient	**G-OH_0**	**G-OH_4**	**G-OH_7**	**G-OH_10**	**G-OH_12**	**G-OH_15**	**G-OH_25**
NR	100	100	100	100	100	100	100
G-OH theoretycal	0	3	6	9	12	15	25
G-OH experimental	0	3.7	6.5	9.5	12.3	15.1	n.d.

[1] Amounts of ingredients are expressed in phr [2] Other ingredients: ZnO 4 phr, stearic acid 2 phr, sulphur 3 phr, 6PPD 2 phr, TBBS 1,8 phr.

Procedure followed for preparing the nanocomposites is described in detail in the experimental part and is summarized in Scheme 5.1.

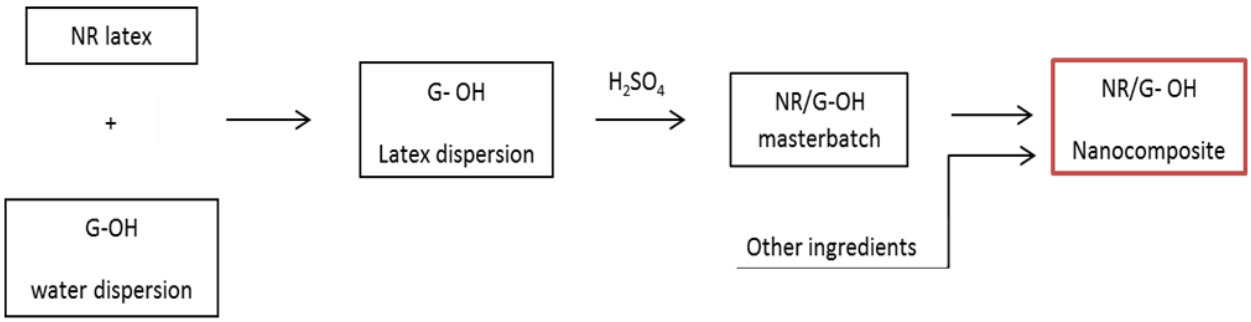

Scheme 5.1 Procedure for preparing the nanocomposites

At first, a masterbatch was prepared by dispersing the nanofiller in the NR latex and sonicating the suspension. As reported in the previous Chapter, the nanosized graphite was chemically modified to insert polar groups (OH) on the edges in order to improve the dispersion in polar media, such as the NR latex. It was also reported in the previous Chapter the stability of G-OH dispersions in water: the increase of the UV absorption with G-OH content in water dispersions was shown. G-OH suspensions in NR latex appeared as “homogeneous black inks”, up to 15.1 phr of G-OH. In Figure 1a, it is shown the dispersion in latex of 15.1 phr of G-OH.

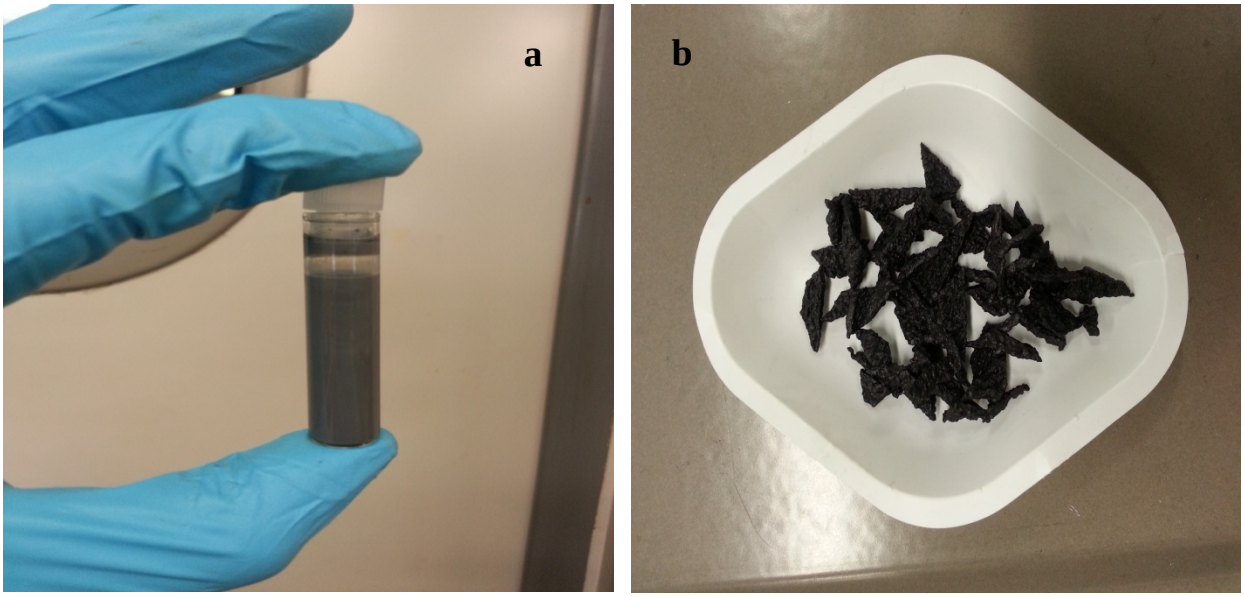

Figure 5.1 Dispersion in NR latex of 15.1 phr G-OH (a); crumbs of NR/G-OH masterbatch (b)

The solid nanocomposite was isolated through precipitation with sulphuric acid. The precipitation of NR latex with acid is well known in the rubber field. In particular, in the field of

nanofiller, the precipitation with sulphuric acid is reported in the case of cationic clays.[1] In Figure 5.1b, precipitated crumbs of NR nanocomposite with G-OH are shown. When 25 phr of G-OH were added to NR latex, G-OH powder was observed in the beaker, indicating that G-OH was not completely incorporated in NR. Taking into consideration this experimental evidence, composites with nominal 25 phr of G-OH were characterized, but data were not used for the elaborations presented below.

Subsequently, nanocomposites were prepared by adding the other ingredients via melt blending in internal mixer of the brabender® type. Temperature was maintained sufficiently low to avoid the so called scorch phenomena, that means undesired crosslinking of polymer chains due to the reaction of the sulphur based ingredients. The elastomeric nanocomposites taken from the internal mixer and passed between the rolls of the two rolls mill were then vulcanized at 170°C for 10 minutes, as described in more detail in the experimental part.

5.3 G-OH content of nanocomposites

G-OH content in the nanocomposites was determined by means of thermogravimetric analysis. In Figure 5.2, TGA of G-OH nanocomposites are shown. The first weight loss is due to pyrolysis of NR and of the organic ingredients and is indicated by the first arrow on the left. The second weight loss is due to the reaction of carbon filler with oxygen. Residual weight, that can be hardly appreciated from the figure, is due to ZnO.

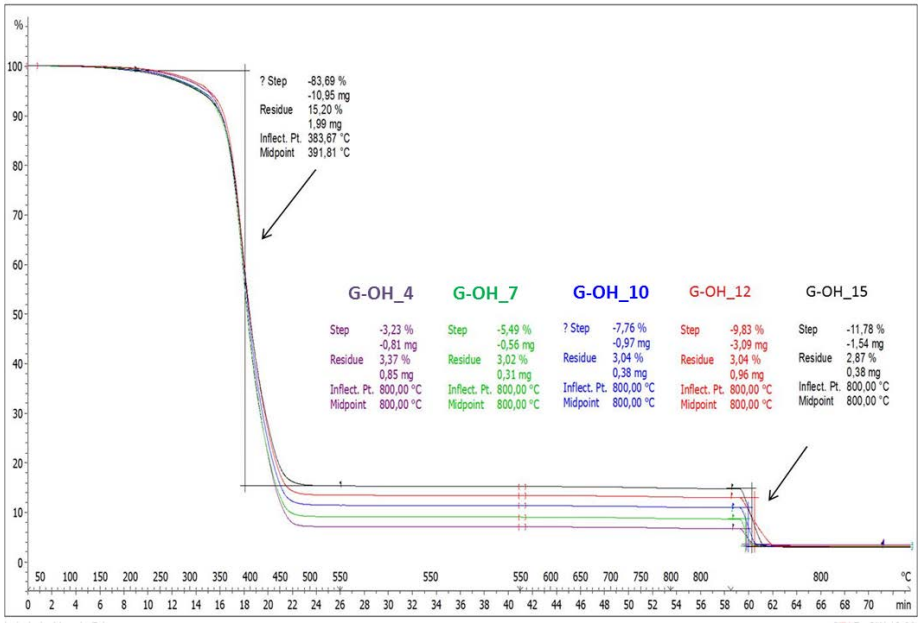

Figure 5.2 TGA thermograph under N_2 of crosslinked G-OH nanocomposites of Table 5.1 (see below)

For the count of experimental phr was used the following procedure. In the TGA analysis, the value of the second loss represents the weight percentage of the filler introduced into the composite. To find the corresponding phr has set the following proportion:

$$phr_{tot}: 100 = \mathbf{phr_{exp}}:\% \ wt_{loss}$$

Where 100 indicates 100% of the mass of the sample used for analysis and TGA phr_{tot} indicates the sum of all components amounts given in phr.

5.4 Structure of the nanocomposites

Structure of the nanocomposites was investigated by means of transmission electron microscopy and X-Ray diffraction.

5.4.1 TEM analysis

In particular, TEM analysis was performed on the nanocomposite containing 9.5 phr of G-OH, as precipitated from the latex. Figure 3 shows the TEM micrograph.

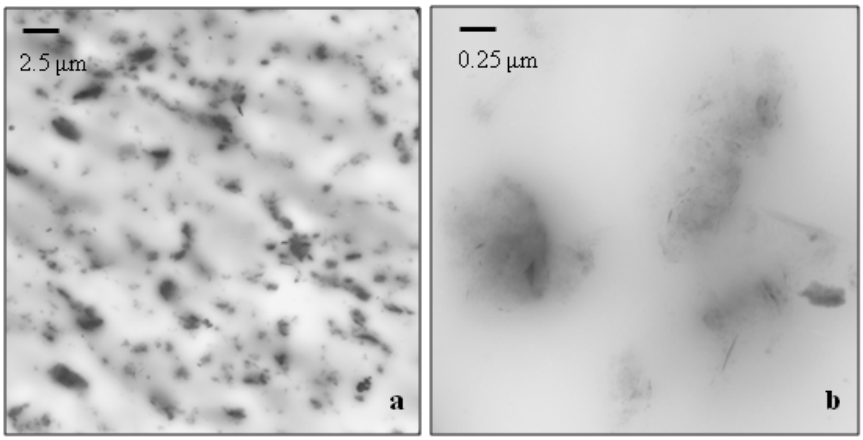

Figure 5.3 TEM micrographs of G-OH_9 nanocomposite, as precipitated from the latex

At low magnification (Fig. 5.3a), aggregates of G-OH and few agglomerates are visible. In particular, the aggregates have sub-micrometric dimensions and the size of agglomerates is lower than 3 µm. The G-OH in NR appears evenly distributed. At high magnification (Fig. 5.3b) it is possible to observe stacked layers with different dimensions, some of which containing only few layers. Very few isolated layers are also visible.

5.4.2 X-Ray diffraction

XRD analysis was taken on crosslinked nanocomposite containing 15.1 phr of G-OH. Figure 5.4 shows the XRD pattern of pristine nanosized graphite (Fig. 5.4a), of G-OH (Fig. 5.4b) and of the nanocomposite based on G-OH (Fig. 5.4c).

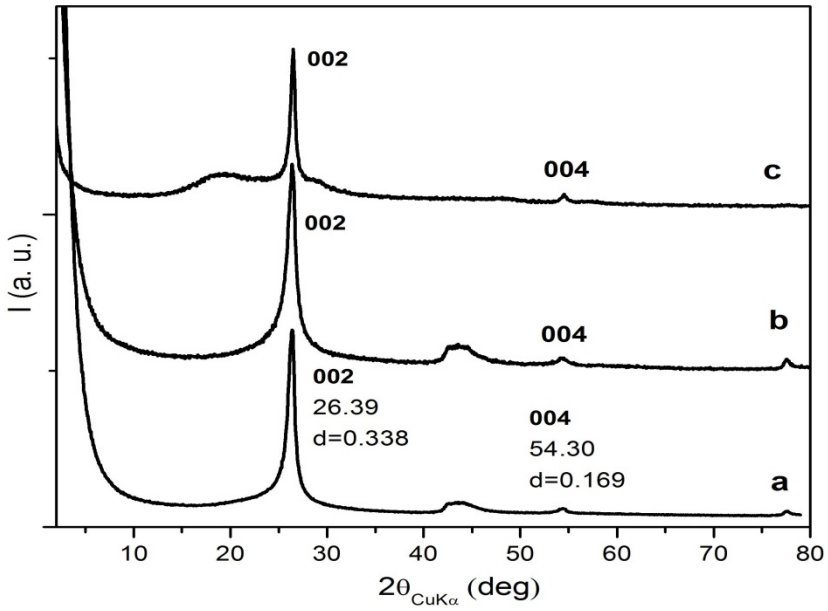

Figure 5.4 XRD pattern of pristine nanosized graphite (Fig. 5.4a), of G-OH (Fig. 5.4b) and of the nanocomposite based on G-OH (Fig. 5.4c)

Patterns in Figure 5.4a and in Figure 5.4b are shown also in Chapter 4, but are here reproduced to facilitate the comparison. As already commented in Chapter 4, (002) reflection, clearly visible in the pattern of pristine nanoG, remains at the same 2θ value in the pattern of G-OH, indicating that the oxidation reaction did not promote expansion of the interlayer distance. (002) reflection remains at the same 2θ value also in the pattern of the nanocomposite. It is possible to comment that expansion of the interlayer distance did not occur either during the preparation of the nanocomposite. It is also worth commenting that such interlayer distance, that can be calculated by applying the Bragg equation to the 2θ value of 002 reflection, is slightly larger, though to a very minor extent, than the one of ordered graphite samples: 0.338 nm in place of 0.335 nm.[2, 7]

The number of stacked layers was calculated by applying the Scherrer equation, already explained in the previous Chapter. Calculated number of stacked layers was, about: 35 in pristine nanoG, 23 in G-OH and 66 in the nanocomposite. It appears that the procedure adopted for oxidizing the nano-graphite to G-OH leads to a reduction of order, with a lower number of layers stacked in the crystalline domain (from about 35 to about 23). Reaggregation of G-OH layers into a crystalline domain occurred when the nanocomposite was vulcanized. It was reported in the literature [3] that the number of layers stacked in crystalline domain, for the same nanoG

used in the present thesis, increased from about 35 to about 70, passing from the pristine nanofiller to the vulcanized nanocomposite. Such reaggregation was attributed to the energy given to the composite during the vulcanization step. Similar comment can be made here.

5.5 Sulphur based crosslinking

Rheometric curves are in Figure 5.5 and data taken from the curves are collected in Table 5.2.

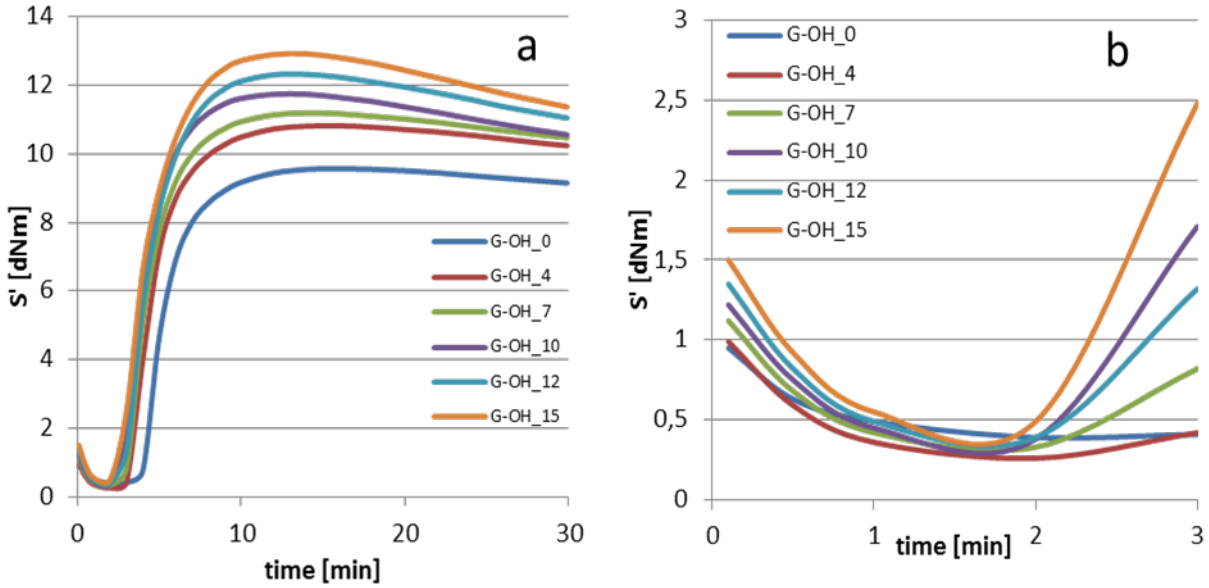

Figure 5.5 Rheometric curves for the crosslinking reaction of nanocomposites of Table 1 (a). Magnification of the curves up to 3 minutes (b)

Table 5.2 Data from crosslinking reactions of nanocomposites containing G-OH as the only filler.

	G-OH_0	G-OH_4	G-OH_7	G-OH_10	G-OH_12	G-OH_15	G-OH_25
M_L	0.39	0.25	0.32	0.36	0.37	0.45	0.68
M_H	9.57	10.83	10.87	11.4	11.97	12.48	13.81
t_{s1}	4.26	3.44	3.18	2.92	3.01	2.97	3.26
t_{90}	8.2	7.55	7.22	6.78	7.29	7.31	8.89

From Figure 5.5a and in particular Figure 5.5b and from the data in Table 5.2, it appears that M_L values, that indicate the viscosity of the nanocomposite, increase, as expected, by increasing the amount of G-OH in the nanocomposite.

The induction time of vulcanization is revealed by t_{s1} parameter. t_{s1} values as a function of the G-OH content are plotted in the graph of Figure 5.6a. t_{s1} values of the nanocomposites with G-OH were also normalized with respect to t_{s1} values of the matrix : the $t_{s1}/t_{s1matrix}$ ratio is plotted in Figure 5.6b.

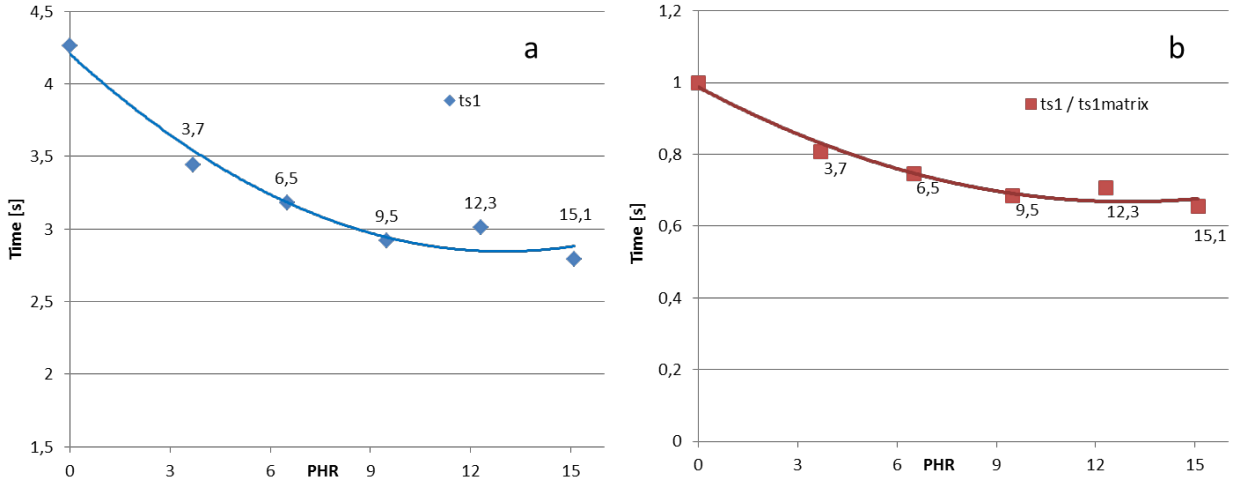

Figure 5.6 t_{s1} vs G-OH content (phr) (a), $t_{s1}/t_{s1\ matrix}$ vs G-OH content (phr) (b) for the crosslinking reactions of nanocomposites of Table 1

It is evident that the induction time of vulcanization consistently decreases by enhancing the amount of G-OH in the nanocomposite. In the literature, it is reported that faster vulcanization reactions are promoted by carbon allotropes, such as carbon black [4], nanosized graphite [3] and carbon nanotubes [5]. In the rubber field, the accelerating effect of carbon allotropes is in general attributed to the improved thermal conductivity and the basic pH. Investigations were not performed in this thesis to clarify the reason of lower induction times. More subtle differences appear for t_{90} values.

Curves in Figure 5.7a and data in Table 5.2 show also that M_H values consistently increase by enhancing the content of G-OH. Graph in Figure 5.7 reports M_H and (M_H – M_L) values as a function of the G-OH content.

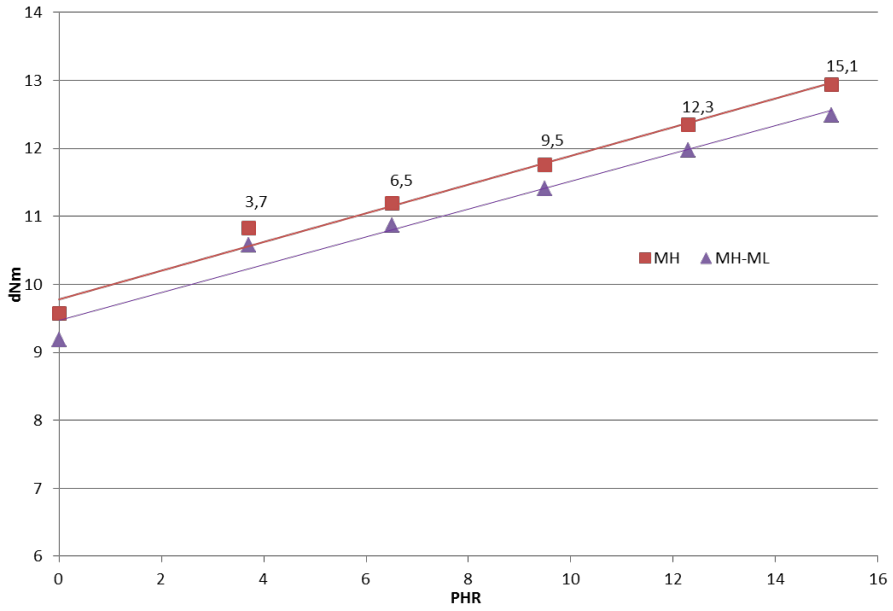

Figure 5.7 M_H and (M_H – M_L) as a function of G-OH content for the crosslinking reactions of nanocomposites of Table 5.1

The linear increase of M_H with G-OH content, at least up to 15.1 phr as G-OH content, suggests that G-OH was evenly dispersed in the NR matrix. This comment is substantially in line with what shown by TEM micrograph shown in Figure 5.4. The minor increase of MH passing from 15 phr to 25 phr as G-OH content can be explained with the unsatisfactory incorporation of G-OH in the NR matrix.

5.6 Dynamic-mechanical properties

Dynamic-mechanical properties were determined by applying sinusoidal stress in the torsion mode to the crosslinked nanocomposites, as described in the experimental part. Figure 5.8 and Figure 5.9 show the dependence of the storage modulus G' and of the loss modulus G", respectively, on the strain amplitude, in semilogarithmic plots. Table 5.3 reports data of G' at minimum strain (0.28%), ΔG' (0.28% – 25%) and of the maximum value of the G" loss modulus.

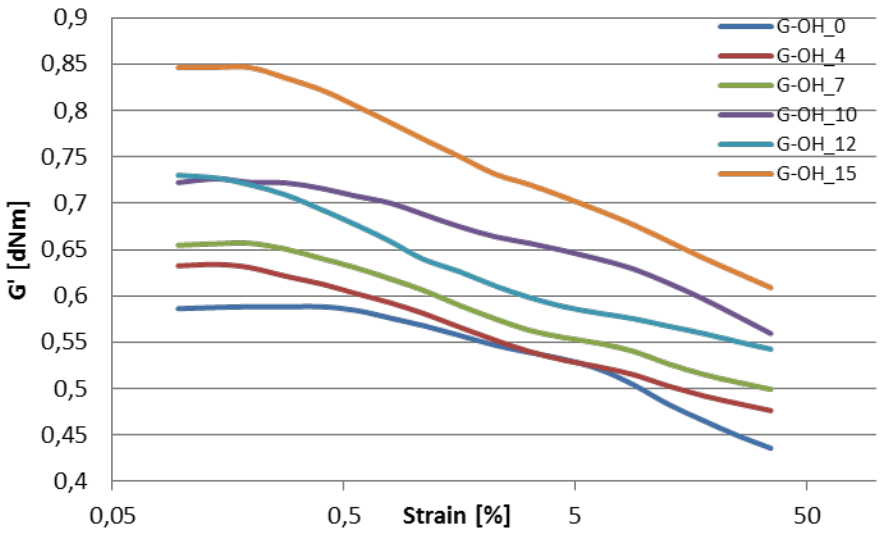

Figure 5.8 Storage modulus G' a s a function of strain amplitude for crosslinked nanocomposites of Table 5.1

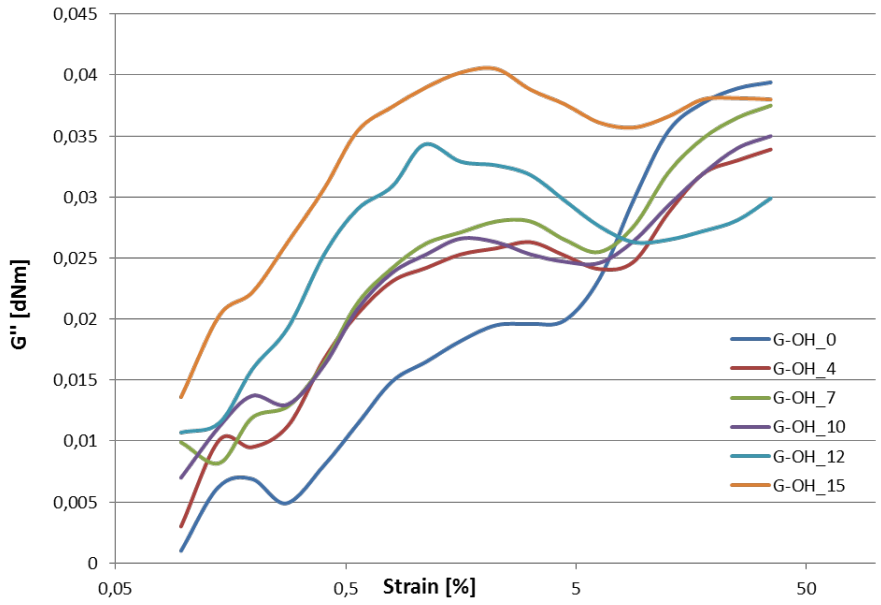

Figure 5.9 Loss modulus G" a s a function of strain amplitude for crosslinked nanocomposites of Table 5.1

Table 5.3 Data on dynamic storage modulus, G', and dynamic loss modulus, G", obtained for G-OH composites of Table 5.1

	G-OH_0	**G-OH_4**	**G-OH_7**	**G-OH_10**	**G-OH_12**	**G-OH_15**	**G-OH_25**
G' (0.28%)	0.588	0.621	0.65	0.722	0.709	0.835	0.856
ΔG' (0.28% – 25%)	0.139	0.137	0.144	0.144	0.158	0.21	0.197
G" (max)	0.039	0.034	0.038	0.035	0.034	0.04	0.039

In Figure 5.8, it is possible to observe that modulus at minimum strain almost consistently increases by enhancing the amount of G-OH in the composites. Appreciable decrease of G', though in limited range as absolute values, can be observed, as the strain amplitude increases, with overlapping of the curves due to composites G-OH_12 and G-OH_10.

The decrease of the modulus with the strain amplitude is a phenomenon known as Payne effect.[6]

Quantitative evaluation of the Payne effect is given by ΔG' values, that, according to the theory, are in line with G" values. In Table 5.3, it is possible to observe that ΔG' values are almost constant up to 9.5 phr as G-OH content, whereas they appear to increase in the composites with G-OH content equal or larger than 12.3 phr.

In Figure 5.9, G" values lie in limited ranges. However, it could be commented that only in the case of nanocomposites with G-OH content from 12.3 phr is possible to see that the curves pass through a maximum. When a filler network is present in the composite material, such shape of the curve indicates the occurring of a maximum of the filler networking phenomenon, that means of the breaking up and re-formation of the filler network. This does not necessarily mean that the filler is above its percolation threshold. In fact, filler aggregates can join together either by direct contact or via layer of polymer shell around them. Moreover, it is known in the field of polymer melts and elastomers that the Payne effect occurs also when the filler is below its percolation threshold. [8-13]

As written in Chapter 2, in filled polymer melts and elastomers, the modulus enhancement as a consequence of the presence of a filler is given by the Guth-Gold-Smallwood equation (Guth, 1945; Guth and Gold, 1938; Smallwood, 1944):

$$E/E_0 = 1 + 0.67f\varphi + 1.62 f^2\varphi^2$$

where, E and E_0 are the initial modulus of filled and unfilled material, respectively, ϕ is the filler volume fraction, the quadratic term accounts for the mutual disturbance caused by the spherical particles and f is a shape factor that allows to apply the equation to non-spherical fillers. Such equation is not valid for ϕ values above a critical threshold ϕ_p, where ϕ_p is the filler volume fraction at which filler percolation occurs, i.e., as written above, filler aggregates join together either by direct contact or via layer of polymer shell around them. Nanofillers are endowed with high surface area and are thus supposed to achieve percolation at very low content in the polymer matrix.

It was thus worthwhile to investigate the occurrence of a percolation threshold in the case of G-OH composites. The existence of a filler percolation threshold was investigated by applying a model proposed by Huber and Vilgis (Huber and Vilgis, 1999) for elastomers filled with spherical nanostructured CB. According to this model, the excess of initial modulus $(E - E_0)/E_0$ has a linear dependence on the filler content below the percolation threshold whereas above this limit it scales with a power law with exponent 4.

A double logarithmic plot of the excess of G' modulus as a function of G-OH volume fraction, elaborated from initial modulus values, is shown in Figure 5.10.

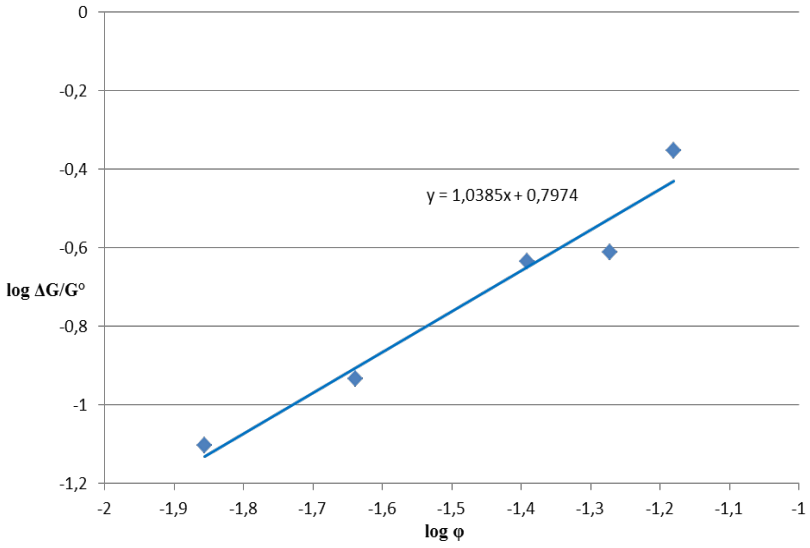

Figure 5.10 Double logarithmic plot of the excess of G' storage modulus $((G' - G'_0)/G_0)$ as a function of G-OH volume fraction (Huber–Vilgis plot)

The plot of Figure 10 reveals that experimental data can be linearly interpolated with one straight line, with 1,039 as the slope. This finding leads to exclude that G-OH is able to give rise to a filler network up to this level of concentration in the polymer matrix. The Huber Vilgis plot was prepared also with data concerning the initial modulus E, obtaining very similar results.

5.7 Quasi-static properties

Tensile measurements were carried out on crosslinked nanocomposites, by applying uniaxial stretching, as described in the experimental part. The graph shown in Figure 5.11 shows the dependence of nominal stress on nominal strain. Values of stresses at different elongations and at break as well as of energy at break are reported in Table 5.4.

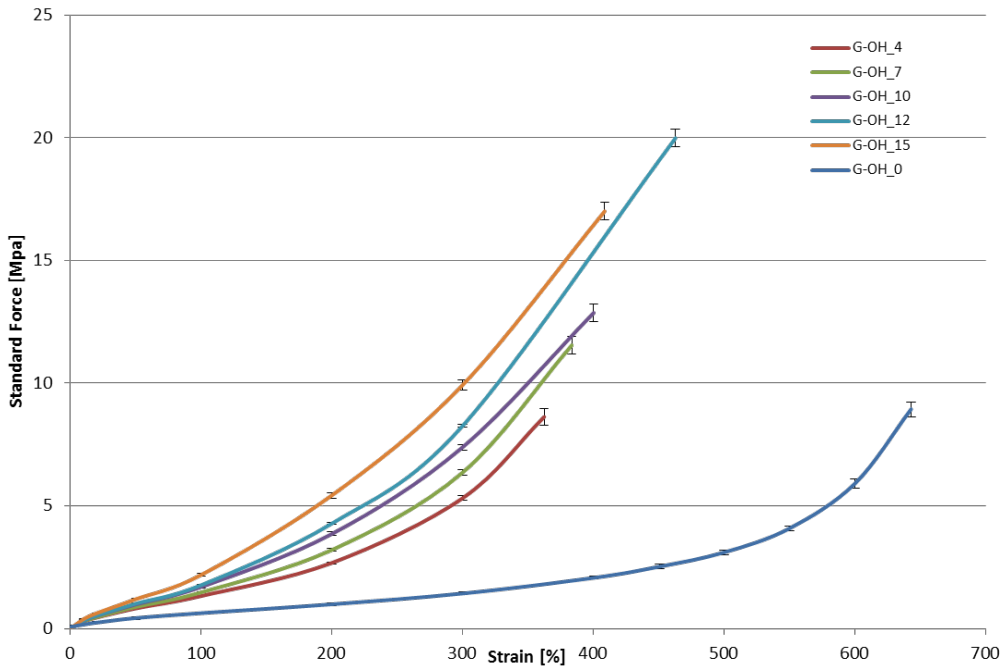

Figure 5.11 Nominal stress–nominal strain curves, with standard deviations, obtained for crosslinked G-OH nanocomposites of Table 5.1

Table 5.4 Tensile properties of crosslinked G-OH nanocomposites of Table 5.1

	G-OH_0	**G-OH_4**	**G-OH_7**	**G-OH_10**	**G-OH_12**	**G-OH_15**
σ_{50} (MPa)	0.43	0.824	0.883	0.982	1.016	1.197
σ_{100} (MPa)	0.635	1.328	1.475	1.697	1.771	2.188
σ_{300} (MPa)	1.441	5.314	6.357	7.39	8.259	9.923
$\sigma_{300} / \sigma_{100}$	2.27	4	4.31	4.356	4.662	4.536
σ_B (MPa)	8.94	8.627	11.548	12.868	19.99	17.007
ε_B (%)	643.13	362.45	383.54	400.29	462.85	408.69
Energy (J/cm^3)	14.55	9.56	16.59	15.29	30.19	23.48

As expected, the lowest values of stresses at every elongation and the largest deformation were obtained for neat NR. G-OH led to the increase of stresses and to the reduction of strain at break. Stresses appear to increase consistently with G-OH content, whereas this cannot be observed for the ultimate properties. The latter finding could be attributed to the presence of agglomerates of G-OH.

From stress-strain curves, values of E initial modulus were derived, as the slope at the origin. They are shown in Table 5.5, together with G' values at minimum (0.28%) strain.

Table 5.5 Initial modulus E, and storage modulus G' at 0.28% strain for crosslinked G-OH nanocomposites of Table 5.1

Sample	**G-OH [phr]**	**G-OH [φ]**	**E [MPa]**	**G' (0.28%) [Mpa]**
Neat	0	0	1.73	0.59
3 phr	3.7	0.014	1.98	0.62
6 phr	6.5	0.023	2.26	0.65
9 phr	9.5	0.041	2.19	0.72
12 phr	12.3	0.054	2.4	0.71
15 phr	15.1	0.066	2.86	0.84

5.8 Composites based on either nanoG or G-OH. Comparison of dynamic-mechanical and tensile properties

In the scientific literature, studies have been reported on nanocompoites based on poly(1,4-*cis*-isoprene) and the same type of nanosize graphite used in this thesis, that means Synthetic Graphite 8427® from Asbury Graphite Mills Inc (3). Such nanosized graphite (nanoG) was used in its pristine state, without any modification. Composites were prepared by melt blending synthetic poly(1,4-*cis*-isoprene) and nanoG in an internal mixer, without any pre-mixing step. As mentioned above, the number of stacked layers in the final composites was calculated to be about 70.

It is interesting to compare the results reported in the literature [3] and obtained in the present thesis.

In Table 5.6 are reported values of G' at minimum strain of composites based on IR and nanoG (3) and on NR and G-OH, prepared in this thesis, normalized with respect to the values of neat polymer matrix: $(G'/G'_0)_{\gamma min}$

Table 5.6 values of G' at minimum strain and E of composites based on IR and nanoG and on NR and G-OH, normalized with respect to the values of neat polymer matrix: $(G'/G'_0)_{\gamma min}$; $(E/E_0)_{\gamma min}$

PHR	**(E/E_0)**		**(G/G_0)**	
	G	***G-OH***	***G***	***G-OH***
0	1	1	1	1
1	1,031		1,02	
2	1,076		1,02	
3,7		1,145		1,051
4	1,122		1,047	
6,5		1,306		1,102
8	1,214		1,093	
9,5		1,266		1,220
12	1,344		1,186	
12,3		1,387		1,203
15,1		1,653		1,424
16	1,489		1,302	

[a] Source for nanoG: articolo nanoG RCT Source for G-OH: this thesis

To better appreciate the comparison, points due to E/E0 and to G/G0 ratios are plotted In Figure 5.12a and in Figure 5.12b, respectively.

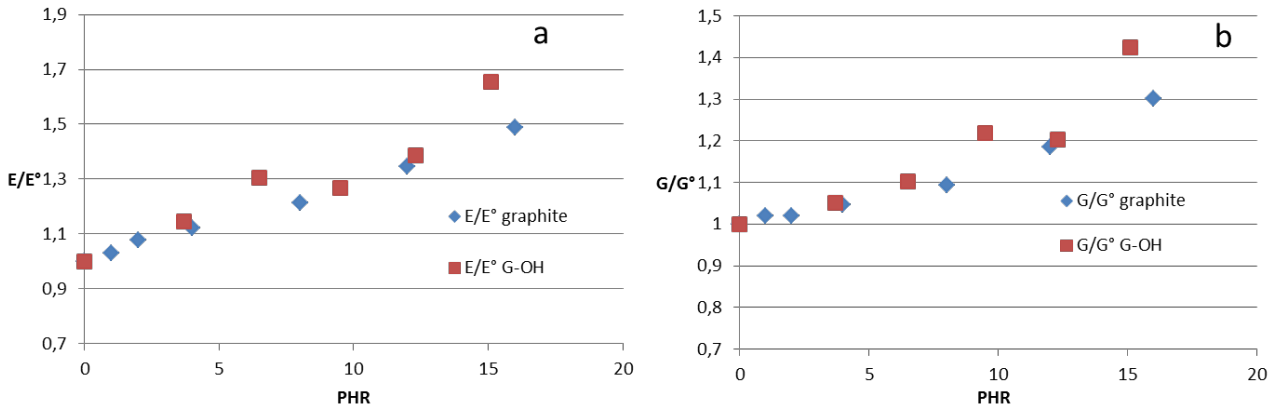

Figure 5.12 Comparison between (E/E°) of elastomers with nanoG and with G-OH (a) and (G/G°) of elastomers with nanoG and with G-OH (b)

It appears that the reinforcement promoted by the two types of nanosized graphite, in its pristine state (nanoG) or oxidized to G-OH, is quite similar. Mechanical reinforcement, at the same volume fraction and below the percolation threshold, depend on the shape factor *f*. In the case of graphite, the shape factor *f* is given by the ratio between the largest lateral dimension and the thickness of the stack. It was reported above that the calculated number of stacked layers in nanoG and G-OH aggregates in the crosslinked composites is almost the same. This result at least allows to assume a similar value of the shape factor *f*.

However, a more careful inspection of the graphs allows to observe that G-OH, mixed with NR first in NR latex and then via melt blending, brings about a slightly higher reinforcement than nanoG, mixed in IR via melt blending. In particular, it seems that G-OH leads to larger reinforcement as the content in the rubber matrix increases. It is clear that this is only an indication, that should be supported by tests performed with higher nanofiller content. Larger mechanical reinforcement by G-OH could be due to better dispersion in the rubber matrix, thanks to the latex blending, as well as to the interaction of the hydroxyl groups with the polar ingredients used for vulcanization.

5.9 Electrical conductivity

Conductivity tests were carried out on the vulcanized samples. For sample with G-OH content up to 15 phr, values of resistivity of the order of 10^{10} were measured. Hence, it can be concluded that, in line with what has been said above, the network between the particles of filler was not created and then the samples were non-conductive. Electrical conductivity was found for the sample with 25 phr as G-OH content. This is an important finding. In fact, it demonstrates that G-OH is a conductive filler. This is in line with the objectives, as it demonstrates that the oxidation with KOH does not disturb the sp^2 hybridization of the carbon atoms.

5.10 Conclusions

Nanocomposites were prepared based on NR and G-OH from the reaction of nanoG with KOH. Latex blending was performed adding, to NR latex, G-OH in different amounts, from about 4 to about 25 phr. Dispersions of G-OH in NR latex were stable and precipitation occurred through addition of sulphuric acid.

Further ingredients for sulphur based crosslinking were then added in an internal mixer and nanocomposites were vulcanized. G-OH was found to promote faster vulcanization reactions: induction crosslinking time decreased with the concentration of G-OH in NR. The maximum modulus M_H increased almost linearly with G-OH concentration.

TEM analysis revealed even dispersion of G-OH.

From dynamic-mechanical measurements in the shear mode, storage modulus G' was observed to increase with G-OH content in the nanocomposites and to decrease with the strain amplitude reduction. Larger increase was observed for about 15 phr as G-OH content and the curve of G'' vs strain amplitude showed a maximum for 12 and 15 phr. In spite of these results, indications were not collected of the occurrence of G-OH percolation.

G-OH caused the enhancement of stresses at all the elongations, in tensile tests, in the presence of some inconsistencies of the ultimate properties.

The mechanical reinforcement obtained with G-OH in NR, from latex blenidng, was compared with the one obtained with NanoG in IR, from melt blending. Preliminary indications show slightly larger reinforcement with G-OH based system.

As the last comment, it is worth saying that the number of stacked G-OH layers in the crosslinked nanocomposite from latex blending was found to be pretty similar to the number of nanoG stacked layers found in IR based nanocomposites from melt blending. In the previous Chapter, Chapter 4, it was reported that the number of stacked layers in G-OH is about 23, with respect to 35 in the pristine nanoG. It seems thus that the reaction of nanoG with G-OH has the potentiality to prepare few layer graphene but that the melt blending step followed by high pressure vulcanization brings back G-OH to the usual crystalline order already detected for nanoG. It could be thus commented that the real potentiality of G-OH in NR nanocomposites have still to be explored.

5.11 References

[1] Wu Y., Wang Y., Zhang H., Wang Y., Yu D., Zhang L., Yang J. (2005) Rubber–pristine clay nanocomposites prepared by co-coagulating rubber latex and clay aqueous suspension, Compos. Sci. Technol. 65: 1195-1202

[2] Hummers, W. S.; Offeman, R. E. J. Am. Chem. Soc. 1958, 80, 1339.

[3] M. Galimberti, Rubber Chemistry and Technology, Vol. 87, No. 3, pp. 417–442 (2014)

[4] S. Agnelli, V. Cipolletti, S. Musto, M. Coombs, L. Conzatti, S. Pandini, T. Riccò, M. Galimberti, "Interactive effects between carbon allotrope fillers on the mechanical reinforcement of polyisoprene based nanocomposites *eXPRESS Polymer Letters 8(6)* (2014) 436

[5] A. De Falco, Journal of Applied Polymer Science, Vol. 113, 2851–2857 (2009)

[6] A. R. Payne, Dynamic properties of filler-loaded rubbers, Chapter 3 in Reinforcement of elastomers, G. Kraus Ed., Interscience Publishers, New York, London, Sydney, pag 69 – 114. 1965

[7] Mauro, M., Maggio, M., Cipolletti, V., Galimberti, M., Longo, P., & Guerra, G. (2013). Graphite oxide intercalation compounds with rotator hexagonal order in the intercalated layers. Carbon, 61, 395-403.

[8] L. Chazeau, J.D. Brown, L.C. Yanyo, S.S. Sternstein Polymer Composites, April 2000, vol 21, p. 202

[9] Sternstein S.S., Zhu A.J. Macromolecules 2002, 35 (vol), 7262 (pag)

[10] Berriot J, Montes H., et al. Macromolecules 2003, 36 (vol), 8107 (pag)

[11] Wang S.G., et al. Macromolecules 2005, 38 (vol), 8816

[12] J. Kalfus, J. Jancar, "Elastic response of nanocomposite poly(vinylacetate)-hydroxyapatite with varying particle shape", Polymer Composites (2007), 365-371.

[13] J. Jancar, J.F. Douglas et al, "Current issues in research on structure-property relationships in polymer nanocomposites", Polymer (2010), 51, 3321-3343.

Chapter VI

6.1 Introduction

In this Chapter is reported preliminary investigation on the synthesis of polyurethanes in the presence of nanosized graphite with high surface area, either pristine or containing hydroxyl groups. The selection of polyurethanes was based on the following reasons:

(i) polyurethanes are the most versatile polymers: thermoplastic, elastomeric, thermoplastic elastomers, thermoset, foams.

(ii) polyurethanes presence in the market is steadily increasing.

(iii) main stumbling block that prevents larger diffusion of PU is their flame resistance. PU can not be classified in the Class A for the flame resistance.

(iv) PU are based on polyols. G-OH bears hydroxyl groups on the graphene layers, essentially on the edges. G-OH are thus likely to become comonomers in the polyurethane chains.

On the basis of these considerations, objectives for preparing nanocomposites based on PU and G-OH was to obtain materials with similar properties but with improved thermal properties, namely the flame resistance.

Polyurethanes were prepared by mixing NanoG or G-OH in the polyol mixture, subsequently performing the polymerization with MDI. It was reported in Chapter 4 the stability of G-OH in the polyol mixture. This should ensure the even dispersion of G-OH in the final polymer.

As the objective was the improvement of the flame resistance, low amount of either nanoG or G-OH was used, as it is typical for nanosized carbon allotropes, such as CNT, that are used at 1, 2 % by weight.

In the present thesis, feasibility of polymerizations was first investigated. Interaction of G-OH with PU chains was studied by means of NMR spectroscopy, analyzing the microstructure of the polymers. Thermal properties of the polymers, in the presence and in the absence of nanofillers, were studied by means of TGA and DSC analysis.

6.2 Synthesis of polyurethanes

6.2.1 Experimental conditions

Polyurethanes were prepared either in the absence or in the presence of the nanosized graphite, either pristine or modified. G-OH-M and G-OH-TM were used as the modified graphites. The procedure adopted for the preparation of PU is summarized in Scheme 6.1.

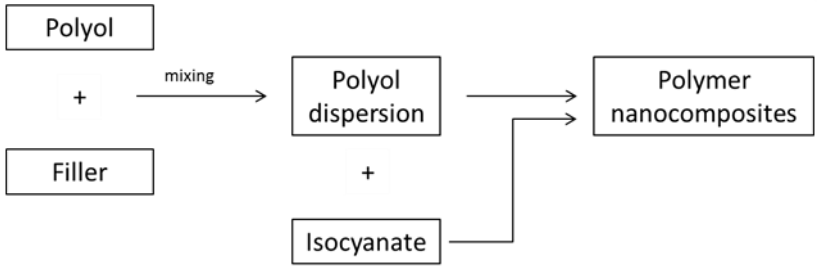

Scheme 6.1 Procedure followed for preparation of polyurethanes nanocomposites

In the absence of the carbon filler, polyol and isocyanate were mixed and then stirred at given temperature and time, obtaining the polymer.

In the presence of the carbon filler, the nanosized graphite was first mixed with polyols. Standard procedure for the preparation of PU was then followed.

In Table 6.1, polymerization conditions for the synthesis of polyurethanes are reported.

Table 6.1 Synthesis of poly(urethanes): polymerization conditions

Run	**Polyol[1] (g)**	**MDI[2] (g)**	**Carbon filler[3]**		**Temperature (°C)**	**time (min)**
			type	**amount**		
1	10	3	-	-	23	5
2	10	3	nanoG	0.1	23	5
3	10	3	G-OH-TM	0.1	23	5
4	10	3	G-OH-M	0.1	23	5

[1] AROPOL SPER 1407; [2]ARODUR 621,6; [3] 0.100 g

Reaction between polyol and MDI is expected to occur through the mechanism reported in Scheme 6.2.

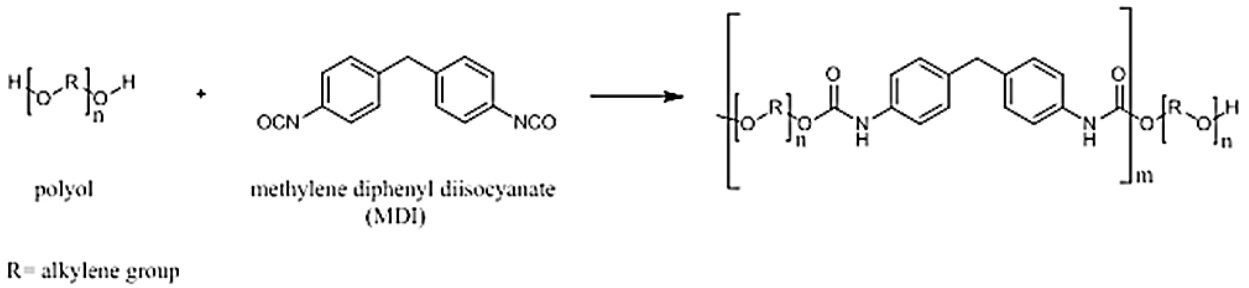

Scheme 6.2 Expected reaction between polyol and MDI

6.3 Characterization of polyurethane nanocomposites

6.3.1 Thermogravimetric analysis

Thermogravimetric analysis (TGA) was used to quantitatively estimate the amount of nanosized graphite in the composite and to study the degradation of PU in the absence and in the presence of nanoG and G-OH. TGA curves of polyurethanes of Table 6.1 are shown in Figure 6.1.

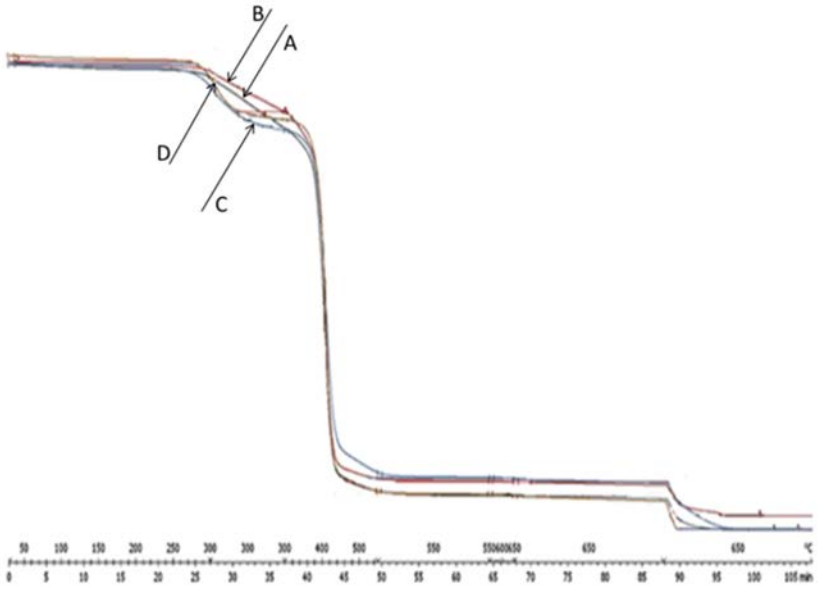

Figure 6.1 TGA thermograms under N_2 of PU from run 1 (A), run 2 (B), run 3 (C) and run 4 (D) of Table 6.1

Weight losses occur at three different temperatures, for all of the PU, with or without nano-graphite.

In Table 6.2 are reported the weight losses of the polymer nanocomposites at different temperatures.

Table 6.2 Weight losses of nanocomposites reported in Table 6.1

Sample	**Temperature**		
	300°C	*407°C*	*649°C*
PU - A	13.36	78.73	6.99
PU/nanoG - B	10.95	80.61	7.30
PU/G-OH-TM - C	12.01	76.34	10.76
PU/G-OH-M - D	12.55	77.92	8.41

Weight losses at different temperatures appear very similar for all of the PUs. It could be noticed a slightly higher weight loss for G-OH based PUs at the lowest temperature.

6.3.2 Microstructure of polyurethanes

Microstructure of polyurethanes was investigated through ^{1}H-NMR spectroscopy. In Figure 6.2, it is shown the NMR spectra of the reagents, polyol (Fig. 6.2a) and MDI (Fig. 6.2b). In Figure 6.3 are reported the NMR spectra of the polymer nanocomposites of Table 6.1.

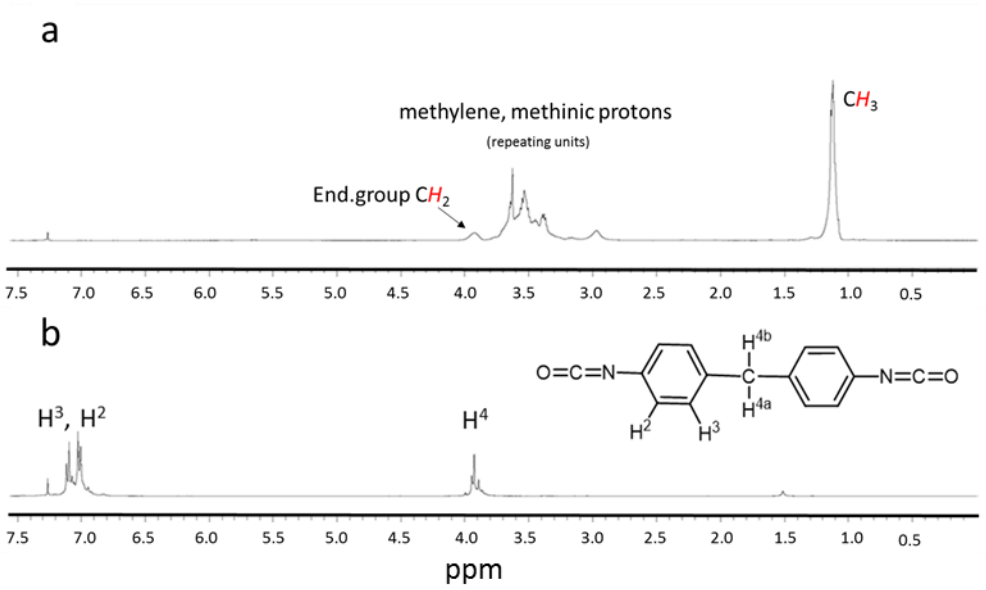

Figure 6.2 400 MHz ^{1}H NMR spectra in $CDCl_3$ of polyol (a) and MDI(b)

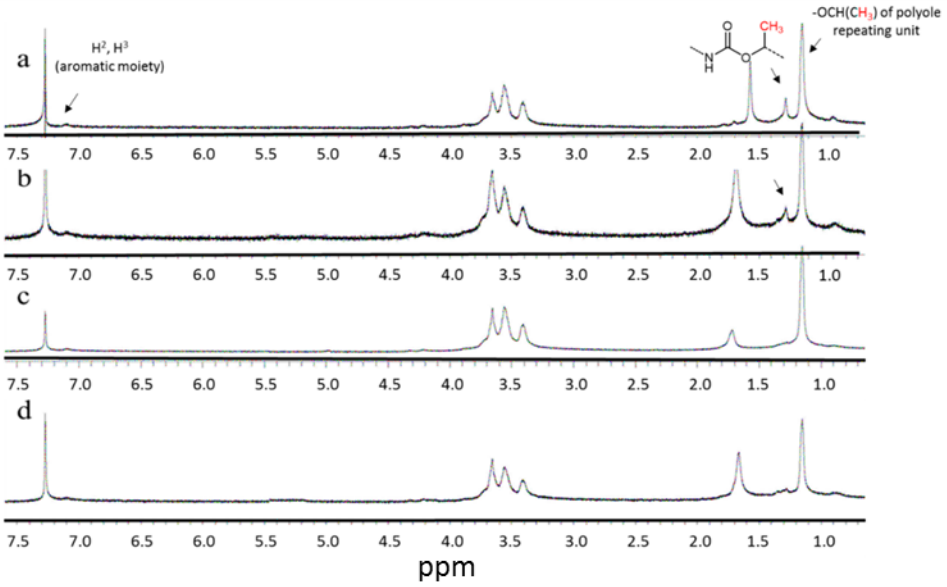

Figure 6.3 400 MHz ^{1}H NMR spectra in $CDCl_3$ PU from run 1 (a), run 2 (b), run 3 (c) and run 4 (d) of table 6.1

It is worth commenting the spectra of Figure 6.3. Spectra in Figure 6.3a and 6.3b are very similar to each other. Spectra of polyurethane from run 1 and 2 of Table 6.1 show two types of methyl group: at 1.09 ppm and at 1.38 ppm there are respectively the that one from the repeating unit of polyol and the methyl group linked to the methine carbon near the carbamic group.

In Figures 6.4c and 6.4d is not visible the signal at 1.38 ppm. It is probably in a small amount because the isocyanate is also involved in a bond with the OH of the G-OH.

These experimental evidences from NMR spectra lead to hypothesize that G-OH takes part in the formation of urethane linkages whereas nanoG does not. In Scheme 6.3, it is shown the formation of urethane group from G-OH and MDI.

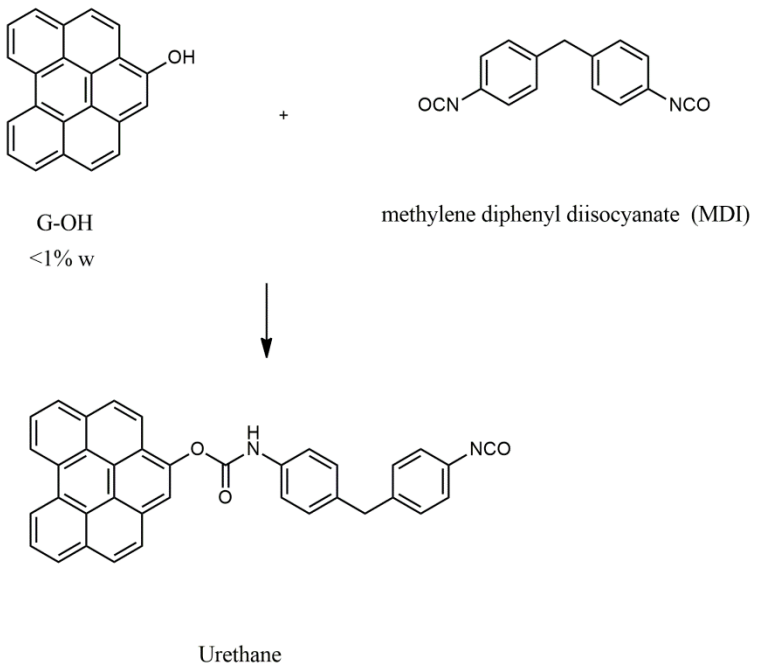

Scheme 6.3 Formation of urethane group from G-OH and MDI (only one OH group on G-OH is indicated)

6.3.3 Thermal transitions

DSC analysis were carried out to investigate thermal transitions of PU sample and, in particular, the effect of the nanofillers on the glass transition of the polymer nanocomposites.

In Figure 6.4 are shown the DSC thermographs of samples reported in Table 6.1

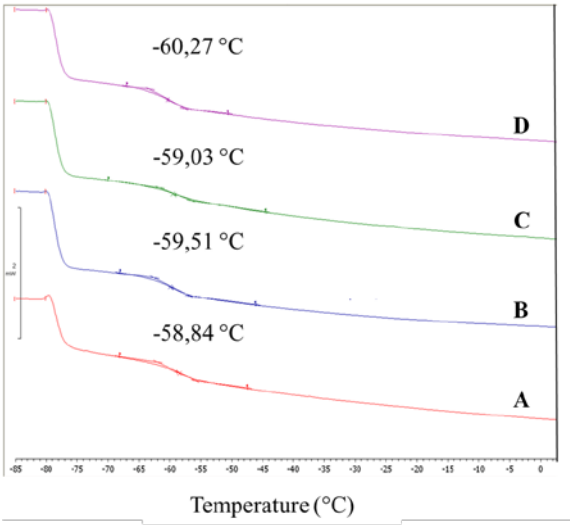

Figure 6.4 DSC analysis of PU from run 1 (A), run 2 (B), run 3 (C) and run 4 (D) of Table 6.1

Differences in Tg appear very low indeed, in line with the limited amount of the carbon nanofiller.

6.3.4 X-Ray analysis

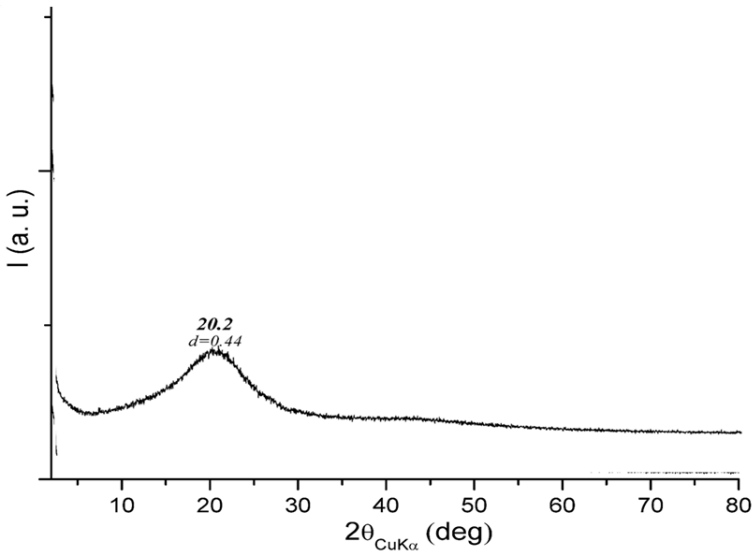

Figure 6.5 XRD patterns of polyurethane from Run 3 of Table 6.1

X-Ray analysis was performed on polyurethane from Run 3 of Table 6.1, containing G-OH-TM. Peaks due to crystalline G-OH cannot be observed. However, this cannot be commented as

indication of exfoliation of G-OH, as the amount of the carbon ananofiller is probably too low to allow the detection of (002) reflection.

6.4 Conclusions

Polyurethanes were prepared in the presence of nanosized graphite containing hydroxyl functional groups, G-OH. Stable dispersion of G-OH in polyol mixture was prepared. Microstructure of PU was modified in the presence of G-OH, suggesting that hydroxyl groups can take part in the polymerization process. Main thermal properties of PU, degradation temperatures and glass transition temperature, were substantially not affected by the carbon filler.

These preliminary data allow to pursue the preparation of PU in larger scale, in order to assess the flame resistance of the nanocomposites.

SECTION III Experimental Parts

Chapter VII

7.1 Materials

Reagents and solvents commercially available were purchased and used without further purification: potassium hydroxide pellets (Carlo Erba Reagenti), high surface area graphite (trade name Synthetic Graphite 8427) from Asbury Graphite Mills Inc., with a minimum carbon wt % of 99.8 and a surface area of 330 m^2/g, 1-dodecanethiol 98+% (Aldrich), maleic anhydride 99% (Aldrich), AIBN (Aldrich), anthracene (Carlo Erba), sulphuric acid 98% (Sigma–Aldrich), chloroform (Aldrich), dichloromethane (Aldrich), ethanol (Fluka), NR latex, sulphuric acid 98% (Sigma–Aldrich), zinc oxide (Zincol Ossidi), stearic acid (Sogis), (1,3-dimethylbutyl)-*N*'-phenylp-phenylenediamine (6PPD) (Crompton), sulphur (Solfotecnica), *N*-tert-butyl-2-benzothiazyl sulfenamide (TBBS) (Flexsys), AROPOL SPER 1407 is a mixture of 92% of polyol Mn~6000 (hydroxyl number 28) and 8% of butanediol, methylene diphenyl diisocyanate (MDI) (ARODUR 621.6), *N*,*N*,*N*-Triethylamine (Aldrich).

7.2 Synthesis of hydroxy–graphite (G–OH) obtained by thermal treatment (G-OH-T)

In a 100 mL round bottom flask equipped with magnetic stirrer were poured in sequence pristine graphite (2.81 g, 39 mmol), KOH powder (2.19 g, 39 mmol) and H_2O (22 mL). The mixture was left to stir at 70°C for 4 hours. After this period, the resulting mixture was first kept to room temperature and removed from the flask using deionized water (5 mL). The so obtained suspension was kept in a Büchner funnel with a sintered glass disc and was purified from the excess of KOH washing repeatedly with distilled water (6x100 mL) under vacuum. The obtained solid was put in an oven to remove excess water. It were obtained 2.60 g of black powder. IR

(KBr) $_{vmax}$ 3282 (O-H stretch), 3000 (aromatic =C-H stretch), 2917 (methylene C-H stretch, ν_{as}), 2848 (methylene C-H stretch, ν_s), 1786 – 1669 (combination bands), 1560 – 1448 (C-C aromatic ring stretch), 1353 (in plane O-H bend), 1108 (C-O stretch), 967 (out of plane, =C-H bend) cm^{-1}.

7.3 Synthesis of hydroxy–graphite (G–OH) obtained by mechanical treatment (G-OH-M)

7.3.1 Method A

The synthesis of hydroxy–graphite (G–OH) was performed using a planetary ball mill S100 from Retsch, having the grinding jar moving in a horizontal plane, with a volume of 0.3 L. The grinding jar was loaded with 6 ceramic balls having a diameter of 20 mm. Graphite (1 g, 14 mmol), KOH powder (20 g, 356 mmol) and H_2O (6.5 mL) were put into the jar, that was allowed to rotate at 300 rpm, at room temperature, for 10 hours. After this time, the mixture was placed in a Büchner funnel with a sintered glass disc and repeatedly washed with distilled water (6 x 100 mL) under vacuum. Finally, the obtained solid was put in an oven to remove excess water. It were obtained 0.65 g of black powder. IR (KBr) $_{vmax}$ 3417 (O-H stretch), 3052 (aromatic =C-H stretch), 2917 (methylene C-H stretch, ν_{as}), 2858 (methylene C-H stretch, ν_s), 1786 – 1669 (combination bands), 1573 – 1504 (C-C aromatic ring stretch), 1382 (in plane O-H bend), 1116 (C-O stretch), 656 (out of plane , =C-H bend) cm^{-1}.

7.3.2 Method B

The synthesis of hydroxy–graphite (G–OH) was performed using a planetary ball mill S100 from Retsch, having the grinding jar moving in a horizontal plane, with a volume of 0.3 L. The grinding jar was loaded with 6 ceramic balls having a diameter of 20 mm. Graphite (13 g, 0.18 mol), KOH powder (100 g, 1.78 mol) were put into the jar, that was allowed to rotate at 300 rpm, at room temperature, for 15 hours. After this time, the mixture was placed in a Büchner funnel with a sintered glass disc. It was repeatedly washed with distilled water (6 x 100 mL) under vacuum. The resulting solid was put in an oven to remove water. It were obtained 12.2 g of black powder. IR (KBr) $_{vmax}$ 3407 (O-H stretch), 3052 (aromatic =C-H stretch), 2934 (methylene C-H stretch, ν_{as}), 2847 (methylene C-H stretch, ν_s), 1714 – 1630 (combination bands), 1579 (C-C

aromatic ring stretch), 1384 (in plane O-H bend), 1117 (C-O stretch), 980 (out of plane , =C-H bend) cm^{-1}

7.4 Synthesis of hydroxy–graphite (G–OH) obtained by thermal and mechanical treatment (G-OH-TM)

In a 100 mL round bottom flask equipped with magnetic stirrer were poured pristine graphite (15 g, 208.3 mmol), KOH powder (11.69 g, 208.3 mmol) and H_2O (117 mL). The mixture was left to stir at 70°C for 4 hours. After this period the resulting mixture was first kept to room temperature and removed from the flask using deionized water (5 mL). The suspension was dried under vacuum and the resulting powder was placed in a planetary ball mill S100 from Retsch, having the grinding jar moving in a horizontal plane, with a volume of 0.3 L. The grinding jar was loaded with 6 ceramic balls having a diameter of 20 mm. The jar was allowed to rotate at 300 rpm, at room temperature, for 5 hours. After this time the powder was moved in four falcon where was added deionized water and centrifuged at 9000 rpm for 10 minutes. The deionized water was changed three times to completely remove all impurities. The obtained solid was put in an oven to remove water traces. It were obtained 13,7 g of black powder. IR (KBr) ν_{max} 3410 (O-H stretch), 2997 (aromatic =C-H stretch), 2900 (methylene C-H stretch, ν_{as}), 2847 (methylene C-H stretch, ν_s), 1640 (C=C alkene stretch), 1580 – 1560 (C=C aromatic ring stretch) 1394 (in plane O-H bend), 1120 (C-O stretch) cm^{-1}.

7.5 Synthesis of graphite(n-dodecan)Sulphane (G-S)

7.5.1 Method A (G-S1)

In a 100 mL two-neck round bottom flask equipped with magnetic stirrer were poured pristine graphite (500 mg, 6.9 mmol), dodecanethiol (2.36 ml, 9.88mmol) and AIBN (50 mg, 304 μmol) as radical initiator. After 20 minutes at room temperature, the mixture was heated at 70°C and maintained at this temperature for 3 hours under nitrogen atmosphere. The resulting mixture was cooled to room temperature and ethanol (7 mL) was added. The solution was centrifuged two times at 3000 rpm for 15 minutes. It were obtained 0.642 g of black powder. IR (KBr) ν_{max} 3000

(aromatic =C-H stretch), 2918 (methylene C-H stretch, ν_{as}), 2849 (methylene C-H stretch, ν_s), 1573 (C=C aromatic ring stretch) cm^{-1}.

7.5.2 Method B (G-S2)

In a 100 mL two-neck round bottom flask equipped with magnetic stirrer were poured pristine graphite (500 mg, 6.9 mmol), dodecanethiol (0.6 ml, 2.5mmol) and AIBN (28 mg, 170 μmol) and ethanol (8 mL, 137 mmol) as solvent. After 20 minutes at room temperature, the mixture was heated at 70°C and maintained at this temperature for 3 hours under nitrogen atmosphere. The resulting mixture was cooled to room temperature and ethanol (7 mL) was added. The solution was centrifuged two times at 3000 rpm for 20 minutes. It were obtained 0.500 g of black powder. IR (KBr) $_{vmax}$ 2918 (methylene C-H stretch, ν_{as}), 2849 (methylene C-H stretch, ν_s), 1573 (C=C aromatic ring stretch) cm^{-1}.

7.6 Diels Alder adduct of maleic anhydride and anthracene (9,10,11,15-tetrahydro-9,10-[3,4]furanoanthracene-12,14-dione)

In a vial equipped with magnetic stirrer were poured anthracene (100 mg, 0.561 mmol) and maleic anhydride (110 mg, 1.68 mmol). The mixture was left to stir at 110°C for 1 hour. After this period the resulting mixture was first kept to room temperature and analyzed by NMR spectroscopy. ^{1}H NMR (400 MHz, $CDCl_3$, δ in ppm): 7.40 (dd, 2H); 7.33 (dd, 2H); 7.20 (ddd, 4H); 4.82 (t, 2H); 3.51 (t, 2H).

7.7 Synthesis of maleic anhydride/graphite adduct (G-A)

7.7.1 Method A (G-A1)

In a closed vial were stirred pristine graphite (500 mg, 6.94 mmol) and maleic anhydride (2.04 g, 20.08 mmol) at 110°C for 1 hour. The resulting mixture was first kept to room temperature, solubilized in chloroform and centrifuged for 15 minutes at 5000 rpm to remove the excess of

maleic anhydride. The supernatant was removed by decant and the procedure was repeated once again. Precipitate was dried with ROTAVAPOR. It were obtained 0.342 g of black powder.

7.7.2 Method B (G-A2)

A mixture of pristine graphite (15 g, 208.3 mmol) and maleic anhydride (40.86 g, 416 mmol) was poured in a 250 mL round bottom flask and stirred at 110°C for 1 hour. After this period was first kept to room temperature and then put in a flask containing an aqueous solution of KOH 1M was added. The mixture was allowed to react overnight. The day after was added an aqueous solution of sulfuric acid (2% w) to neutralize the solution. The resulting mixture was placed in a Büchner funnel with a sintered glass disc and repeatedly washed with distilled water (6 x 100 mL).The solid was put in an oven to remove traces of water. It were obtained 14.85 g of black powder. IR (KBr) $_{\nu max}$ 1780 (anhydride C=O stretch) 1640 (C=C alkene stretch), 1573 - 1517 (C=C aromatic ring stretch), 1302 (carboxylic C=O stretch), 1359 (OH bending); 1120 (C-O stretch) 969 (out of plane, = C-H bend) cm^{-1}.

7.8 Stability test of hydroxy–graphite (G–OH) obtained by thermal and mechanical treatment (G-OH-TM)

7.8.1 Solubility in H_2O

Aqueous solutions of G-OH at different concentrations (1 mg/mL; 0,8 mg/mL; 0,6 mg/mL; 0,5 mg/mL; 0,3 mg/mL; 0,2 mg/mL; 0,1 mg/mL; 0,05 mg/mL; 0,025 mg/mL; 0,01 mg/mL) were prepared. Each solution was sonicated for 15 minutes using an ultrasonic bath (260 W) and subsequently UV-vis absorption was measured. The solution (10 mL) of each sample was put in a Falcon™ 15mL Conical Centrifuge Tubes and centrifuged at: 2000 rpm for 5 minutes, 4000 rpm for 10 minutes, 4000 rpm for 30 minutes and 4000 rpm for 60 minutes. UV-vis absorptions were measured immediately after each centrifugation and after 5 minutes, 10 minutes, 30 minutes, 60 minutes, 120 minutes, 4 days and 8 days.

7.8.2 Solubility in polyol

G-OH powder and polyol were poured in a flask (1 mg/mL; 0,8 mg/mL; 0,6 mg/mL; 0,5 mg/mL; 0,3 mg/mL; 0,2 mg/mL; 0,1 mg/mL; 0,05 mg/mL; 0,025 mg/mL; 0,01 mg/mL) mixed for 10

minutes at 10000 rpm using an ULTRATURRAX stirrer. The solution (10 mL) of each sample was put in a Falcon™ 15mL Conical Centrifuge Tubes and centrifuged at: 2000 rpm for 5 minutes, 4000 rpm for 10 minutes, 4000 rpm for 30 minutes and 4000 rpm for 60 minutes. UV-Vis absorptions were measured immediately after each centrifugation and after 5 minutes, 10 minutes, 30 minutes, 60 minutes, 120 minutes, 4 days and 8 days.

7.9 Preparation of nanocomposites from NR Latex

A standard procedure was adopted for the preparation of nanocomposites. It were prepared six different compound with different amount of filler: 0 phr, 3 phr, 6 phr, 9 phr, 12 phr, 15 phr. For each compound in a 1L becker it were prepared an aqueous suspension of hydroxy–graphite (G–OH) (1% wt) then stirred at room temperature with magnetic stirrer for 15 min and sonicated for 15 min. Meanwhile in a 1L becker was poured latex and water in order to dilute latex 1:3 vol / vol. The obtained suspension of latex was stirred at room temperature with magnetic stirrer for 10 min. After that the aqueous suspension of hydroxy–graphite (G–OH) (1% wt) was added to the latex suspension and stirrer again with magnetic stirrer for 15 min and sonicated for 15 min. Subsequently, during the stirring, was added the coagulating agent, an aqueous solution (2%) of sulphuric acid. The coagulated compound was cut into small pieces and washed with water until neutral pH and dried at room temperature for several days.

These compounds were prepared nanocomposites with an internal mixer (Brabender®) with an inner chamber of 12 cc. Figure 7.1 shows a typical Brabender®

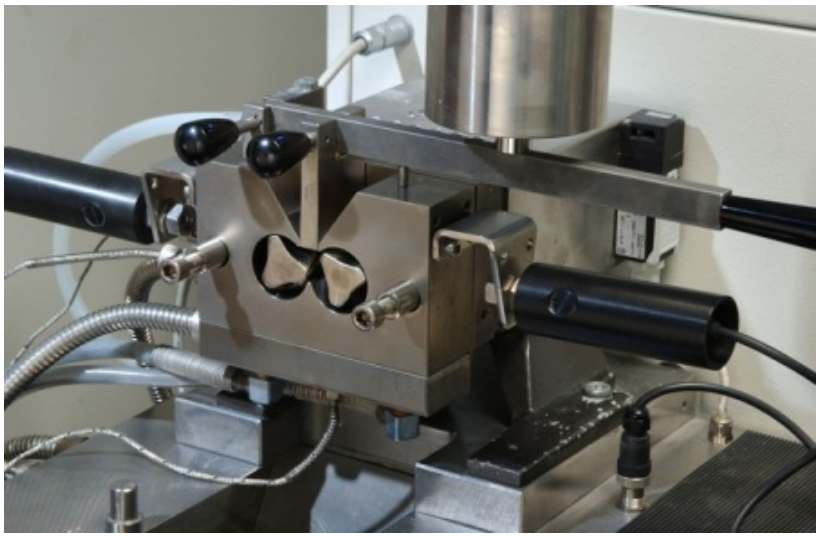

Figure 7.1. Brabender® for laboratories.

First the compounds were masticated for 1 min, then stearic acid and zinc oxide were added and mixed together for 2 min, finally were added 6PPD, TBBS and sulphur and mixed together for 2 min. All quantities were calculated to maintain the same phr for each substance, except G-OH, and to have 10cc of the composite at a time. The reason for this choice was not fill 100% of the chamber of the mixer 12 cc in order to improve the mixing.

7.10 Crosslinking

Crosslinking reaction was studied at 151°C with a Monsanto oscillating disc rheometer (MDR 000), determining the minimum modulus M_L, the maximum modulus M_H, the modulus M_{final} at the end of the crosslinking reaction, the time t_{s1} required to have a torque equal to $M_L + 1$, the time t_{90} required to achieve 90% of the maximum modulus M_H.

7.11 Synthesis of polyurethanes

A standard procedure was adopted for polymerization reactions. Run 3 of Table 6.1 is reported as an example. In a polymerization mold were mixed G-OH-TM (0.1 g, 1.39 mmol) and AROPOL SPER 1407 (10 g) using an ULTRATURRAX stirrer for 5 minutes at 10000 rpm.

Subsequently was added ARODUR 621,6 (3 g, 12 mmol) and stirred with an ULTRATURRAX stirrer for 15 seconds. The resulting mixture was allowed to react for 5 minutes.

7.12 Characterization

7.12.1 Powder X-Ray Diffraction

Wide-angle X-Ray diffraction (WAXD) patterns were obtained in reflection, with an automatic Bruker D8 Advance diffractometer, with nickel filtered Cu–Kα radiation. Patterns were recorded in 10° – 100° as the 2θ range, being 2θ the peak diffraction angle. Distance between crystallographic planes was calculated from the Bragg law. The $D_{hk\ell}$ correlation length, in the direction perpendicular to the hkl crystal graphitic planes, was determined applying the Scherrer equation $D_{hk\ell} = K\,\theta / (\beta_{hk\ell} \cos \theta_{hk\ell})$ **(1)** where: K is the Scherrer constant, λ is the wavelength of the irradiating beam (1.5419 Å, Cu-Kα), $\beta_{hk\ell}$ is the width at half height, and $\theta_{hk\ell}$ is the diffraction angle. The instrumental broadening, b, was determined by obtaining a WAXD pattern of a standard silicon powder 325 mesh (99%), under the same experimental conditions. The width at half height, $\beta_{hk\ell} = (B_{hk\ell} - b)$ was corrected, for each observed reflection with $\beta_{hk\ell} < 1°$, by subtracting the instrumental broadening of the closest silicon reflection from the experimental width at half height, $B_{hk\ell}$.

7.12.2 Thermogravimetric analysis (TGA)

TGA tests under flowing N_2 (60 mL/min) were performed with a Mettler TGA SDTA/851 instrument according to the standard method ISO9924-1. Samples (10 mg) were heated from 30 to 300°C at 10°C/min, kept at 300°C for 10 min, and then heated up to 550°C at 20°C/min. After being maintained at 550°C for 15 min, they were further heated up to 650°C with an heating rate of 30°C/min and kept at 650°C for 20 min under flowing air (60 mL/min).

7.12.3 FT-ATR and FT-IR

The FT-ATR spectra were recorded between 450 and 4000 cm^{-1} by using a Perkin Elmer FT-IR Spectrum One equipped with Universal ATR Sampling Accessory with diamond crystal.

7.12.4 UV-Vis

UV-Vis absorption measurements were made using a Hawlett Packard 8452A Diode Array Spectrophotometer. The suspensions of adduct (3 mL) were placed by pipette Pasteur, in quartz cuvettes of 1 cm optical path (volume 1 or 3 mL) and analyzed by a spectrophotometer UV-Vis. Resets the instrument with pure solvent and has one UV spectrum from 200-340 nm. It was recorded a white the solvent employed. The UV-visible spectrum reported intensity the absorption as a function of the wavelength of the radiation between 200 and 750 nm.

7.12.5 Differential scanning calorimetry (DSC)

DSC analyses under N_2 (80 mL/min) atmosphere were performed with a Mettler DSC 823e calorimeter. Each sample (4.5 mg ± 0.05 mg) was kept at 50°C for 5 min, cooled to -85°C at 10C/min, kept 10 min at this temperature, heated up to 50°C at 5°C/min.

7.12.6 Transmission electron microscopy (TEM)

Morphology of the composites was investigated by Transmission Electron Microscopy (TEM) with a Zeiss EM 900 microscope applying an accelerating voltage of 80 kV. Ultrathin sections (about 50 nm thick) were obtained by using a Leica EM FCS cryoultramicrotome equipped with a diamond knife (sample temperature: 1308C; knife temperature: 608C). The distance between consecutive platelets within clay stacks was measured on digitalized TEM micrographs, obtained at high magnification (>50,000), by using an image analysis software (Image Pro Plus1).

7.12.7 Centrifugation

Centrifugations were performed using an ALC - Centrifugette 4206.

7.12.8 Surface area analysis BET

Nitrogen adsorption at liquid nitrogen temperature (77 K) was used to measure surface areas of OMMT and polymer/OMMT aerogels with a Nova Quantachrome 4200e instrument. Before the adsorption measurement, OMMT powders were degassed at 100°C under vacuum for 24 h, while polymer/clay aerogels were degassed at 40°C, in the same conditions. The surface area values were determined by using 11-point BET analysis.

7.12.9 Nuclear Magnetic Resonance Spettroscopy (NMR)

^{1}H-NMR and ^{13}C-NMR spectra were recorded on a Bruker 400 MHz (100 MHz ^{13}C) instrument at 298 K. Chemical shifts were reported in ppm with the solvent residual peak as internal standard (DMSO-*d*6: δ_H= 2.50 ppm, $CDCl_3$: δ_H= 7.26 ppm).

7.12.10 Sonication

2 L ultrasonic bath (power 260 W) Soltec Sonica Ultrasonic Cleaner.

7.12.11 Dynamic-mechanical test: Strain Sweep

Tests were performed with a Monsanto R.P.A. 2000 rheometer in the torsion mode. A first strain sweep (0.1 - 25% shear strain amplitude) was performed at 50 °C and 1 Hz, then the sample was kept in the instrument at the minimum strain amplitude (γmin = 0.1%) for 10 min, to achieve equilibrated conditions. Dynamic tests were finally performed at 50°C at increasing strain amplitude (0.1 - 100% shear strain amplitude) with a frequency of 1 Hz.

7.12.12 Quasi static properties

Tensile tests were carried out at room temperature by means of a dynamometer (Zwick Roell Z010) with optical extensometer. The clamps rate was 1mm/min and the chamber load was 10 kN. (ISO 37 / UNI 6065)

Conclusions

In this thesis, nanosized graphite with very high surface area was successfully modified through the reaction with the following reagents: (i) KOH, (ii) maleic anhydride, (iii) 1-dodecanethiol.

Thanks to the successful reaction with KOH, hydroxyl groups were selectively introduced, in appreciable amount. They were essentially in peripheral positions, as the interlayer distance of graphene layers was not modified. However, the number of stacked layers, calculated from X-Ray analysis, was reduced (from 35 to 23) and the TEM micrographs confirmed the preparation of few layers graphene. It is worth underlining that the reaction was carried out in the absence of solvents or catalysts, with green methods such as ball milling or the simple heating of the reaction flask. More than that, it was demonstrated that is possible to prepare few layers graphene without using harsh reaction conditions, dangerous or toxic reagents, and using water as the solvent to favour this event. Methods used in the field and considered as the best practice, such as the Hummers method, require a further step to reduce oxidized graphite. Such step is not required by using the method presented in this thesis. In fact, nanocomposites based on NR and G-OH show electrical conductivity, though so far not at very low level of G-OH (25 phr). This demonstrates that the oxidation with KOH does not disturb the sp^2 hybridization of carbon atoms.

Thanks to the successful reaction with maleic anhydride, were introduce on nanoG anhydride groups and, after hydrolysis, carboxylic groups. Reactions have to be optimized, in order to better remove unreacted anhydride and to improve the selectivity in the introduction of carboxylic groups.

Thanks to the successful reaction with 1-dodecanethiol, hydrocarbon chains were introduced and it was demonstrated that a carbon allotrope with high surface area reacts with sulphur.

G-OH from the reaction of nanoG with KOH was selected for the preparation of nanocomposites with natural rubber and polyurethane as the polymer matrix. In fact, nanoG with polar functional groups was required in order to allow: (i) the dispersion of the carbon allotrope in NR latex and in polyols (ii) the interaction with polyurethanes and the reactivity with isocyanates. G-OH from reaction with KOH was selected in consideration of the green methods adopted, the complete removal of KOH up to neutral pH, the selectivity in the introduction of OH functional groups, the reduction of number of stacked layers.

Stable solutions of G-OH from KOH were prepared in water, up to 4 mg/mL as G-OH concentration, in NR latex and in polyols.

Nanocomposites in NR were prepared by latex blending, with G-OH content from about 4 to about 25 phr, followed by addition of ingredients for sulphur based crosslinking, via melt blending. Almost linear correlation was found between G-OH content and the reduction of induction time of vulcanization and the increase of the maximum modulus of the composites. Mechanical reinforcement consistently increased with G-OH content, as shown by the values of storage G' modulus and stresses at all the elongations in stress-strain curves. Indications were not collected of the occurrence of G-OH percolation. However, it is worth noting that reduction of G' with strain amplitude, that means the known Payne effect, was observed below the percolation threshold.

Preliminary indications show slightly larger mechanical reinforcement with G-OH in NR, from latex blending, than with NanoG in IR, from melt blending, with the latter data taken from the literature.

Experimental evidences suggest that G-OH reacts with isocyanates and take part in the formation of PU. Polyurethane based on a low amount of G-OH (less than 1%) had main thermal properties, such as degradation temperatures and glass transition temperature, substantially similar to the ones of neat PU.

In a nutshell

Results of this thesis demonstrate that the reaction of nanosized high surface area graphite with KOH is a suitable way for introducing hydroxyl functional groups in the carbon allotrope. Nancomposites based on G-OH and NR show electrical conductivity (at 25 phr as G-OH content), showing that the oxidation with KOH leaves substantially unaltered the sp^2 hybridization of carbon atoms. Stable solutions of such nanosized graphite with hydroxyl groups, G-OH, can be prepared in water, NR latex and polyols. G-OH can be evenly dispersed in NR and PU matrices. G-OH improves the mechanical reinforcement of NR based nanocomposites and takes part in the formation of PU.